

NASA
TP
1801
c. 1

NASA Technical Paper 1801

LOAN COPY
AFWL TECHN
KIRTLAND AF

0067655



TECH LIBRARY KAFB, NM

Analytic Model for Washout of $\text{HCl}(\text{g})$ From Dispersing Rocket Exhaust Clouds

G. L. Pellett

MAY 1981





NASA Technical Paper 1801

Analytic Model for Washout of $\text{HCl}(\text{g})$ From Dispersing Rocket Exhaust Clouds

G. L. Pellett
*Langley Research Center
Hampton, Virginia*



National Aeronautics
and Space Administration

**Scientific and Technical
Information Branch**

1981

CONTENTS

SUMMARY	1
INTRODUCTION	2
SYMBOLS	4
DEVELOPMENT OF WASHOUT MODEL	8
HCl Absorption and Resultant pH of Falling Droplets	8
Applicability of Irreversible Absorption Assumption	9
Washout Coefficient for Monodisperse Rain	11
Washout Coefficient for Polydisperse Rain	13
Washout Coefficient Based on Marshall-Palmer Distribution	14
Washout Coefficient Based on Kelkar Raindrop Intensity Data	15
HCl(g + aq) Washout From SRM Exhaust Scavenging	18
Correction of Fenton-Purcell Λ Expression	18
Alternate Analysis of Fenton-Purcell Scavenging Data	19
Summary of Λ Expressions for HCl(g) Washout	20
Resultant pH of Polydisperse Rain	22
SRM EXHAUST CLOUD DISPERSION	24
Standard Meteorological Regimes for Cape Canaveral	24
Characteristics of Altitude-Stabilized SRM Source Clouds	24
Source-Strength Considerations	25
Summary of Exhaust Cloud Characteristics	25
Vertical HCl Column Density Determinations	27
WASHOUT OF DISPERSING SRM EXHAUST CLOUDS	29
Application to a Dispersing SRM Cloud	29
Resultant pH From a Dispersing SRM Cloud	30
Resultant Acid Deposition From a Dispersing SRM Cloud	31
Collective Results for Dispersive Decay of σ and Potential Rain pH	32
Examples of Acidic Rain Deposition Characteristics	34
Dispersive Decays of Average HCl Concentration	35
Test of Precipitation Scavenging Subroutine in MDM-5(II)	36
SUMMARY OF RESULTS	37
CONCLUDING REMARKS	39
APPENDIX A - REVIEW OF SCAVENGING STUDIES	41
Knutson and Fenton	41
Fenton and Purcell	42
APPENDIX B - STANDARD METEOROLOGICAL REGIMES FOR CAPE CANAVERAL	45
APPENDIX C - CHARACTERISTICS OF ALTITUDE-STABILIZED SRM SOURCE CLOUDS	46
REFERENCES	47
FIGURES	51

SUMMARY

This work contributes to the study by the National Aeronautics and Space Administration (NASA) of the possibility that precipitation scavenging of HCl from large solid rocket (SRM) exhaust clouds may lead to unacceptably acidic rain in the Cape Canaveral, Florida, area before atmospheric dispersion has reduced the potential hazard to safe limits. Washout coefficients are derived, a previously developed $\text{HCl}(g)$ washout model for rain scavenging of SRM clouds is refined and generalized, and the model is applied to nine independently determined SRM cloud dispersion cases.

Derived washout coefficients $\Lambda = AH^b$, given in sec^{-1} , are summarized in terms of rainfall rate H , given in mm rain/hr, and empirical constants (A, b) as follows: Washout of $\text{HCl}(g)$ was based on the modified Frössling equation for convective diffusion of $\text{HCl}(g)$ to a falling droplet; $(A = 1.80 \times 10^{-4}, b = 0.565)$ applied for the Marshall-Palmer (M-P) raindrop size distribution, and $(1.08 \times 10^{-4}, 0.625)$ applied for Kelkar's extensive raindrop size-intensity data for average rains. Washout of $\text{HCl}(g + aq)$ was also derived, based on recent laboratory data on rain scavenging of diluted and humidified SRM exhaust aerosol; $(1.52 \times 10^{-4}, 0.658)$ applied for the M-P distribution. Since this result stemmed from limited data and was statistically equivalent to Λ for $\text{HCl}(g)$ washout, it is provisionally recommended that the geometric mean Λ for $\text{HCl}(g)$, i.e. $(1.39 \times 10^{-4}, 0.595)$, be used to characterize HCl washout from SRM clouds.

The washout model treats the idealized case of an independently generated vertical rainfall that overrides and scavenges an independently advecting and dispersing SRM cloud under stable stratification conditions in the lower troposphere. The resultant pH of rain and HCl deposition rate are characterized in terms of (a) initial source strength of HCl ; (b) dispersive decay of vertical $\text{HCl}(g)$ column density σ expressed in terms of case-specific empirical constants α and β and downwind distance (time), viz, $\sigma = \alpha X^{-\beta}$; and (c) mean wind speed, downwind location of rainfall onset, Λ , and H . Cumulative areal deposition of HCl G_x is characterized in terms of ground coordinates when (a) to (c) are specified and the SRM cloud geometry is assumed to be an expanding right circular cylinder.

The washout model was applied to a refined "spring fair weather" (SFW) Space Shuttle case and eight Titan III (60 percent less exhaust) dispersion cases. These σ decays were previously deduced by application of a multilayer Gaussian diffusion model to seven standard meteorological regimes for overland advection at Cape Canaveral. The Titan III dispersive decays of σ and hence potential pH, defined as volumetric average pH at first onset of rainfall, differed greatly among the seven regimes. A range of more than 2 pH units was spanned at $X \geq 100$ km downwind and $t \geq 2$ hr. At shorter distances the total span was less, but still exceeded 1 pH unit for $X > 10$ km and $t > 0.2$ hr. Environmentally significant pH's (≤ 1.5) for infrequent exposures were shown possible at $X \leq 50$ km and $t \leq 5$ hr for the two most severe, least disper-

sive Titan III cases. This result contrasts with a measured volumetric average pH of 4.61 ± 0.22 (monthly standard deviation) for rains at Cape Canaveral over the last 2 years.

Detailed examples of downwind rainwater pH and G_x , for both potential and progressive washout, are shown for the least and most dispersive Titan III cases and the refined SFW Shuttle case. Both pH and G_x increased with H, as a consequence of $b < 1.0$. High H occurring close to the launch site resulted in much greater G_x than lower H occurring farther out. Nearly complete HCl washout could occur within 30 km at high H. Although potential pH applies strictly at rainfall onset, progressive washout at low H over large X resulted in slow pH change. Thus, damage to ground-receiver surfaces may tend to be greater (lower pH) and more extensive (longer footprint) at lower H.

Several factors affect the validity of the predicted pH's and HCl depositions. First, the model application specifically excludes convective activity and, particularly, dynamics of rainout processes when HCl and alumina interact with natural clouds. This exclusion reduces the utility of the model, since convective activity occurs frequently at Cape Canaveral. Clearly a more realistic atmospheric dynamics model is needed along with parameterizations of the essential cloud microphysics-scavenging processes. Second, uncertainties related to the dispersion calculations, and hence σ decay inputs, affect the validity of predictions, especially at large X. Inclusion of (a) convective loss of HCl from the SRM cloud's upper boundary, (b) HCl sorption at ground level, and (c) a more realistic treatment of horizontal wind shear effects would have increased potential rain pH. However, the values of σ were based on variances derived from relatively small-scale turbulence measurements; variances scaled more appropriately to cloud size would have resulted in smaller but more realistic values of β at large X and t, similar to those observed experimentally for recent Titan III clouds. This modification would decrease potential rain pH. Such competing effects require complex analyses, and their net effects are presently not predictable. Third, the model applies for idealized HCl washout by rain of specified intensity and average polydispersity. Naturally occurring rains vary widely in both respects, and their temporal-spatial characteristics are only roughly predictable. Finally, the washout of $HCl(g + aq)$ still remains an uncertainty. Although $HCl(g)$ will predominate over $HCl(aq)$ on chlorided-alumina nuclei after significant cloud dilution at low-to-moderate humidities, the present values of Λ for $HCl(g + aq)$ may be significantly in error at very high humidities (approximately ≥ 95 percent), which frequently exist at Cape Canaveral.

INTRODUCTION

NASA has been examining the possible environmental impacts of its Space Shuttle Program for about 8 years. Formal Environmental Impact Statements were published in July 1972 (ref. 1) and April 1978 (ref. 2). One of the cited potential problem areas, atmospheric pollution, stems mainly from use of a solid-propellant rocket motor (SRM) booster design. The tropospheric portion of this environmental problem centers on the possible effects of relatively large, localized, low-level releases of SRM exhaust products, which include more than 70 metric tons of hydrogen chloride (HCl) and about 110 metric tons

of aluminum oxide particles (0.01 to 20 μm) emitted per launch below 4-km altitude. More specifically, the possibility exists that precipitation scavenging of HCl may lead to localized deposition of unacceptably acidic (hydrochloric acid) rain on nearby land areas or protected waters before atmospheric dispersion has effectively reduced the potential hazard to safe limits.

One purpose of this paper is to refine and generalize a previously developed model (ref. 3) which characterized the idealized washout of gaseous HCl and resultant deposition of acidic rain from an advecting and dispersing SRM cloud. A second purpose is to characterize the possible effects that various meteorological conditions at Cape Canaveral, Florida, may have on acidic rain deposition.

Obviously the development of understanding and quantitative methodology for predicting HCl scavenging and for assessing possible environmental consequences of various acid rain deposition is an essential precursor to specification of safe, realistic launch constraints. The original Environmental Impact Statement (EIS) for the Space Shuttle Program (July 1972) states, ". . . for the (predicted) overland trajectories of the exhaust cloud, the possible harmful effects of rain containing HCl will be analyzed prior to each firing. If the calculations predict unfavorable conditions, the launch will be postponed." The recent revision of the EIS (Final, April 1978) states, ". . . the results of this program . . . to model the occurrence of acidic rain . . . and to predict the acidity of rainfall that might occur . . . will provide a model to define in advance the go-no-go (launch constraints) criteria to minimize unacceptable environmental effects from acidic rainfall."

The absorption of $\text{HCl}(\text{g})$ by free-falling aqueous droplets was previously studied experimentally (ref. 3). The data were shown to be well characterized by the modified Frossling equation with an appropriate binary diffusion coefficient¹ for HCl in air. Also, an idealized rain scavenging model was developed and used to characterize the washout of $\text{HCl}(\text{g})$ from SRM exhaust clouds (ref. 3). This model treated the simplified case of an independently generated vertical rainfall that overrides and scavenges by washout processes an independently dispersing SRM exhaust cloud. The model was developed to apply strictly at low-to-moderate SRM cloud relative humidities, where $\text{HCl}(\text{g})$ tends to predominate over the aqueous acid aerosol component after a few minutes of cloud dilution, and under stable stratification conditions in the lower troposphere.

The model in reference 3 was used to predict the resultant characteristics of acid rain deposition for an SFW Space Shuttle SRM exhaust cloud dispersion

¹Although the initially assumed binary diffusion coefficient D_{AB} of $0.20 \text{ cm}^2/\text{sec}$ for HCl in N_2 (air) was shown to fit the four column-length-residence-time sets of droplet absorption data well and thus was used throughout the reference 3 analysis, the four data sets were best fit statistically by $D_{\text{AB}} = 0.175 \text{ cm}^2/\text{sec}$. It was subsequently found that use of a theoretical equation based on modern kinetic theory and the Lennard-Jones expression for intermolecular forces (ref. 4) led to a calculated value of $0.170 \text{ cm}^2/\text{sec}$ at 25°C and 1 atm. This latter value was adopted for the present paper and then corrected to $0.187 \text{ cm}^2/\text{sec}$ at 15°C and 0.85 atm.

case, derived independently from application of a Gaussian multilayer diffusion model, MDM-4(II), that was developed at the NASA Marshall Space Flight Center (MSFC). The SFW dispersion case was based on one of seven standard meteorologies documented for the Cape Canaveral area. These meteorologies were originally selected to represent a range of characteristic cases of overland advection with turbulent diffusion in the planetary boundary layer in order to establish an initial basis for assessing postlaunch HCl concentration histories at the Earth's surface (ref. 5).

In the present paper, the idealized washout model is first refined and generalized and then is applied to nine independently determined exhaust cloud dispersion cases (ref. 6 and an unpublished paper by G. L. Pellett) which were derived from the set of seven standard meteorological conditions. The model improvements and additions consist of (a) including more representative values for air properties and HCl diffusion coefficient; (b) developing a more comprehensive analytic approach for generalizing HCl(g) absorption and washout and thus resultant rain pH and HCl deposition characteristics; (c) deriving two new HCl(g) washout coefficient expressions based on the modified Frössling equation and integrated over both the well-known Marshall-Palmer (M-P) raindrop size distribution and the previously used Kelkar raindrop size-intensity data; and (d) deriving a new HCl(g + aq) washout coefficient expression for SRM exhaust aerosol based on a detailed review and analysis of published laboratory data on rain scavenging of solid rocket exhaust and integrated over the M-P distribution. While the previous washout model was applied only to the Shuttle SFW meteorological case, the refined washout model is applied to (a) an improved version of the Shuttle case, (b) all seven standard meteorological cases for the smaller but chemically similar Titan III SRM propelled vehicle, which exhausts ≈ 40 percent of that for the Shuttle in the altitude range 0 to 4 km, and (c) an abnormal (pad abort) Titan III case. The Titan III cases provide a basis for detailed comparisons with existing in-cloud data on Titan III launch effluents and also associated acidic rainfall in one case. Finally, the characteristics of acidic rainfall which might result from either vehicle under various meteorological conditions are clearly demonstrated; i.e., explicit analytic predictions of downwind rainwater pH and HCl ground deposition are given for various meteorologies, assumed onsets of rainfall, and rainfall intensities.

Use of trade names or names of manufacturers in this paper does not constitute an official endorsement, expressed or implied, of such products or manufacturers by NASA.

SYMBOLS

- A empirical constant in power-law expression for washout coefficient (eq. (41)), sec^{-1}
- b empirical exponent in power-law expression for washout coefficient (eq. (41)), dimensionless

$C(\text{HCl})$	concentration of $\text{HCl}(\text{g} + \text{aq})$ in diluted SRM exhaust, as used by Fenton and Purcell (ref. 25) and expressed in dimensionless volume/volume units, ppmv
$\hat{C}(\text{HCl})$	peak value of measured in-cloud HCl concentration, expressed in dimensionless volume/volume units, ppmv
c_f	molar air density, 3.60×10^{-5} mol air/cm ³ at 15°C and 0.85 atm
D_{AB}	binary diffusion coefficient for HCl in N_2 or air; 0.187 cm ² /sec is used at 15°C and 0.85 atm (see footnote 1)
D_x	effective diameter of cylindrical (right circular) SRM exhaust cloud in horizontal plane, m
d	raindrop diameter, cm
$E(a,d)$	collection efficiency for falling drop of diameter d which collects aerosol particles and droplets of radius a ; efficiency represents fractional collection of particles and/or droplets within geometric cross-sectional area πd^2 , dimensionless
G_x	cumulative deposition of aqueous HCl (in rainwater) on ground, at location X along SRM cloud-centroid path, g HCl/m^2
$G_{x,y}$	cumulative deposition of aqueous HCl (in rainwater) on ground, at location (X,Y) along SRM cloud path, g HCl/m^2
\dot{G}_x	rate of deposition of aqueous HCl (in rainwater) on ground, at location X along SRM cloud-centroid path, g $\text{HCl}/\text{hr}\text{-m}^2$
H	rainfall accumulation rate, mm rain/hr
H_m	upper bound of surface mixing layer, m
k_x	gas-phase mass-transfer coefficient, mol $\text{HCl}/\text{cm}^2\text{-sec}$
M_A	mass concentration of $\text{HCl}(\text{g} + \text{aq})$ in diluted SRM exhaust, as used by Fenton and Purcell (ref. 25), g HCl/m^3
$m(\text{HCl})$	molarity of aqueous HCl in droplets; mixing-cup average molarity for polydisperse rain, mol HCl/L
m_0	initial mass of HCl in SRM exhaust cloud, g HCl
n	number of raindrops per unit volume of air, cm ⁻³
Δn_i	incremental number of raindrops per unit volume for size class i , cm ⁻³
$\dot{\Delta} n_i$	raindrop intensity for raindrops of size class i , m ⁻² -sec ⁻¹

$p(\text{HCl})$	average concentration of $\text{HCl}(\text{g})$ in parcel of diluted SRM exhaust, expressed in dimensionless volume/volume units, ppmv
$p_0(\text{HCl})$	initial value of $p(\text{HCl})$ before $\text{HCl}(\text{g})$ washout begins at $t = 0$, ppmv
pH	measure of acidity due to $\text{H}^+(\text{aq})$; defined for an idealized solution of fully dissociated $\text{HCl}(\text{aq})$ by $\log_{10} [1/m(\text{HCl})]$
Q_I	effective heat release for solid rocket propellant combustion, cal/g propellant (1 cal = 4.184 J)
R_A	rate of HCl scavenging by individual droplets, g HCl/sec
Sh	Sherwood number based on droplet diameter (eq. (3)), dimensionless
t	elapsed time after onset of ground deposition due to HCl washout, sec
t_e	exposure time for droplet absorption during fall through parcel of gas containing HCl , sec
t_0	elapsed time corresponding to X_0 , hr
t'	transit time for droplet to fall to Earth's surface from altitude z , sec
U_C	mean unidirectional wind speed which describes horizontal motion of SRM exhaust cloud, m/sec
V_∞	droplet terminal velocity during free fall through parcel of air, cm/sec
W_A	molar flow of $\text{HCl}(\text{g})$ to droplet surface during $\text{HCl}(\text{g})$ absorption, mol HCl/sec
X	unidirectional downwind distance from launch site, $X_0 + X_{CS}$, km
X_0	virtual source distance upwind from SRM cloud stabilization point at $X_{CS} = 0$, km
X_{CS}	unidirectional downwind distance from SRM cloud stabilization point, km
X_r	unidirectional downwind distance from launch site where onset of uniform rain occurs (before arrival of SRM cloud), km
X_{A0}	mole fraction of $\text{HCl}(\text{g})$ in equilibrium at gas-droplet interface
$X_{A\infty}$	mole fraction of $\text{HCl}(\text{g})$ in bulk gas

Y perpendicular distance from cloud-centroid path, km
 Z_m SRM cloud-centroid height, m
 z vertical distance for droplet fall through SRM exhaust cloud, m
 z_{top} height of SRM cloud top above ground, m
 α, β constants which define power-law decay of $HCl(g)$ column density σ in dispersing SRM exhaust cloud; α is equivalent to ppmv-m at $X = 1$ km, and β is dimensionless exponent of X in equation (48)
 Λ washout coefficient defined by equation (8) and generalized by equation (41), sec^{-1}
 ν_f kinematic viscosity of air, $0.172 \text{ cm}^2/sec$ at $15^\circ C$ and 0.85 atm
 ρ_{air} mass density of air, 1041 g air/m^3 at $15^\circ C$ and 0.85 atm
 σ vertical $HCl(g)$ column density, ppmv-m

Subscript:

pot potential

Abbreviations:

CC cloud centroid
 CFP cold front passage
 F-P Fenton and Purcell
 FFW fall fair weather
 FW, Pre-CF fair weather pre-cold front
 LLSB low-level sea breeze
 MDM multilayer diffusion model
 M-P Marshall and Palmer
 Post-CF post-cold front
 SB sea breeze
 SFW spring fair weather
 SRM solid rocket motor

DEVELOPMENT OF WASHOUT MODEL

The first two sections of this development follow closely that given in reference 3, but the coefficients have been reevaluated to conform to the revised $\text{HCl}(\text{g})$ diffusion coefficient and the newly defined ambient conditions at 15°C and 0.85 atm, which more closely represent average conditions aloft at Cape Canaveral. Subsequent equations depend on these coefficients. The next section on washout coefficient for monodisperse rain serves a dual, although not immediately obvious, purpose. First, it defines the washout process in terms of droplet characteristics, and this leads to a set of analytic expressions that can be used independently to characterize washout by droplets of specified size. Second, it serves to define expressions that are needed later in the derivation of washout by polydisperse rain, when raindrop intensity data (e.g., Kelkar) are used to evaluate washout coefficients at various rainfall intensities.

HCl Absorption and Resultant pH of Falling Droplets

Hydrogen chloride is a highly soluble gas, and within an SRM cloud, $\text{HCl}(\text{g})$ transfer to a falling droplet may be considered to be gas-phase diffusion limited. For low mass-transfer rates and where gas-phase mass-transfer resistance controls, droplet absorption can be described by (ref. 7)

$$-W_A = k_x \pi d^2 \frac{X_{A0} - X_{A\infty}}{1 - X_{A0}} \quad (1)$$

Now X_{A0} will always be much smaller than unity in an SRM cloud. Furthermore, it will be shown later that, for all practical cases of $\text{HCl}(\text{g})$ washout (i.e., for ≥ 0.5 -mm rain/hr falling through a dispersing SRM cloud), X_{A0} will always be much smaller than $X_{A\infty}$. This is due to the high solubility of HCl and to the expected range of $\text{HCl}(\text{g})$ column densities and concentrations. However, note that, for the potentially reversible case of in-cloud scavenging, X_{A0} and $X_{A\infty}$ will tend to converge as HCl equilibrium is approached in cloud aerosol droplets, since they are much smaller and also have substantially longer residence times. Thus

$$W_A = k_x \pi d^2 X_{A\infty} \quad (2)$$

The Frössling semiempirical mass-transfer correlation (ref. 8), as modified by Ranz and Marshall (ref. 9), has been successfully applied to a number of cases of mass transport to (or from) a sphere immersed in a moving fluid (ref. 7). The dimensionless Sherwood number (diameter basis) is given in terms of the Reynolds and Schmidt numbers as

$$\text{Sh} = \frac{k_x d}{c_f D_{AB}} = 2 + 0.60 \left(\frac{dV_\infty}{\nu_f} \right)^{1/2} \left(\frac{\nu_f}{D_{AB}} \right)^{1/3} \quad (3)$$

By taking values for the properties of air at 15°C and 0.85 atm (see symbols) and adopting a value for the binary diffusion coefficient ($D_{AB} = 0.170 \text{ cm}^2/\text{sec}$ at 25°C and 1 atm, corrected to $D_{AB} = 0.187 \text{ cm}^2/\text{sec}$ at 15°C and 0.85 atm; see footnote 1), equation (3) becomes

$$Sh = 2 + 1.407(dv_{\infty})^{1/2} \quad (4)$$

Recognizing that $p(\text{HCl}) = 10^6 X_{A\infty}$ and substituting for k_x and $X_{A\infty}$ in equation (2), a pair of expressions² is obtained for the molar absorption rate:

$$W_A = 10^{-6} c_f D_{AB} \pi d (Sh) p(\text{HCl}) \quad (5a)$$

$$W_A = 10^{-11} \left(4.23d + 2.98d^{3/2} v_{\infty}^{1/2} \right) p(\text{HCl}) \quad (5b)$$

The resulting molarity of HCl in a falling droplet after an absorption exposure time t_e is

$$m(\text{HCl}) = 6 \times 10^{-3} c_f D_{AB} d^{-2} (Sh) p(\text{HCl}) t_e \quad (6a)$$

$$m(\text{HCl}) = 10^{-8} \left(8.08d^{-2} + 5.68d^{-3/2} v_{\infty}^{1/2} \right) p(\text{HCl}) t_e \quad (6b)$$

Assuming that the absorbed HCl is 100 percent dissociated to H^+ , ignoring for a moment the initial H^+ concentration in a rain droplet, and taking the exposure time for a droplet falling at terminal velocity through a cloud of dilute $\text{HCl}(g)$, z meters thick, $t_e = 100z/v_{\infty}$ (no net vertical air motion in the SRM cloud), the final pH of a fallen droplet obtained is

$$\text{pH} = \log \frac{10d^2 v_{\infty}}{6c_f D_{AB} p(\text{HCl}) z (Sh)} \quad (7a)$$

$$\text{pH} = \log \frac{10^6 d^2 v_{\infty}}{\left[8.08 + 5.68(dv_{\infty})^{1/2} \right] p(\text{HCl}) z} \quad (7b)$$

Applicability of Irreversible Absorption Assumption

The applicability of equations (2) to (7) to an SRM cloud is now checked for a typical case. An analysis of the SFW Shuttle exhaust cloud dispersion case, described later, led to predicted values of $p(\text{HCl})$ and z at various

²The second expression is included to indicate d and v_{∞} dependencies and also to facilitate user computations.

distances from the launch site. Two sets of values within the main region of interest, 10 to 100 km, have been used in equation (7b) to calculate pH and molarity for rain droplets in the size range of interest, 0.3 to 0.03 cm. Results are shown in table I along with X_{AO} values corresponding to equilibrium vapor pressures of the respective HCl solutions at 15°C and 0.85 atm (calculated from ref. 10 vapor-pressure formulas).

TABLE I.- SAMPLE CALCULATIONS AND CHECK ON APPLICABILITY OF EQUATION (2)
FOR DROPLETS FALLING THROUGH AN SRM EXHAUST CLOUD*

d, cm	V_{∞} , cm/sec	pH (100% ionized to H ⁺)	$m(\text{HCl}) = 10^{-\text{pH}}$, mol HCl/L in droplet	$X_{A\infty}$, HCl in bulk gas	X_{AO} , [†] HCl at gas-liquid interface
$p_O(\text{HCl})z = 2 \times 10^4$ ppmv-m at X = 10.9 km downwind distance*					
0.3	860	1.59	0.0257	5×10^{-6}	0.0001×10^{-6}
.1	430	.676	.211	5	.0057
.05	218	.006	.986	5	.140
.03	123	-.536	3.44	5	7.94
$p_O(\text{HCl})z = 10^3$ ppmv-m at X = 67.5 km downwind distance*					
0.3	860	2.89	0.0013	0.25×10^{-6}	$<0.00001 \times 10^{-6}$
.1	430	1.98	.0105	.25	.00002
.05	218	1.31	.0493	.25	.00035
.03	123	.76	.172	.25	.0038

*Based on fully modified SFW Shuttle exhaust cloud dispersion case developed later in this paper: $p_O(\text{HCl})z = 10^6 X^{-1.64}$ and $m_O = 61 \times 10^6$.
[†] X_{AO} is based on empirical fit (ref. 10) of equilibrium HCl vapor-pressure data for 15°C aqueous HCl and 0.85 atm.

In general, the calculated pH values in table I indicate acidities less than 1 mol HCl/L. The obvious exception is for droplets smaller than 0.05 cm falling at a close distance (11 km) to the launch site. Although the basic assumption used in deriving equation (2), i.e., $X_{A\infty} \gg X_{AO}$, is valid for 0.05-cm droplets falling at 11 km downwind, it fails for droplets of smaller size (e.g., 0.03 cm) that fall close to the launch site. However, at larger distances (or alternately, with initially lower HCl column densities and/or shortly after washout begins), the irreversibility assumption is adequate for droplets as small as 0.03 cm; at a distance of 68 km, the assumption is highly valid for all droplet sizes.

Thus, for this range of raindrop size, taking into consideration the relative contributions of various droplet sizes to integrated HCl(g) washout (dis-

cussed later), the use of equation (2) in the present model is considered adequate for rainfall rates >0.5-mm rain/hr at all relevant distances (≥ 10 km) from the launch site or, alternately, whenever HCl column density is smaller than 2×10^4 ppmv-m.

Washout Coefficient for Monodisperse Rain

In order to describe the effective transient $\text{HCl}(g)$ concentration in an SRM cloud t seconds after the SRM cloud encounters a steady overriding rain, a solution to the scavenging-rate equation for irreversible washout (refs. 11 to 14) is required. Thus

$$\frac{dp(\text{HCl})}{dt} = -\Lambda p(\text{HCl}) \quad (8)$$

The washout coefficient Λ can be seen to satisfy its operational definition as the ratio of scavenging rate to the concentration of the scavenged component. The solution of equation (8) which applies to a finite thickness z (m) of the SRM cloud is

$$p(\text{HCl})z = p_0(\text{HCl})z \exp(-\Lambda t) \quad (9)$$

For idealized monodisperse rain, of droplet size d and number density n , it can be shown from (a) the operational definition of Λ and (b) rearrangement of equation (5a) that the washout coefficient is simply

$$\Lambda = \frac{10^6 W_A n}{p(\text{HCl}) c_f} = \pi D_{AB} d (Sh) n \quad (10)$$

Since the monodisperse rainfall rate is defined by

$$H = 6000 \pi d^3 v_{\infty} n \quad (11)$$

rearrangement of equation (11) and substitution for n in equation (10) yields a pair of alternative expressions for the washout coefficient for monodisperse rain:

$$\Lambda = \frac{HD_{AB}(Sh)}{6000d^2v_{\infty}} \quad (12a)$$

$$\Lambda = 3.12 \times 10^{-5} H \left(2d^{-2} V_{\infty}^{-1} + 1.407 d^{-3/2} V_{\infty}^{-1/2} \right) \quad (12b)$$

Note, from equation (12a), that Λ is essentially proportional to D_{AB} since Sh is only weakly dependent on D_{AB} in equation (3).

Since equations (7) and (12) contain (a) droplet terminal velocity V_{∞} , which depends on d (refs. 14 and 15) and on air properties, and (b) Sh , which depends on both d and V_{∞} , it is desirable to express the product $Sh/(d^2 V_{\infty})$ in terms of d only to facilitate calculations of pH and Λ for the monodisperse rainfall case.

Values of $Sh/(d^2 V_{\infty})$ were calculated for convective diffusion of HCl (in air at $15^{\circ}C$ and 0.85 atm) to water droplets falling at terminal velocity. Equation (4) was used to calculate Sh . The water droplet terminal velocities tabulated in Mason (ref. 15) for $20^{\circ}C$ and 1 atm were corrected to conditions of $15^{\circ}C$ and 0.85 atm by applying a factor of 1.0665 . This factor was calculated from an expression developed by Foote and Du Toit (ref. 16), and it is assessed by Mason (ref. 15). Results which illustrate the slightly curvilinear power-law variation of $Sh/(d^2 V_{\infty})$ with d are shown in figure 1. A best-fit straight line is described by

$$\frac{Sh}{d^2 V_{\infty}} = 0.022 d^{-2.15} \quad (13)$$

A more accurate fit, also shown in figure 1, is

$$\frac{Sh}{d^2 V_{\infty}} = 2.61 (10d)^{-2.15} + 0.175 \ln (10d) \quad (14)$$

Either equation (13) or equation (14) can be substituted into equations (7a), (9), and (12a) to obtain expressions that characterize washout by monodisperse rainfall. Use of the simpler but less accurate expression, equation (13), results in

$$pH = \log \frac{1.125 \times 10^7 d^{2.15}}{p(HCl)_z} \quad (15)$$

$$p(HCl)_z = p_0(HCl)_z \exp(-6.86 \times 10^{-7} d^{-2.15} H t) \quad (16)$$

$$\Lambda = 6.86 \times 10^{-7} H d^{-2.15} \quad (17)$$

where $p(\text{HCl})_z$ is the effective vertical $\text{HCl}(\text{g})$ column density (in ppmv-m) t seconds after the onset of rain deposition.

Substitution of equation (16) into equation (15) yields a combined expression that can be used to calculate the pH of monodisperse-droplet rain at ground level any time after onset of rainfall deposition:

$$\text{pH} = \log \frac{1.125 \times 10^7 d^{2.15}}{p_0(\text{HCl})_z} + 2.98 \times 10^{-7} d^{-2.15} H t \quad (18)$$

Note that pH applies only to H^+ derived from HCl ; also, $t = 0$ applies in a practical sense when the idealized monodisperse rainfall first reaches ground level.

Washout Coefficient for Polydisperse Rain

For naturally occurring polydisperse rain, droplet size spectra can be characterized by various frequency-distribution functions $d(n)/d(d)$ (in drops/cm⁴), which depend on rainfall rate and type of rain (refs. 14, 15, and 17). These functions can be used to define (see ref. 14) an integrated intensity; by using equation (11),

$$H = 6000\pi \int_0^\infty d^3 v_\infty \frac{d(n)}{d(d)} d(d) \quad (19)$$

and the washout coefficient for highly soluble gases, from equation (10),

$$\Lambda = \pi D_{AB} \int_0^\infty d(\text{Sh}) \frac{d(n)}{d(d)} d(d) \quad (20)$$

Note that the generalized integral expression for Λ in terms of rain-droplet collection efficiency $E(a,d)$ is given (refs. 11 to 14) by

$$\Lambda = \int_0^\infty \frac{\pi d^2}{4} E(a,d) v_\infty \frac{d(n)}{d(d)} d(d) \quad (21)$$

where collection efficiency for convective diffusion with irreversible absorption is

$$E(a,d) = \frac{4D_{AB}(Sh)}{dV_{\infty}} \quad (22)$$

Expressions for $E(a,d)$, which apply for Brownian diffusion, interception, and impact collection of aerosol particles and/or droplets of radius a by raindrops of diameter d are discussed by Slinn (ref. 14) and Pruppacher and Klett (ref. 17).

Although equation (20) can be integrated by using numerical substitution to obtain Λ at various H for any given raindrop spectra, the following alternative approach was taken to eliminate the implicit dependence on V_{∞} (contained in Sh). This approach greatly simplifies subsequent numerical integrations for Λ by having functions that contain only d and H . Values of $d(Sh)$ were calculated for convective diffusion of HCl (in air at $15^{\circ}C$ and 0.85 atm) to water droplets falling at terminal velocity. Results which illustrate the slightly curvilinear power-law variation of $d(Sh)$ with d are shown in figure 2. A best-fit straight line is

$$d(Sh) = 52d^{5/3} \quad (23)$$

Now that $d(Sh)$ is accurately expressed as a simple function of d only, substitution of equation (23) into equation (20) leads to a convenient integral expression which can be used to evaluate Λ for rains of known droplet size distribution

$$\Lambda = 52\pi D_{AB} \int_0^{\infty} d^{5/3} \frac{d(n)}{d(d)} d(d) \quad (24)$$

Washout Coefficient Based on Marshall-Palmer Distribution

The Marshall-Palmer (M-P) raindrop size distribution (ref. 18) has been used in a number of studies to calculate precipitation scavenging characteristics. (See ref. 14.) The expression for the M-P differential number distribution for raindrops with diameters between d and $d + d(d)$ is given by

$$\frac{d(n)}{d(d)} = 0.08 \exp(-41H^{-0.21}d) \quad (25)$$

Before the M-P distribution is adopted for use in this analysis, it is important that its principal attributes and limitations be recognized. Mason's initial assessment (ref. 15) of the M-P expression for raindrop size distribution, equation (25), was that it provided a good average fit to the experimental data of Laws and Parsons (ref. 19), apart from a tendency to overestimate the numbers of small drops. Based on four more recent independent sets of data (up to 1962, ref. 20), Mason (ref. 15) concluded, "While the Marshall-Palmer distribution represents quite well the average size distribution of a large number of samples from continuous cyclonic or warm-frontal rain, or the characteristics of the rain averaged over a considerable interval of time, samples taken over periods of only a few minutes may show considerable deviations from these spectra." Slinn (ref. 14) discussed the problem of defining an appropriate raindrop size distribution, especially for predictions of the washout coefficient. He compared empirical formulas for seven different size distributions and asserted, "The difference between real data and these smooth empirical functions can be very large, especially for convective storms where frequently they're not even qualitatively similar." Slinn also pointed out that even for continuous frontal rain, as studied by Waldvogel (ref. 21) and Joss, the parameters in the M-P distribution had large variations during a single storm. Finally, Pruppacher and Klett (ref. 17) provided a very recent and comprehensive assessment of the M-P and other distribution functions used to characterize rainfall under a variety of conditions.

By considering the limitations of the M-P raindrop size distribution and also recognizing that this distribution still remains an acceptable standard for predictive comparisons, it can now be applied to the determination of $HCl(g)$ washout coefficient as a function of rainfall intensity. Substitution of equation (25) into equation (24) with $D_{AB} = 0.187 \text{ cm}^2/\text{sec}$ followed by numerical integration over the finite droplet size range $0.01 \leq d \leq 0.6 \text{ cm}$ for each of several H-values in the range $0.1 \leq H \leq 100 \text{ mm/hr}$ leads to the results shown in figure 3. The calculated results (circles) are well characterized by the empirical fit

$$\Lambda = 1.80 \times 10^{-4} H^{0.565} \quad (26)$$

Washout Coefficient Based on Kelkar Raindrop Intensity Data

Experimental data in the form of raindrop intensity (in drops/ $\text{m}^2\text{-sec}$) versus size can also be used to deduce the washout coefficient and its dependence on rainfall rate. Kelkar (ref. 22) published the results of an extensive set of ground-level raindrop measurements and gave the intensity of raindrops as a function of droplet diameter for several different rainfall rates. The data used in the present analysis represent averages of grouped results (table 2 of ref. 22) obtained during 8 rain periods, with 49 000 drops counted. They are confined to general rains, as opposed to Kelkar's other studies of drizzles, light showers, moderate showers, and monsoon thunderstorm rains (ref. 23). The data are grouped into sets, with averaged values of the rainfall intensity and the number of drops/ $\text{m}^2\text{-sec}$ tabulated for 21 intensity groups (0.20 to 34 mm/hr) and 16 diameter groups (0 to 0.25 mm up to 3.75 to 4.00 mm in 0.25-mm increments).

In order to utilize the Kelkar raindrop intensity data to calculate Λ for polydisperse rains, we first denote these incremental data by $\Delta \dot{n}_i$ for the i th class of mean diameter d_i and corresponding terminal velocity V_∞ , and then express the incremental data in terms of Δn_i :

$$\Delta \dot{n}_i = 10^4 V_\infty \Delta n_i \quad (27)$$

Equation (20) is rewritten as

$$\Lambda = \pi D_{AB} \int_0^\infty \left(\frac{Sh}{d^2 V_\infty} \right) d^3 V_\infty \frac{d(n)}{d(d)} d(d) \quad (28)$$

Dividing equation (28) by equation (19) gives

$$\frac{\Lambda}{H} = \frac{D_{AB} \int_0^\infty \left(\frac{Sh}{d^2 V_\infty} \right) d^3 V_\infty \frac{d(n)}{d(d)} d(d)}{6000 \int_0^\infty d^3 V_\infty \frac{d(n)}{d(d)} d(d)} \quad (29)$$

When equation (13) is substituted as the simple power-law expression for $Sh/d^2 V_\infty$, the respective integrals of equation (29) are approximated by finite sums, and $10^{-4} \Delta \dot{n}_i$ is substituted for $V_\infty \Delta n_i$, the following expressions for Λ are obtained:

$$\Lambda = \frac{H D_{AB}}{6000} \frac{\sum_{i=1}^N (0.022 d_i^{-2.15}) d_i^3 \Delta \dot{n}_i}{\sum_{i=1}^N d_i^3 \Delta \dot{n}_i} \quad (30)$$

$$\Lambda = \frac{H D_{AB}}{6000} \left(\frac{Sh}{d^2 V_\infty} \right)_m \quad (31)$$

where the weighted mean is defined by

$$\left(\frac{Sh}{d^2 v_\infty}\right)_m = \frac{0.022 \sum_{i=1}^N d_i^{0.85} \Delta \dot{n}_i}{\sum_{i=1}^N d_i^3 \Delta \dot{n}_i} \quad (32)$$

Kelkar's averaged raindrop intensity data were used to calculate $\left(\frac{Sh}{d^2 v_\infty}\right)_m$ through application of equation (32) to his 21 sets of combined droplet intensity data, each corresponding to an average rainfall rate. The results shown in figure 4 indicate that

$$\left(\frac{Sh}{d^2 v_\infty}\right)_m = 3.47H^{-0.375} \quad (33)$$

represents a good empirical fit of the data over the entire experimental range of rainfall rate. Substitution of equation (33) into equation (31) results in an expression for the washout coefficient for $HCl(g)$ based on $D_{AB} = 0.187 \text{ cm}^2/\text{sec}$ and the Kelkar raindrop intensity data:

$$\Lambda = 1.08 \times 10^{-4} H^{5/8} \quad (34)$$

Respective values for Λ calculated directly from equation (30) for each of Kelkar's 21 sets of averaged raindrop intensity data are shown in figure 3 (squares) and are faired with a straight line representing equation (34).

The somewhat more accurate expression for $Sh/d^2 v_\infty$, equation (14), could have been substituted into equation (29) to define a refined (and more complex) finite sum expression for Λ analogous to equation (30). But this treatment of the Kelkar data did not appear to be justified in view of the relatively large drop size interval used; e.g., especially over the inclusive lower bound interval (0 to 0.025 cm), where the relative difference in accuracy between equations (14) and (13) is the greatest.

The expression for $HCl(g)$ washout coefficient based on Kelkar's data, equation (34), can be compared with Engelmann's graphically illustrated Λ for iodine (I_2) washout (ref. 11), which was based on an independent numerical evaluation of equations (3) and (20) using the same Kelkar rain intensity data. The present author's measurement of Engelmann's slope (0.62) for $\log \Lambda$ versus

log H indicated nearly exact agreement with the present $H^{5/8}$ dependence. Also, the estimated ratio of multiplying factors (2.6 for 25°C and 1 atm) was very close to an estimated ratio of molecular diffusion coefficients, as calculated from the inverse square root of the molecular-weight ratio (2.64). Thus, the present determination of Λ for $\text{HCl}(g)$ washout, using Kelkar's data, is consistent with Engelmann's independent prediction of Λ for washout of I_2 vapor.

$\text{HCl}(g + aq)$ Washout From SRM Exhaust Scavenging

The $\text{HCl}(g)$ washout coefficients can now be compared with scavenging results obtained from experimental studies of solid-propellant exhaust. Consecutive studies by Knutson and Fenton (ref. 24) and Fenton and Purcell (ref. 25) of the Illinois Institute of Technology Research Institute (IITRI) are of particular relevance, since they represent the only published attempts known to this writer to measure rain scavenging rates in laboratory studies of solid rocket exhaust. Because of the potential importance of results derived from these data, these studies are first thoroughly reviewed and critiqued in appendix A. Then the Fenton-Purcell (F-P) result is corrected, and the data are reanalyzed in the following two subsections.

Correction of Fenton-Purcell Λ Expression

Close inspection of the Λ expressions derived by Fenton and Purcell (see appendix A and also p. 53 of ref. 25) clearly indicates that both are incorrect algebraically. The ratio $M_A^{0.824}/M_A$ was written to be $M_A^{0.176}$ instead of $M_A^{-0.176}$. This error has a relatively large effect on the calculated values of Λ at all relevant HCl concentrations (0.1 to 100 ppmv). The power-corrected F-P equation should be

$$\Lambda = 4.21 \times 10^{-8} \rho_{\text{air}} M_A^{-0.176} H^{0.773} \quad (35a)$$

when ρ_{air} is expressed in g air/m³.

Substitution for ρ_{air} and M_A in the power-corrected F-P Λ expression leads to

$$\Lambda = 1.41 \times 10^{-4} p(\text{HCl})^{-0.176} H^{0.773} \quad (35b)$$

for the presently selected atmospheric conditions at 15°C and 0.85 atm. Results calculated from this power-corrected expression are shown in figure 5 for HCl concentrations ranging from 0.1 to 100 ppmv. Comparable results for the original F-P expression (not shown) were incorrectly low by a factor of 10 for 1 ppmv HCl , for example. Finally, note that the single solid line representing this writer's analysis of the F-P data (shown later) crosses through the various

power-corrected F-P results for different HCl concentrations. Details of the analysis are derived in the next subsection of this paper.

Although the HCl concentration dependence of the power-corrected F-P expression is relatively weak, it is evident in figure 5 that significant increases in Λ with decreasing $p(\text{HCl})$ would result for a realistic range of $p(\text{HCl})$. A review of the F-P results, however, indicates that the statistical significance of the derived HCl concentration dependence was not demonstrated. Furthermore, this dependence appears doubtful because of the large data scatter, inclusion of the previously discussed high-concentration reference 24 data, and the presence of large run-to-run variations in relative humidity.

Alternate Analysis of Fenton-Purcell Scavenging Data

An alternate analysis of the F-P data is now presented to (a) examine the validity of the corrected washout coefficients and (b) find a simpler expression for Λ which is consistent with the data. Note that Fenton and Purcell based their reference 25 analysis on the major a priori assumption that the parameter $R_A/\rho_{\text{air}}V_{\infty}d^2$ correctly scales the combined effects of variable droplet diameter and droplet fall speed on scavenging rate. In order to (a) allow a straightforward examination of this assumption and (b) eliminate the apparently weak dependence of Λ on HCl concentration (statistical significance uncertain), it was assumed provisionally that the experimental rate of chloride scavenging R_A is directly proportional to chamber HCl (g + aq) concentration $C(\text{HCl})$ for each of the three droplet-size—fall-speed combinations investigated.

The present author's calculated (from tabulated data) scavenging rates R_A are plotted against $C(\text{HCl})$ in figures 6, 7, and 8 for average droplet diameters of 0.055, 0.11, and 0.30 cm, respectively. All 29 usable data runs, contained in table VI of reference 25 and asserted to be reliable, were included in these log-log plots. Experimental chamber relative humidities are shown adjacent to each point. Although the data scatter is substantial and some runs are clearly of lower quality than others because of the relatively large rainwater chloride corrections required sometimes (starred data), the entire data set is used throughout the present analysis. The 45° lines in each plot represent mean values of $R_A/C(\text{HCl})$ in accordance with the previous assumption of linear concentration dependence. Inspection of the data fails to indicate the presence of a statistically significant effect of chamber relative humidity on R_A , which is in agreement with the F-P assessment.

The mean values of $R_A/C(\text{HCl})$, which effectively represent washout coefficients on a per-droplet basis for each monodisperse droplet size, are plotted as a function of d in figure 9. The least-squares expression

$$R_A/C(\text{HCl}) = 1.24 \times 10^{-7}d^{2.13} \quad (36)$$

is a good correlation of the data. The vertical bars indicate 1 standard deviation of the mean values. Since the molar collection rate per droplet is given by $W'_A = R_A/36.45$ (prime denotes HCl (g + aq) collection), equation (36) is equivalent to

$$\frac{10^6 W_A'}{c_f C(\text{HCl})} = 94.5 d^{2.13} \quad (37)$$

when the present value for c_f at 15°C and 0.85 atm is used.

The corresponding washout coefficient for polydisperse rain is now defined by an integral expression, similar to that defined previously, as

$$\Lambda = \int \frac{10^6 W_A'}{c_f C(\text{HCl})} \frac{d(n)}{d(d)} d(d) \quad (38)$$

After substituting the M-P raindrop size distribution function, equation (25), Λ can be evaluated numerically from

$$\Lambda = \int_{0.01}^{0.6} (94.5 d^{2.13}) [0.08 \exp(-41H^{-0.21}d)] d(d) \quad (39)$$

Calculated values for Λ at various rainfall rates (circles) are shown in figure 10. An excellent fit of these results for $\text{HCl}(g + aq)$ washout is

$$\Lambda = 1.52 \times 10^{-4} H^{0.658} \quad (40)$$

Equation (26) for $\text{HCl}(g)$ washout is also plotted in figure 10. Note that both apply to the same ambient and droplet size distribution and integration conditions. Surprisingly, the respective values of Λ for these independent cases are remarkably close over the normal range of rainfall rate. In fact, they are statistically identical when the data scatter in figure 9 (± 30 per cent) is considered. Unfortunately, the reason for this coincidence of scavenging results cannot be evaluated quantitatively without measurements of aerosol size distribution and analytic considerations of aqueous aerosol growth and scavenging, as discussed previously.

Summary of Λ Expressions for $\text{HCl}(g)$ Washout

The HCl washout coefficients based on the M-P raindrop size distribution and the Kelkar raindrop intensity data are characterized by a generalized empirical expression

$$\Lambda = AH^b \quad (41)$$

The values of A and b for these HCℓ(g) washout cases are summarized in table II, along with values for the geometric mean of the two determinations. The author's previously evaluated expression (ref. 3), based on an alternate treatment of the same Kelkar data, an outdated binary diffusion coefficient (0.20 cm²/sec), and standard air properties at 25°C and 1 atm, is shown for comparison; although the previous value of A, 1.11 × 10⁻⁴, was very close to the present one, 1.08 × 10⁻⁴, this small difference partly reflects compensating effects.

TABLE II.- SUMMARY OF HCℓ WASHOUT COEFFICIENTS IN TERMS OF GENERALIZED EXPRESSION $\Lambda = AH^b$

HCℓ ()	Temperature, °C	Pressure, atm	Source	Scavenging rate	Raindrop distribution; Λ -equation	A, sec ⁻¹	b
g	15	0.85	Present	Modified Frössling	M-P; eq. (26)	1.80 × 10 ⁻⁴	0.565
g	15	0.85	Present	Modified Frössling	Kelkar; eq. (34)	1.08 × 10 ⁻⁴	0.625
g	15	0.85	Present	Modified Frössling	Geometric mean of M-P, Kelkar; eq. (42)	1.39 × 10 ⁻⁴	0.595
g	25	1.00	Previous (ref. 3)	Modified Frössling	Kelkar	1.11 × 10 ⁻⁴	0.625
g + aq	15	1.00	Knutson and Fenton (ref. 24)	Data with 50% of modified Frössling	M-P	.83 × 10 ⁻⁴	0.567
g + aq	15	0.85	Presently corrected F-P result, eq. (35a)	Data	M-P; eq. (35) (note ppmv HCℓ in A-factor)	1.36 × 10 ⁻⁵ p(HCℓ) ^{-0.176}	0.773
g + aq	15	0.85	Present analysis of F-P (ref. 25)	Calculated from data	M-P; eq. (40)	1.52 × 10 ⁻⁴	0.658

The SRM exhaust rain scavenging results reviewed on pages 18 to 20 and 41 to 44 of this paper are also summarized in table II. While Knutson and Fenton (ref. 24) used 0.173 cm²/sec for their HCℓ(g) diffusion coefficient at 15°C and 1 atm and air properties under the same conditions, multiplication of their A value by 2 (= 1.66 × 10⁻⁴) yields a value of Λ which is approximately equivalent to the present result (first row) when the difference in atmospheric pressure is fully accounted for. Although the corrected F-P expression (eq. (35)) yields Λ values that agree roughly with those derived from the reanalysis of their data (eq. (40)), the latter is preferred because of its simplicity and also the absence of a clear experimental dependence of Λ on HCℓ concentration and humidity.

Two recommendations are now offered. First, since (a) equation (40) for $\text{HCl}(g + aq)$ washout is statistically equivalent to equation (26) for $\text{HCl}(g)$ washout over the relevant H range and (b) the physics of $\text{HCl}(g)$ washout are more firmly established, it is provisionally recommended that rocket exhaust HCl washout analyses be based on values of Λ which apply to rain scavenging of $\text{HCl}(g)$. If at some later point new aerosol size distribution information and detailed SRM cloud microphysics and scavenging calculations lead to well-defined alternative expressions that apply, for example, at high humidities (approximately ≥ 95 percent), then reconsideration will be necessary. Second, it is recommended that the geometric mean of the M-P and Kelkar integrated $\text{HCl}(g)$ washout coefficients (both based on the modified Frossling equation) be used for predictive purposes; i.e.,

$$\Lambda = 1.39 \times 10^{-4} H^{0.595} \quad (42)$$

This compromise is considered both a reasonable and conservative expression for characterizing $\text{HCl}(g)/\text{HCl}(g + aq)$ washout under the presently selected atmospheric conditions at 15°C and 0.85 atm, since neither of the raindrop size intensity distributions is considered unequivocal.

Resultant pH of Polydisperse Rain

Using the $\text{HCl}(g)$ washout coefficient, defined for average, naturally occurring, polydisperse rains by equation (41), $\Lambda = AH^b$, a general expression for the pH of rain at ground level can be derived. First, for the monodisperse rain case, equation (12a) is rearranged as

$$\frac{Sh}{d^2 v_\infty} = \frac{6000\Lambda}{HD_{AB}}$$

and then substituted for $Sh/(d^2 v_\infty)$ in equation (7a) to eliminate the explicit dependence of pH on d , v_∞ , and Sh ; thus

$$\text{pH} = \log \left[\frac{H}{3600c_f \Lambda p(\text{HCl})z} \right] \quad (43)$$

Substituting equation (9) for $p(\text{HCl})z$ gives

$$\text{pH} = \log \left[\frac{H}{3600c_f \Lambda p_0(\text{HCl})z} \right] + \frac{\Lambda t}{\ln 10} \quad (44)$$

Note that for ground deposition considerations $t > 0$ pertains to time lapse after uniform-size raindrops of diameter d (used in eq. (18)) first reach ground level. Thus, while washout actually occurs at some earlier average time $t - t'$, its effect is not measured at ground level until $t > 0$.

Since Λ is the only term in equations (43) and (44) which depends on the distribution of raindrop size (assuming fixed H), equation (41) may be substituted for Λ to yield an expression for the pH of polydisperse rain at ground level; thus

$$\text{pH} = \log \left[\frac{H^{1-b}}{3600c_f A p_O (\text{HCl}) z} \right] + \frac{AH^b t}{\ln 10} \quad (45)$$

When the geometric mean Λ in equation (42) (i.e., $A = 1.39 \times 10^{-4}$ and $b = 0.595$) is used, equation (45) reduces to

$$\text{pH} = \log \left[\frac{5.55 \times 10^4 H^{0.405}}{p_O (\text{HCl}) z} \right] + 6.04 \times 10^{-5} H^{0.595} t \quad (46)$$

Several features of equation (45) should be noted. First, it consists of two A - and H -dependent terms: one relates to $\text{HCl}(g)$ column density at the onset of rainfall deposition, and one represents the effect of progressive washout. Second, it represents the mixing-cup (volume-weighted average) pH of steady rainfall received at ground level; thus, it has been assumed that differences in transit times $\delta t'$ for the various droplet sizes which contribute most to (dominate) volumetric average pH are small compared with incremental values of t which alter pH significantly in equation (45). In practice, an instantaneous mixing-cup average pH would not be realized exactly, since droplets of different size do have different transit times through the SRM cloud. Thus, a finite sampling time is appropriate for practical application of equation (45), particularly during initial stages of rainfall and, in general, for any natural rainfall, since large spatial and temporal variations in raindrop size distribution usually occur during a given rainfall event. Note that for calculation of the final total acidity pH_f of a rain that has an initial acidity pH_0 , the relation

$$\text{pH}_f = -\log (10^{-\text{pH}} + 10^{-\text{pH}_0}) \quad (47)$$

can be used. This satisfies the problem of an incorrect asymptotic limit for pH in equations (7), (15), (18), and (43) to (46) for very long washout times and/or very low vertical $\text{HCl}(g)$ column densities.

SRM EXHAUST CLOUD DISPERSION

Specific applications of the NASA/MSFC cloud rise preprocessor and the variously modified Gaussian multilayer diffusion models (MDM) of exhaust cloud dispersion for tropospheric air quality predictions at ground level are described in references 26 to 32. Some of these references focus on the inherent mathematical and physical limitations of this basically statistical analytic approach (ref. 32), parametric studies of the principal variables upon which the MDM models are based (refs. 26 and 32), and comparisons of calculated rocket effluent concentrations at ground level with those obtained from other advective diffusion models (ref. 32).

The parameters used in this paper to characterize HCl source strength m_0 and vertical HCl column density σ are documented by this author in reference 6 and an unpublished paper. The original SRM cloud dispersion calculations, from which these parameters were derived, were obtained through use of the NASA/MSFC cloud rise preprocessor and Gaussian MDM described and documented in references 28 to 30 for operational prediction of toxic fuel hazards. Dispersion calculations using Model 4, version II of the MDM codes, designated here as MDM-4(II), comprise the basis of parameters used throughout this study. Simultaneous inclusion of the precipitation scavenging subroutine is indicated by the designation of MDM-5(II).

Standard Meteorological Regimes for Cape Canaveral

The meteorological regimes selected for this work consist of the set of standard meteorologies (ref. 5) that were originally used to assess atmospheric dispersion of rocket exhaust effluents in the Cape Canaveral, Florida, area. They represent the major meteorological conditions which lead to overland transport and are likely to be encountered in the Cape Canaveral area. The meteorological profiles of temperature, wind speed, and wind direction for all seven meteorological regimes are shown in figures 11(a) to 11(g), as obtained from references 33 and 28 (for sea breeze (SB)), and are discussed in appendix B. Meteorological data for specific launch occasions are generally tabulated in separate publications (e.g., refs. 34 to 36).

Characteristics of Altitude-Stabilized SRM Source Clouds

The SRM cloud rise preprocessor portion of the MDM-4(II) model numerically calculates the vertical and horizontal distribution of HCl which results from buoyant cloud rise with turbulent air entrainment under a specified potential temperature gradient (refs. 26 to 36). The resulting vertical source-strength distribution is then assigned a multilayer structure, based on the meteorologi-

cal profiles, which includes a specific geometric shape in the vertical cross section to define the initial distribution of exhaust mass in the altitude-stabilized SRM cloud. In the case of Model 4, a conical body of revolution, having a diamond-shaped cross section symmetrical about the vertical centroid axis, is used to bound the horizontal layers. Examples for the SB, cold front passage (CFP), and post-cold front (Post-CF) cases are shown in figure 12 and are discussed in appendix C.

Source-Strength Considerations

Although the vertical-line—source-strength input function (propellant mass burn rate versus altitude) is accurately known for any prescribed Titan III or Shuttle mission, the cloud rise process determines resultant vertical and horizontal SRM exhaust distributions, which apply after altitude stabilization has occurred. Thus, the calculated layer source strengths, which lead to corresponding initial HCl concentrations in the MDM subdivided stabilized SRM cloud, always differed from the accurately known input source-strength increments. Moreover, the resultant cumulative HCl source strength in the surface mixing layer was always smaller than the cumulative input of HCl mass exhausted up to the defined stabilization altitude. Finally, both the resultant layer and cumulative HCl source strengths varied significantly as functions of the various potential temperature profiles.

Input histories and resultant HCl source strengths which pertain to the chemically similar SRM boosters for both Space Shuttle and Titan III launch vehicles are shown in figure 13. The cumulative HCl inputs to the MDM for both Shuttle (ref. 37) and Titan III (ref. 28) launches are based on propellant consumption rates and launch mission trajectories. They differ by a factor of 2.44 up to an altitude of 2.0 km. The resultant preprocessed fall fair weather (FFW) cumulative HCl source strength in the MDM stabilized cloud for Titan III is also shown in figure 13 for altitudes up to 2 km. The so-called original spring fair weather (SFW) cumulative source strength in the MDM stabilized cloud, used in previous acid rain calculations (ref. 3), is shown as a single point (4 km, 89 t HCl). In view of the Mission 2, November 1973 design (ref. 37), it is too large by about 30 t for a 4-km upper cloud altitude boundary.

Summary of Exhaust Cloud Characteristics

Table III summarizes, for Titan III launches and the seven standard meteorological regimes at Cape Canaveral, Florida, SRM exhaust cloud characteristics deduced from application of the MDM-4(II) in reference 6 and an unpublished paper by G. L. Pellett. In some cases the mean transport wind speed for the cloud U_C , which relates distance to time in the model, differs significantly from the wind speeds of the individual layers.

TABLE III.- SRM EXHAUST CLOUD CHARACTERISTICS, AS DEFINED FROM APPLICATION OF MDM-4(II) TO TITAN III
LAUNCHES, FOR SEVEN STANDARD METEOROLOGICAL CASES AT CAPE CANAVERAL, FLORIDA

Meteorological regime	Meteorology abbreviation	Cloud-centroid height, Z_m , m	Surface mixing-layer depth, m	MDM upper cloud boundary, m	Effective cloud thickness at $X \geq 5$ km, m	Mean wind speed for cloud, U_c , m/s	Mean wind direction (North $\equiv 0^\circ$), deg	Cloud stabilization time, sec	Calculated distance, pad to cloud stabilization (from U_c), km	Empirical virtual source distance, X_0 , km	HC% source strength, m_0 , g
Fall fair weather	FPW	1322	1000	2000	1000	6.127	105	364	2.23	10	14.88×10^6
Spring fair weather	SFW	1380	2000	2000	2000	7.0314	140	416	2.93	4.0	14.48
Low-level sea breeze	LLSB	959	300	2000	1700	6.752	145	199	1.34	3.5	8.634
Sea breeze	SB	993	800	2200	1400	9.923	165	247	2.45	5.0	10.12
Fair weather, pre-cold front	FW, Pre-CF	875	200	1400	1180	2.453	224	160	.39	3.0	11.89
Cold front passage	CFP	1230	2000	2000	2000	6.696	66	301	2.02	4.0	15.07
Post-cold front	Post-CF	1341	1400	2000	600	8.712	69	442	3.85	2.5	11.30
Post-cold front (pad abort)	Post-CF (pad abort)	1506	1400	2000	600	9.284	69	342	3.18	2.5	15.86

The cloud stabilization times from the model were used to estimate downwind drift distances from the launch pad to the point where cloud altitude stabilization theoretically occurs. These cloud stabilization drift distances are compared with the empirically determined virtual source distances X_0 (X_0 was needed to obtain straight-line power-law fits of σ versus X). Finally, the resultant HCl source strengths for the stabilized SRM clouds m_0 are also summarized in table III. They apply from the Earth's surface to the MDM upper cloud boundary and are conserved throughout the SRM cloud dispersion history (in the absence of rain), since no loss terms were applied at the SRM cloud boundaries.

Vertical HCl Column Density Determinations

The MDM-4(II) calculated downwind vertical HCl profiles and the empirical power-law fits of σ versus downwind distance $X = X_{CS} + X_0$ are illustrated in reference 6 and an unpublished paper by G. L. Pellett for each of the Titan III cases studied. The original SFW Shuttle case used in reference 3 is reproduced in figure 14, and the present power-law-decay-modified SFW Shuttle cases (two) are shown in figure 15. The solid line in figure 15 represents the original source strength; the dashed line, the present fully modified source-strength case.

The decay expressions for vertical HCl column density $\sigma = \alpha X^{-\beta}$ are summarized in table IV for the Titan III and Shuttle cases, along with HCl source strength, mean transport wind speed, and other relevant exhaust cloud properties derived from the MDM-4(II) calculations. Corresponding time-dependent decay expressions for σ are also given. The empirical fits for σ were excellent throughout the data range, $1 \leq X \leq 100$ km, for all the Titan III meteorological cases studied. It will be shown later that the demonstration of adequate power-law expressions for σ leads to substantial analytic simplification, especially for subsequent calculation and parameterization of acid rain characteristics. Some effects of meteorology on expressions for σ in table IV are now discussed. Although the deduced values of α can be referred to as an HCl column density source strength at unit distance, the reader should recognize that α is inherently sensitive to X_0 . In turn, X_0 is influenced in the MDM-4(II) cloud rise calculations by the vertical profiles of temperature and wind speed as well as the placement of vertical layer boundaries. Thus, the physical significance of α is approximate and is not precisely defined.

A noteworthy internal consistency exists for the two Post-CFP meteorological cases, which apply to a normal launch and a pad abort situation. The respective X_0 and β values were identical, and the ratio of α values (and σ values) (0.71) was identical to the ratio of m_0 values. In the absence of other similar paired calculations for Titan III's, it is not known whether a simple linear scaling law would apply to other meteorological cases.

A roughly similar comparison can be made between the fully modified Shuttle SFW and Titan III SFW cases, but it is not as exact since additional multilayer structure bounded at an altitude of 4000 m was used for calculating the Shuttle case, whereas the Titan III case was terminated at 2000 m. While the respective β values differed (1.64 and 1.98), the X_0 values were the same (4.0 km), and

TABLE IV.- EMPIRICAL SRM EXHAUST CLOUD PROPERTIES CHARACTERIZING DOWNWIND DISPERSIVE DECAY OF VERTICAL HCl COLUMN DENSITY

Deduced from application of MDM-4(II) to Titan III launches for seven standard meteorological cases at Cape Canaveral, Florida; the present power-law-decay-modified SFW Shuttle case is shown for both originally used source strength $m_0 = 89 \times 10^6$ g HCl (ref. 3) and presently reduced source strength $m_0 = 61 \times 10^6$ g HCl consistent with more recent Shuttle mission design (ref. 37)

Meteorology abbreviation	Cloud-centroid height, z_m , m	MDM upper cloud boundary, m	Effective cloud thickness at $X_{CS} \geq 5$ km, m	Mean wind speed for cloud, U_C , m/s	HCl source strength, m_0 , 10^6 g	Empirical parameters for vertical HCl column density, σ , ppmv-m					
						$\sigma = \alpha(X_{CS} + X_0)^{-\beta} = \alpha X^{-\beta}$			$\sigma = \alpha(t_{CS} + t_0)^{-\beta} = \alpha t^{-\beta}$		
						α , ppmv-m	X_0 , km	β	α , ppmv-m	t_0 , hr	β
Titan III cases											
FFW	1322	2000	1000	6.127	14.88	1.6×10^5	10	0.84	11.9×10^3	0.453	0.84
SFW	1380	2000	2000	7.0314	14.48	2.6	4.0	1.98	.433	.158	1.98
LLSB	959	2000	1700	6.752	8.634	4.3	3.5	1.32	6.35	.144	1.32
SB	993	2200	1400	9.923	10.12	14.0	5.0	1.81	2.17	.140	1.81
FW, Pre-CF	875	1400	1180	2.453	11.89	2.0	3.0	.93	26.3	.340	.93
CFP	1230	2000	2000	6.696	15.07	4.5	4.0	1.93	.968	.166	1.93
Post-CF	1341	2000	600	8.712	11.30	.60	2.5	1.13	1.22	.080	1.13
Post-CF (pad abort)	1506	2000	600	9.284	15.86	.85	2.5	1.13	1.65	.075	1.13
Space Shuttle cases											
SFW (original source strength)	----	4000	----	7.50	89.0	14.6	4.0	1.64	6.56	0.148	1.64
SFW (modified source strength)	----	4000	----	7.50	61.0	10.0	4.0	1.64	4.49	.148	1.64

the ratio of α values (3.85) was fairly close to the ratio of m_0 values (4.21). In terms of corrected distance from launch site, the point at which the ratios of σ values and m_0 values were equal to 4.21 was $X = 1.3$ km, which is still close to the launch site. Thus, these comparisons between Titan III and Shuttle for SFW meteorology suggest that approximately linear scaling of σ with source strength applied.

WASHOUT OF DISPERSING SRM EXHAUST CLOUDS

Application to a Dispersing SRM Cloud

Equation (45) and related expressions for predicting rain pH and ground deposition of HCl can be applied to independently dispersing SRM clouds once the temporal and spatial variation of vertical HCl column density is specified in terms of time and/or ground coordinates. The power-law decay of σ which resulted from application of MDM-4(II) is now defined by the integral expression

$$\sigma = \int_0^{z_{\text{top}}} p_{0,z}(\text{HCl}) dz = p_0(\text{HCl})z = \alpha X^{-\beta} \quad (48)$$

where $p_{0,z}(\text{HCl})$ is the HCl (g) concentration at altitude z , $p_0(\text{HCl})$ represents a vertically averaged concentration over z , X is the downwind distance from launch site, and α and β represent empirical constants.

For simplicity, it is now assumed that the SRM cloud geometry is an expanding right circular cylinder of diameter D_x (axis vertical) with mass conservation for HCl at concentration $p_0(\text{HCl})$. Since the HCl scavenging model applies to irreversible absorption and thus exhibits a direct proportionality between rain molarity and HCl (g) column density, the actual distribution of HCl (g) in the vertical direction is unimportant. In order to calculate rain pH and ground deposition per unit area along the SRM cloud-centroid path (CC path), the horizontal distribution of vertical HCl column density along the projected cloud diameter is normally assumed uniform. For calculation of two-dimensional acid footprints, or ground deposition isopleths, the variation of vertical HCl column density with ground coordinates X and Y must either be uniform beneath the SRM cloud or else specified.

Substitution of equations (41) and (48) into equation (9) yields an expression for the reduction of vertical HCl column density by dispersive decay and washout for $X > 0$ and $t \geq 0$; thus

$$p(\text{HCl})z = \alpha X^{-\beta} \exp(-AH^b t) \quad (49a)$$

Substitution of equation (48) is made with the tacit assumption that SRM cloud dispersion is unaffected by the development and presence of an overriding rain; thus, the SRM cloud is denoted as independently dispersing.

Now let U_C (in m/sec) represent the steady mean wind speed that characterizes SRM cloud transport, and X_r (in km) represent the closest distance from launch site where a steady, overriding, vertical rainfall commences before arrival of the SRM cloud. Thus $t = 1000(X - X_r)/U_C$ sec represents the effective time lapse after the SRM exhaust cloud encounters rainfall. Substitution of this expression for t in equation (49a) leads to an equation, in terms of downwind distances only, which describes the combined effects of dispersion and washout on vertical HCl column density for $0 < X_r \leq X$; thus

$$p(HCl)_z = \alpha X^{-\beta} \exp\left[-1000AH^b(X - X_r)/U_C\right] \quad (49b)$$

Resultant pH From a Dispersing SRM Cloud

An expression for the pH of polydisperse rain at ground level is obtained by substituting equation (48) into equation (45) and letting $t = 1000(X - X_r)/U_C$. For $X \geq X_r \geq 1$ km,

$$pH = \log\left(\frac{H^{1-b}}{3600c_fA\alpha}\right) + \beta \log(X) + \left(\frac{AH^b}{\ln 10}\right)\left(\frac{X - X_r}{U_C/1000}\right) \quad (50)$$

For the geometric mean Λ (eq. (42)), equation (50) reduces to

$$pH = \log\left(\frac{5.55 \times 10^4 H^{0.405}}{\alpha}\right) + \beta \log(X) + 6.04 \times 10^{-2} H^{0.595} \frac{X - X_r}{U_C} \quad (51)$$

In equation (50) there are three terms which affect rainwater pH: The first relates to a combination of rainfall intensity, washout coefficient, and HCl source strength at unit distance; the second depends solely on SRM cloud dispersion; and the third accounts for progressive removal of $HCl(g)$ through washout. Exclusion of the latter term, which is equivalent to setting $X = X_r$, allows formation of an expression for potential rain pH, defined herein as the rainwater pH at ground level just after the first onset of rain. Succinctly, it represents the maximum rain acidity to be expected in the event of rain occurrence downwind; thus

$$pH_{pot} = \log\left(\frac{H^{1-b}}{3600c_fA\alpha}\right) + \beta \log(X_r) \quad (52)$$

Resultant Acid Deposition From a Dispersing SRM Cloud

The areal deposition rate (flux) for aqueous HCl , at any point X on the SRM cloud-centroid (CC) path where washout is occurring overhead, is (averaged over passage of finite SRM cloud)

$$\dot{G}_x = 36.45 \times 10^{-\text{pH}_H} \quad (53)$$

For a uniformly mixed cylindrical SRM cloud of effective diameter D_x , conservation of HCl (in the absence of wet or dry deposition, absorption at the Earth's surface, and convective losses at the top) dictates that

$$m_o = 36.45 c_f \left(\pi D_x^2 / 4 \right) (\alpha X^{-\beta}) \quad (54)$$

Thus the effective SRM cloud diameter along the CC path is

$$D_x = \left[\left(\frac{4}{36.45 \pi c_f} \right) \left(\frac{m_o X^\beta}{\alpha} \right) \right]^{1/2} \quad (55)$$

Since the time lapse for complete passage of the SRM cloud over any point on the CC path is D_x/U_c , the stationary ground receiver on this path will experience a total deposition per unit area of

$$G_x = \dot{G}_x D_x / 3600 U_c \quad (56)$$

Substitution of equations (53) and (55) into equation (56) yields an intermediate result in terms of rainwater pH; thus

$$G_x = \left(\frac{2}{3600} \right) \left(\frac{36.45}{\pi c_f} \right)^{1/2} 10^{-\text{pH}_H} \left(\frac{m_o X^\beta}{\alpha U_c^2} \right)^{1/2} \quad (57)$$

Substitution of equation (50) for pH and rearrangement of terms leads to a generalized predictive expression for cumulative (total) areal HCl deposition along the CC path for all $X \geq X_r$:

$$G_x = \left[\frac{4}{\pi} (36.45 c_f) \right]^{1/2} (A H^b U_c^{-1}) (m_o \alpha X^{-\beta})^{1/2} \exp \left[-1000 A H^b U_c^{-1} (X - X_r) \right] \quad (58)$$

For the geometric mean Λ (eq. 42)), equation (58) reduces to

$$G_x = 5.68 \times 10^{-6} H^{0.595} U_c^{-1} (m_o \alpha X^{-\beta})^{1/2} \exp[-0.139 H^{0.595} U_c^{-1} (X - X_r)] \quad (59)$$

Ground receivers located at some distance Y (in km) normal to the CC path will experience, for the well-mixed cylindrical-cloud case, the same transient pH value but cumulative areal depositions of

$$G_{x,y} = 2G_x \left[0.25 - \left(\frac{Y}{D_x} \right)^2 \right]^{1/2} \quad (60)$$

for all $Y < D_x/2$.

The total HCl deposition experienced at $X = X_r$ after the first onset of rainfall and for complete SRM cloud passage is defined herein as potential deposition and is obtained by setting $X = X_r$ in equation (58). For the present value of c_f (3.60×10^{-5} mol air/cm³), the potential deposition is simply

$$G_{x,pot} = 0.0409 (A H^b U_c^{-1}) (m_o \alpha X^{-\beta})^{1/2} \quad (61)$$

Collective Results for Dispersive Decay of σ and Potential Rain pH

The power-law decay of σ for eight Titan III cases is shown as a function of corrected distance from launch site X in figure 16 and also as a function of elapsed time after launch $X/3.6U_c$ in figure 17. The fully modified SFW Shuttle case is shown as a dashed line in each figure. Two additional ordinate scales, illustrating the corresponding values of potential rain pH for rainfall rates of 1.5 and 25 mm/hr, are also shown in figures 16 and 17. This dual scale is deduced from either equation (46) with $t = 0$ or equation (52) using the geometric mean washout coefficient.

The most noticeable feature of figures 16 and 17 is that the dispersive decay of σ and potential rain pH differ greatly among the seven standard meteorological regimes. A range of more than 2 orders of magnitude in σ and potential acidity (more than 2 pH units) is spanned at $X \geq 100$ km downwind and/or $t \geq 2$ hr postlaunch elapsed time. At shorter distances and times the total span in σ and potential acidity is somewhat less but still exceeds an order of magnitude for $X > 10$ km and $t > 0.2$ hr. These results tend to confirm earlier expectations of large variations in atmospheric dispersion under widely different meteorological conditions, and they serve to emphasize the need for developing a comprehensive atmospheric dynamics model (e.g., see refs. 10 and 38) to deal effectively with this large source of variability.

A second important feature of figures 16 and 17 is that environmentally significant potential rain acidities (e.g., $pH \leq 1.5$ results in short-term

damage to vegetation; see refs. 39 and 40) are shown to be possible for relatively large downwind distances from launch site and for long elapsed times. If the validity of the two meteorological cases, which tend to define upper bounds for σ (FFW and FW, Pre-CF), is accepted, then initial rain pH values between 1.0 and 1.5 (for $1.5 \leq H \leq 25$ mm/hr) could occur at downwind distances up to 50 km and elapsed times up to 5 hours. Although these estimates are derived from the two least dispersive meteorological cases, they are not considered excessively conservative. For example, somewhat more severe stagnation conditions are conceivable; no additional uncertainty bounds have been imposed; and the real possibility³ of a significantly increased raindrop collection efficiency due to a predominance of large (≥ 10 - μ m diameter) aerosol droplets has not been accounted for. While the predictions in figures 16 and 17 also indicate values of potential rain pH of 2 or less at downwind distances up to 200 km and elapsed times exceeding 10 hr, one must recognize that the validity of these longer range results becomes less certain with increasing distance and time.

Some competing effects, which both reduce and increase the potential rain acidity, are now identified. First, the MDM calculations do not include loss of HCl from the SRM cloud's upper boundary or HCl sorption at ground level. Also, they do not include variable advection (wind speed and direction) for the respective MDM cloud layers. Inclusion of these processes would tend to reduce σ and, hence, increase potential rain pH at progressively larger distances. Second, the variances used in the present MDM-4(II) calculations were originally based on field data which applied to relatively small-scale atmospheric turbulence (refs. 34 to 36). It is well known (ref. 42), however, that as the relevant turbulence scale increases for atmospheric dispersion of very large plumes, the appropriate variances and overall dispersion rates tend to become weaker power-law functions of the characteristic scale size (e.g., source cloud diameter) and downwind distance. Thus, the exponent β , which characterizes the decay of σ with X, could decrease to ≈ 0.5 at large X, in a fashion similar to that observed in large-scale dispersion studies (ref. 42) and that actually observed for Titan III exhaust clouds. The most extreme and best documented example out of eight Titan III cases observed thus far (ref. 43) was for the September 5, 1977, launch. Here, 45 data points for maximum in-cloud HCl concentration, obtained over the postlaunch period of 3 to 300 min, were characterized by $\beta = 0.54$ in the empirical expression

$$\hat{C}(\text{HCl}) = 55t^{-0.54}$$

In summary, the sets of potential rain acidity results in figures 16 and 17 characterize the range of dispersive decay σ and initial rain (potential) pH that might be expected for Titan III launches. Respective envelopes bounding the collective results would encompass all seven standard meteorological conditions at Cape Canaveral but would not include the other uncertainties mentioned.

³Informal communication of unpublished results obtained by A. N. Dingle and B. Heikes, University of Michigan, Ann Arbor, Michigan. See also references 10 and 41.

The upper limit for the potential rain pH ordinate is based upon an assumed rainfall rate of 25 mm/hr. The areas beyond $X = 100$ km downwind and 10 hr postlaunch should be treated with an additional level of uncertainty, as discussed previously. Thus the respective inclusive envelopes of these results define a regime of most probable initial rain (potential) pH when it is recognized that the model application is restricted to conditions of low-to-moderate SRM cloud humidity (HCl mostly in gas phase) and to ground locations beneath the SRM CC on which an independently generated overriding rainfall commences under stable stratification conditions aloft.

Examples of Acidic Rain Deposition Characteristics

Before detailed examples of calculated rain pH and HCl deposition due to SRM cloud washout are presented, consider briefly the characteristics of natural rain and contrast these with the regime of concern for individual launch events, where potential rain pH may be <3 and sometimes <1 . Figure 18 shows some characteristics of rain acidity for the Florida area (refs. 44 and 45) and also a set of parametric relationships among potential pH, effective SRM cloud thickness, and vertically averaged HCl(g) concentration. The pH was calculated from equation (46) at a conservative rainfall intensity of 25 mm/hr.

The volume-weighted average rain pH in the Cape Canaveral area was determined to be 4.61 ± 0.22 (monthly standard deviation), based on an extensive study of rainwater characteristics (ref. 45) over the period July 1977 to June 1979. Although the range of rain pH for north-central Florida during the 1967-1968 period (5.3 to 6.8) is based on only four measurements (ref. 44) and is therefore not necessarily representative, these unusually high values are consistent with a downward temporal trend in pH deduced for the northeastern United States over the last 25 years (refs. 46 to 50). More specifically, a recent comprehensive study of rainwater characteristics in Florida (ref. 51) leads to the conclusion that a significant decline in pH and bicarbonate concentration has occurred for northern and central Florida over the past two decades.

The open circles in figure 18 represent potential pH corresponding to the source-strength-modified SFW Shuttle case illustrated in figure 15. Obviously, these predictions of single-event rain acidity are significant even for relatively large distances when compared with the pH of natural precipitation.

Detailed predictions of downwind pH (eq. (50) or (51)) and cumulative HCl deposition G_x (eq. (58) or (59)) are illustrated in figures 19 to 24 for the FFW Titan III, SFW Titan III, and fully modified SFW Shuttle cases. Potential quantities, pH_{pot} from equation (52) and $G_{x,pot}$ from equation (61), which apply at the first onset of rain are shown as dashed lines. Examples of progressive washout for various assumed onsets of rainfall at each of three different intensities are shown as solid lines. Cumulative areal deposition applies along the CC path; off-axis deposition can be calculated from equation (60), with the effective SRM cloud diameter D_x evaluated from equation (55). Note that attainment of CO_2 equilibration at $pH = 5.7$ implies that 100 percent washout of the HCl has occurred upwind. Nearly complete wash-

out can readily occur within 30 km at high rainfall rates. Finally, the corresponding downwind growth of SRM cloud diameter is shown in figure 25 for each of these three cases.

Several observations of the pH and G_x results shown in figures 19 to 24 are now cited briefly. While rain acidity decreases with increasing rainfall rate, total deposition increases. Also, high rainfall rates occurring close to the launch site result in significantly greater depositions than lower rainfall rates occurring farther out. The progressive increase in downwind potential rain pH, due exclusively to dispersive decay of HCl column density for any given rainfall rate, is much slower for the FFW case than the SFW Titan III case. These cases constitute the two limiting dispersion extremes with respect to downwind distance. Note that for both the FFW and SFW cases the pH of a light drizzle (1 mm/hr), beginning at 15 km downwind and continuing out to 100 km, increases very slowly with respect to potential pH (e.g., 0.6 to 0.8 pH units), and is about equivalent to the potential pH for heavy rainfall (25 mm/hr) onset at ≈ 80 km.

While the main thrust of this section has centered on the prediction of acid rain characteristics, some closing remarks on the possible consequences of SRM cloud washout are now given. In general, rain acidity derived from washout of an overhead SRM cloud will tend to determine the respective transient rates of acid reaction with various exposed surfaces, either manmade or natural. The duration (and acidity) of any primary exposure, and hence degree of reaction during exposure, will depend on SRM cloud characteristics, wind speed, and location. Subsequent cleansing of nontrapping surfaces and dilution of accumulated acid rain will occur if rainfall continues after SRM cloud passage. In this case quenching or reduction of the rate of acid attack will tend to occur, the extent depending partly on the nature of each surface. However, regardless of any subsequent cleansing phenomena, and also recognizing the low probability of event reoccurrence, one must still consider the possibility that localized exposures to rain containing HCl and aluminum oxychlorides may have both short and long term effects on the local ecology (refs. 39 and 40). Long term damage effects may depend not only on the concentration history of acidic rain, but also on the deposition histories of both acidic rain and subsequent rainwater dilutions, as well as total accumulated deposition and a host of other environmental parameters. Further guidance in defining possible long term effects may be obtained from recent studies of regional acid rain problems in parts of Europe and the northeastern United States (refs. 46 to 51). Although some of the more obvious and serious environmental effects have already been defined in these studies, it is clear that understanding of the problem is far from complete.

Dispersive Decays of Average HCl Concentration

Dispersive decays of corresponding vertically averaged HCl concentration were deduced for the eight Titan III cases, and the results are shown as functions of X and elapsed time in figures 26 and 27, respectively. These averaged peak-center-line HCl concentrations were computed from expressions for σ by (a) estimating effective cloud thicknesses which applied for

$X_{CS} \geq 5$ km as indicated in table IV, and (b) dividing the appropriate expressions for σ in table IV by the corresponding cloud thicknesses.

Since the dispersive decays of HCl concentration in figures 26 and 27 correspond to decays of potential rain pH in figures 16 and 17, comparisons of these figure sets facilitate preliminary assessments of acid rain potential based on measurements of in-cloud HCl. Such comparisons have proven useful in correlating in-cloud HCl concentrations with simultaneous rain composition data. (See ref. 43.)

A comparison of the calculated results in figure 27 with experimental measurements of peak in-cloud HCl concentrations for eight Titan III launches is illustrated in figure 28 (reproduced from ref. 43). Since the calculated dispersion results were derived from a set of standard meteorologies for the Cape Canaveral area, they have no direct relationships to the actual launch cases. However, certain first-order features of the respective sets are in agreement.

First, to a good approximation, all the experimental in-cloud HCl concentration data appeared to be adequately characterized by single-term power-law-decay expressions, such as shown to apply for the modeled results. Next, the total range of measured HCl concentrations is approximately bounded by the total range of predicted concentrations after ≈ 0.2 hr (lower limit of model validity) and up to the indicated termination of each launch data fit (at 0.5 to 5 hr). Moreover, the respective ranges of highest to lowest HCl concentration were large; e.g., the ratios of highest to lowest HCl were ≈ 100 for both sets and increasing after 1 hr postlaunch. Despite this intersection of the experimental and calculated sets of HCl decay histories, four of the measured in-cloud peak HCl concentrations decayed significantly slower with time than the slowest calculated ($\beta = 0.83$ for FFW). Notably, the worst-case model calculations of HCl concentration (highest values) were partly confirmed experimentally. The apparent tendency of the dispersion model to overpredict the rate of decay of peak HCl concentrations is consistent with the derivation of MDM empirical dispersion coefficients, which are essentially based on correlations of relatively small-scale turbulence measurements. Thus, while there is surprisingly good overall agreement with respect to HCl concentrations, the present MDM application is believed to be deficient in that it fails to account for the reduced effect of large-scale turbulent diffusion, bounded by an inversion layer, that inevitably applies to large stabilized SRM exhaust clouds several minutes after launch.

Test of Precipitation Scavenging Subroutine in MDM-5(II)

The present analytic HCl(g) washout model allows an independent check on the output of the multilayer (and essentially numerical) calculations of MDM-5(II). The comparison made here was to examine the progressive washout of HCl from an SRM cloud, as now described. (Deposition calculations were not available.) The FFW meteorology was selected; a washout coefficient corresponding to 7.7 mm rain/hr was specified ($\Lambda = 4.68 \times 10^{-4} \text{ sec}^{-1}$); and the elapsed time from cloud stabilization for onset of rain was defined ($t_1 = 394$ sec). Two calculations of vertical HCl(g) profiles were needed, one with MDM-5(II) that

allowed evaluation of σ (with rain) and a reference calculation with MDM-4(II) that defined σ (no rain). The latter was equivalent to the results presented in figure 16. Equating σ (with rain)/ σ (no rain) with the ratio $p(\text{HCl})/p_0(\text{HCl})$, and plotting selected results as a function of distance from cloud stabilization X_{CS} led to the results shown in figure 29. The straight line, which agrees very well with the calculated points, was obtained from an alternate form of equations (49), i.e.,

$$p(\text{HCl})/p_0(\text{HCl}) = \exp \left[-\Lambda \left(1000 \frac{X_{CS}}{U_C} - t_1 \right) \right]$$

Note that $p(\text{HCl})/p_0(\text{HCl}) = 1$ at $X_{CS} = 2.41$ km, which corresponds to the onset of rain at $t_1 = 394$ sec. Results of a similar test of MDM-5(II) using the SFW meteorology are shown in figure 30 and indicate equally good agreement. The difference in downwind $\text{HCl}(g)$ washout histories between figures 29 and 30 is due entirely to the difference in average SRM cloud speed U_C .

These comparisons demonstrate that calculated $\text{HCl}(g)$ washout, evaluated by equations (9) and (49) for the present analytic model, was quantitatively equivalent to that evaluated numerically by using MDM-5(II). As a final note it is suggested that the simplicity of the present model, which requires only a single determination of σ decay in the absence of rain, allows subsequent evaluations of σ and various HCl washout and deposition characteristics with greatly reduced computational effort. Thus, a comprehensive matrix of lengthy MDM-5(II) calculations is no longer required to evaluate the effects of various combinations of assumed rain onset time and washout coefficient corresponding to assumed rainfall intensity. It is conceivable that this might prove valuable for real-time predictions and probability assessments of acid rain hazards during prelaunch countdowns.

SUMMARY OF RESULTS

A previously developed $\text{HCl}(g)$ washout model for rain scavenging of solid rocket (SRM) exhaust clouds was refined and applied to nine independently determined SRM exhaust cloud dispersion cases. The model refinements consist of (a) including more representative values for air properties and HCl diffusion coefficient; (b) developing a more comprehensive analytic approach for generalizing $\text{HCl}(g)$ absorption, washout, and resultant rain pH and HCl deposition characteristics as functions of droplet diameter, terminal velocity, raindrop size distribution and intensity, and exhaust cloud dispersion characteristics; (c) deriving two new $\text{HCl}(g)$ washout coefficient expressions, based on an experimentally verified convective diffusion equation (modified Frössling) and integrated over both the Marshall-Palmer (M-P) raindrop size distribution and the previously used Kelkar raindrop size-intensity data; and (d) deriving a new $\text{HCl}(g + aq)$ washout coefficient expression for SRM exhaust aerosol, based on a detailed review and analysis of published laboratory data on rain scavenging of SRM exhaust and integrated over the M-P distribution.

The model treats the idealized case of an independently generated vertical rainfall that overrides and scavenges an independently dispersing SRM exhaust cloud under stable stratification conditions in the lower troposphere. The first two relationships for washout coefficient Λ versus rainfall intensity H derived in this paper characterize washout of $\text{HCl}(g)$. These apply at low-to-moderate ambient relative humidities, where it can be assumed that $\text{HCl}(g)$ will predominate over the aqueous acid aerosol component after a few minutes of SRM cloud dilution. The geometric mean of these two power-law expressions, $\Lambda = 1.39 \times 10^{-4} H^{0.595} \text{ sec}^{-1}$, is recommended for subsequent predictions of $\text{HCl}(g)$ washout under idealized average conditions.

The third Λ expression characterizes $\text{HCl}(g + aq)$ washout for diluted and humidified SRM exhaust aerosol. This expression has the same analytic form and is both statistically and numerically equivalent, to a good approximation, to that obtained for $\text{HCl}(g)$ washout. Thus it is provisionally recommended that the geometric mean $\text{HCl}(g)$ washout coefficient should also be applied to characterize $\text{HCl}(g + aq)$ washout from SRM exhaust clouds under moderate ambient humidity conditions (≤ 95 percent), where significant quantities of $\text{HCl}(aq)$ may coexist with $\text{HCl}(g)$.

The washout model has been generalized for application to SRM exhaust clouds as follows. The resultant pH of rain and HCl deposition rate are characterized in terms of (a) the initial source strength of HCl ; (b) a power-law decay of vertical $\text{HCl}(g)$ column density $\sigma = \alpha X^{-\beta}$, where X is downwind distance from the launch site and α and β are empirically determined constants; and (c) the downwind distance (time) at which a steady overriding rainfall commences at a specified intensity. The cumulative deposition of HCl is then characterized in terms of ground coordinates when (a) to (c) are specified and the SRM cloud geometry is assumed to be an expanding right circular cylinder.

The washout model was applied to a refined "spring fair weather" (SFW) Space Shuttle exhaust cloud dispersion case and eight Titan III dispersion cases. All nine cases were based on independently calculated downwind dispersive decays of σ , deduced previously from application of the NASA Marshall Space Flight Center Gaussian multilayer diffusion model, MDM-4(II), to seven standard meteorological regimes. These regimes were originally selected to represent a range of characteristic cases of overland advection with turbulent diffusion in the planetary boundary layer for the Cape Canaveral, Florida, area.

Results obtained from application of the washout model to the eight Titan III cases indicated that the dispersive decays of potential rain pH, i.e., volumetric average pH at the first onset of rainfall, differed greatly among the seven standard meteorological regimes. A range of more than 2 pH units was spanned at $X \geq 100$ km downwind and/or $t \geq 2$ hr postlaunch elapsed time. At shorter distances and times, the total span was less but still exceeded an order of magnitude for $X > 10$ km and $t > 0.2$ hr. These large spreads in potential pH are consistent with earlier expectations of atmospheric dispersion under widely different meteorological conditions. They also highlight the need for developing a more realistic and comprehensive atmospheric dynamics (with cloud microphysics-scavenging processes) model to deal effectively with this uncertainty. Environmentally significant potential rain acidities ($\text{pH} \leq 1.5$) for one-time exposures were shown to be possible (for $H \leq 25$ mm/hr) at downwind

distances up to 50 km and elapsed times of 5 hr for the two most severe, least dispersive Titan III cases. This result contrasts with a measured volumetric average pH of 4.61 ± 0.22 (monthly standard deviation) for naturally occurring acidic rains in the Cape Canaveral area over the last 2 years.

Detailed examples showing calculated downwind histories of rainwater pH and HCl deposition (for both potential and progressive washout) were shown for the least and most dispersive Titan III cases (fall fair weather (FFW) and SFW) and a modified SFW Shuttle case. In general, rain acidity decreased with increasing rainfall rate while deposition increased; this is a consequence of the <1.0 power-law dependence of washout coefficient on rainfall rate. High rainfall rates occurring close to the launch site resulted in much greater depositions than lower rainfall rates occurring farther out. Nearly complete washout of HCl from an SRM cloud could occur within 30 km at high rain intensities. Progressive washout at a low rainfall intensity (e.g., 1 mm/hr) over large distances (e.g., 15 to 100 km) results in relatively slow decay of rainwater acidity (0.6 to 0.8 pH unit). Thus, damage to ground-receiver surfaces may tend to be greater (lower pH) and more extensive (longer footprint) at lower rainfall intensities.

CONCLUDING REMARKS

Several factors affect the validity of the predicted pH values and ground depositions. The greatest uncertainties stem from the basic idealized assumptions used to formulate the problem. The assumptions of an independently dispersing SRM cloud that experiences washout from an independently generated overriding rainfall under stable stratification conditions specifically exclude (a) significant convective activity associated with storm dynamics and (b) rainout processes stemming from the interaction of SRM cloud components, $\text{HCl}(g)$ and $\text{HCl}(aq)$ on chlorided-alumina nuclei, with natural clouds. Since rainfall in the Cape Canaveral area is frequently associated with significant convective activity, it seems imperative that a more realistic atmospheric dynamics model be developed with appropriate parameterizations of the essential cloud microphysics-scavenging processes.

Additionally, uncertainties related to the input σ decays also affect the validity of the predictions, especially at large distances (e.g., $X \geq 100$ km). A refined inclusion of (a) convective loss of HCl from the SRM cloud's upper boundary, (b) HCl sorption at ground level, and, probably, (c) a more realistic treatment of horizontal wind shear effects for each layer would have increased potential rain pH. Since the decays of σ stemmed from MDM-4(II) calculations based on relatively small-scale turbulence measurements, use of variances scaled more appropriately to cloud size would have resulted in smaller but more realistic values of β at large X and t , similar to those observed for Titan III clouds. The effect in this case would be to decrease potential rain pH at large X . Clearly these competing effects require complex analyses beyond the scope of this paper.

Finally, the rain scavenging relationships derived in this paper apply for washout of $\text{HCl}(g)$ and $\text{HCl}(g + aq)$ by rain of specified intensity and average polydispersity. Naturally occurring rains vary widely in both respects, and their characteristics are very difficult to predict. Rainout of HCl associated

with convective cloud activity may be important or dominant under many conditions, but these processes have not been examined herein. Although $\text{HCl}(g)$ will tend to predominate over $\text{HCl}(aq)$ on chlorided-alumina nuclei after a few minutes of cloud dilution at low to moderate ambient humidities, the applicability of the deduced $\text{HCl}(g + aq)$ washout coefficient is most questionable at very high relative humidities, say ≥ 95 percent, which frequently exist at Cape Canaveral. Thus since washout coefficients for aerosols depend uniquely and significantly on aerosol size distribution and since the distribution of aerosol sizes and the $\text{HCl}(aq)$ concentration exhibit complex microphysical time and concentration dependencies, refinements in the description of $\text{HCl}(g + aq)$ washout may require detailed cloud microphysics calculations.

Langley Research Center
National Aeronautics and Space Administration
Hampton, VA 23665
March 13, 1981

APPENDIX A

REVIEW OF SCAVENGING STUDIES

Knutson and Fenton

In the study of Knutson and Fenton (ref. 24) 0.09-cm water drops, at terminal velocity, scavenged the exhaust of a small, solid-propellant rocket motor in a 5.5-m-diameter spherical chamber. Bubblers were used to determine chamber HCl concentration, which included HCl(g) and HCl(aq) aerosol attached to Al₂O₃ particulates. A log-log plot of Cl⁻ scavenged against chamber Cl⁻ concentration indicated approximately a unity slope based on eight data points. However, the resultant proportionality constant was approximately 0.5 times the value predicted by the modified Frössling correlation (eq. (3)). These authors also observed that relative humidity in the range 69 to 98 percent had no effect on scavenging rate, based on this plot. Relative humidity was calculated from total initial water content, at measured dry bulb temperature, without accounting for subsequent HCl(aq) aerosol formation and solute vapor pressure lowering effects. The authors calculated a washout coefficient expression based on drop-let HCl(g) absorption at 0.5 times the rate expressed by the modified Frössling correlation, the M-P raindrop size distribution, and $D_{AB} = 0.173 \text{ cm}^2/\text{sec}$ at 15°C and 1 atm. Numerical integration and empirical fitting of the results led to their recommended expression for HCl washout (ref. 24):

$$\Lambda = 8.3 \times 10^{-5} H^{0.567} \quad (\text{A1})$$

Unfortunately, the significance and utility of the Knutson and Fenton washout coefficient (eq. (A1)) is unclear. First, the effective air-exhaust mass ratio was about 225 for six of the eight useful data runs. This contrasts with exhaust cloud ratios of $\geq 10^5$ after a few minutes coupled with a much greater availability of water vapor in the real case. Thus, co-condensation of HCl(g) and H₂O(g) in the chamber experiments, forming HCl(aq) on chlorided-alumina nuclei (see refs. 3, 52, 53, and 54) and on the walls (discussed in ref. 24), favored large HCl partitioning and water vapor pressure reduction effects. That is, a relatively high concentration of hygroscopic particles competed for a relatively limited supply of water vapor.

As a check, the present author calculated the properties of a flat-surface (no Kelvin effect) locally equilibrated HCl(aq) aerosol based on the cited experimental data and an iterative analytical solution of the respective partitioning equations for HCl and H₂O by using the methodology outlined in reference 43. For run 7 in reference 24, equilibrium HCl(aq) aerosol formation would reduce the relative humidity from 98 to 86.4 percent and would leave only 7.76 ppmv HCl(g) out of the measured 200 ppmv HCl(g + aq) during the rain scavenging period. Similarly, for run 8 in reference 24, relative humidity would be reduced from 87 to 83 percent, thus leaving only 16.5 ppmv HCl(g) out of the measured 100 ppmv HCl(g + aq). The respective molalities of HCl(aq) are 3.08 and 3.64 for runs 7 and 8. These results indicate that only small percentages of the chamber HCl existed as HCl(g) (3.9 and 16.5 percent, respectively) and

APPENDIX A

the remainder existed as concentrated $\text{HCl}(\text{aq})$ aerosol with a relatively fine but essentially unknown size distribution. Therefore, since washout of $\text{HCl}(\text{aq})$ aerosol by raindrops is typically an order of magnitude less efficient for micrometer-sized droplets than for $\text{HCl}(\text{g})$ but is strongly dependent on aerosol size distribution (refs. 14 and 17), the data of reference 24 are of limited usefulness, even though the observed overall trend (0.5 times Λ for $\text{HCl}(\text{g})$) is in the expected direction for moderately small (e.g., 1- to 5- μm diameter) aerosol sizes. Parenthetically, note that a predominance of submicrometer aerosol sizes could decrease this factor to values approaching 0.1, while a predominance of 10- μm aerosol sizes could increase the factor to $\gg 1$. (See ref. 14.)

Fenton and Purcell

The follow-on IITRI study by Fenton and Purcell (ref. 25) was an attempt to overcome some of the experimental difficulties of the first study; a number of ancillary measurements were also conducted. In particular, they sought to conduct rain scavenging measurements on laboratory-produced rocket exhaust clouds at lower HCl concentrations than before, typical of poststabilized SRM clouds. The solid propellant used was essentially the same; the rocket motor and propellant mass were similar but about 50 percent smaller; and the nozzle was identical.

The rocket motors were fired into the same spherical (5.5 m) test chamber used previously, but the experimental approach differed significantly from this point on. At preselected times partly diluted SRM exhaust in the primary spherical chamber was conducted into a Teflon⁴ 1.5- m^3 experimental chamber via a specially designed aerosol transport tube, which incorporated a peripheral transpiration air sheath and allowed further dilution and efficient transport of the aerosol.

The raindrop generator used to produce uniform-size droplets was essentially the same as before (ref. 24). However, three different droplet sizes (0.055, 0.11, and 0.30 cm) were utilized instead of the single size (0.09 cm) used previously. Terminal velocity was claimed to have been achieved at the raindrop generator exit for the two smallest sizes but not for the 0.30-cm droplets. A glass funnel attached to an N_2 purged holding flask was used to collect the rain. This replaced the mineral oil collection pan used previously. Exit ports located along the periphery of the funnel were used to remove a matched flow of N_2 sheath gas. Parenthetically, a denser gas such as argon would have been superior.

The concentration of HCl in the test chamber was measured with a Geomet, Inc., chemiluminescent detector rather than an aqueous bubbler (impinger) system used previously. A single comparison of the two methods indicated that the bubbler system measured about 10 percent more chloride. This small difference may not have been experimentally significant, but it was consistent with expectations of additional aluminum oxychloride salts trapped as chlorided-alumina particulates by the bubbler. This result coupled with Geomet $\text{HCl}(\text{aq})$ calibration

⁴Teflon: Registered trademark of E. I. du Pont de Nemours & Co., Inc.

APPENDIX A

checks appeared to confirm that the Geomets used to monitor HCl in the Teflon test chamber were measuring HCl(g + aq) but not chloride associated with the alumina.

The results of 33 rain scavenging tests are summarized in table VI of reference 25. As a check the present author independently calculated R_A values by (a) assuming various effective scavenging heights consistent with the aforementioned setup, (b) using the tabulated rain collection data to evaluate corrected raindrop chloride concentrations to at least two significant figures, and (c) using the cited average raindrop diameters. An assumed scavenging height of 145 cm was found to give reasonable agreement with all but four of the tabulated R_A values (2a, 2b, 4a, and 4f in table VI of ref. 25). These appeared to represent calculation-typographical errors, and with one exception (4f), were not obvious misfits in their final parameterized-data correlation (fig. 18 of ref. 25).

Fenton and Purcell sought to generalize these scavenging data by defining a quasi-dimensionless group of variables, $R_A/\rho_{air}V_{\infty}d^2$, in g HCl absorbed/g air. They plotted (on a log-log scale) this parameter as a function of drift-corrected HCl(g + aq) concentration, $C(HCl)$. Note that in the absence of a more specific definition for $C(HCl)$ it must be assumed that ppmv units apply to $C(HCl)$.

Although the parameterized-data scatter was relatively large in figure 18 of reference 25, best-fit empirical expressions were stated to be

$$\begin{aligned} \frac{R_A}{\rho_{air}V_{\infty}d^2} &= 2.82 \times 10^{-7}C(HCl)^{0.824} \\ &= 6.72 \times 10^{-5}M_A^{0.824} \end{aligned}$$

For the latter, M_A was defined as the equivalent mass concentration of HCl, in g HCl/m³. Clearly the first expression, in terms of $C(HCl)$, does not agree (factor of ≈ 1.2 to ≈ 2.5 high) with the best-fit line drawn in figure 18 of reference 25. Additionally, it can be shown that the latter expression in terms of M_A is inconsistent with the first expression when an appropriate value for laboratory air density is used and is in greater disagreement with the best-fit line shown in figure 18 of reference 25 than the $C(HCl)$ expression. Reasons for these disagreements are not apparent.

Fenton and Purcell then evaluated Λ as follows. They used the expression for parameterized raindrop scavenging rate to evaluate a washout coefficient for polydisperse rain. They defined an integral equation equivalent to

$$\Lambda = \frac{1}{M_A} \int R_A \frac{d(n)}{d(d)} d(d) \tag{A2}$$

APPENDIX A

$$\Lambda = \frac{1}{M_A} \int \left(6.72 \times 10^{-5} M_A^{0.824} \right) \left(\rho_{\text{air}} v_{\infty} d^2 \right) \frac{d(n)}{d(d)} d(d) \quad (\text{A3})$$

Fenton and Purcell used the M-P raindrop distribution (eq. (25)) and an approximate power-law expression for droplet terminal velocity to perform numerical integrations for calculation of Λ as a function of H . These values of Λ were stated to be best fit by the expression (incorrect, exponent for M_A should be negative)

$$\Lambda = 4.21 \times 10^{-8} \rho_{\text{air}} M_A^{0.176} H^{0.773}$$

Using $\rho_{\text{air}} \approx 1216 \text{ g air/m}^3$ for their standard conditions, they obtained a final expression (also incorrect) for the washout coefficient:

$$\Lambda = 5.12 \times 10^{-5} M_A^{0.176} H^{0.773}$$

APPENDIX B

STANDARD METEOROLOGICAL REGIMES FOR CAPE CANAVERAL

The meteorological regimes for this work consist of the entire set of standard meteorologies (ref. 5) that were originally used to assess atmospheric dispersion of rocket exhaust effluents in the Cape Canaveral, Florida, area. These regimes represent the major meteorological conditions which lead to overland transport and are likely to be encountered in the Cape area.

The meteorological profiles of temperature, wind speed, and wind direction for all seven meteorological regimes are shown in figures 11(a) to 11(g), as reproduced from references 33 and 28 (SB). The profiles are based on averages of selected data obtained from Cape Canaveral rawinsonde releases and from the NASA 150-Meter Meteorological Tower at Kennedy Space Center, as tabulated in reference 5. Inspection of these profiles indicates large differences in the thermal structure and wind characteristics aloft. Note that significant deviations occur, at various levels, from the preprocessor-calculated average values of wind speed U_C and wind direction θ_C (summarized in table III of main body of this paper), that were used in MDM-4(II) to describe average SRM cloud advective motion after altitude stabilization. Thus, horizontal wind shear effects are not directly accounted for in the MDM-4(II) calculations since individual layers in the multilayer structure are not allowed to advect independently, even though average values for each layer are specified in the program output. Instead, the effects of horizontal and vertical wind shear, relative to average SRM cloud advective speed and direction, are simulated in each layer by respective sets of horizontal (cross direction) and vertical turbulence parameters applied to each layer. These parameters are standard deviations of the wind azimuth σ'_A and elevation angle σ'_E fluctuations. While these standard deviations can be obtained from a comprehensive set of local meteorological data for the Cape Canaveral area (refs. 34 to 36), they can also be deduced from the profile measurements, such as those shown in figures 11(a) to 11(g). The latter procedure was used for the seven standard meteorologies employed in this study; the methodology is described in references 26 to 32 and the specific parameters used are tabulated in an unpublished paper by G. L. Pellett.

APPENDIX C

CHARACTERISTICS OF ALTITUDE-STABILIZED SRM SOURCE CLOUDS

An example of the geometric definition of a Titan III stabilized SRM exhaust cloud is shown in figure 12(a) for the sea breeze (SB) meteorological regime at Cape Canaveral, as obtained from reference 28. The calculated height of the cloud centroid $Z_m = 832$ m is based on an early value for the effective heat release $Q_I = 691$ cal/g propellant; 2790 cal/g is used presently. The fine-layered surface mixing layer has an upper bound ($H_m = 800$ m) based on the onset of temperature inversion at 800 m as shown in figure 11(d). The stem of the so-called column cloud begins at 1300 m with a radius of 200 m. The reason for assigning 1300 m as the transition from the so-called stabilized ground cloud to the stabilized column cloud is apparent in figure 11(d), where the temperature inversion terminates and the gradient of local (and potential) temperature turns negative.

A second stabilized SRM cloud is shown in figure 12(b) for the post-cold front passage meteorological regime applied to the case of an on-pad abort of the Titan III vehicle (Post-CF, pad abort). In this case, obtained from reference 28 and based on $Q_I = 691$ cal/g, the calculated height of the CC is $Z_m = 1132$ m, compared with 751 m for the normal launch case (Post-CF) and 832 m for the previously discussed SB case. Thus, both the vertical temperature profile and the input source strength influence the determination of Z_m . Note also that the height of the surface mixing layer ($H_m = 1400$ m, fig. 11(g)) is greater than in the SB case but is not defined strictly at the minimum temperature point (1700 m) in figure 11(g). Instead, H_m is defined at the turning point in potential temperature.

A third Titan III SRM cloud, also obtained from reference 28 and based on $Q_I = 691$ cal/g, is shown in figure 12(c) for the cold front passage (CFP) case. The corresponding vertical temperature gradient in figure 11(f) was not so steep as in some cases, resulting in a relatively low CC height ($Z_m = 675$ m). However, the temperature profile did not exhibit an inversion up to 2000 m, and thus the surface layer was assigned a depth of $H_m = 2000$ m; the multilayer structure was arbitrarily terminated at this point. Geometric definitions for the remaining meteorological cases were based on application of the same principles first described. Plots of the layer structures and initial vertical distributions of HCl for the present cases ($Q_I = 2790$ cal/g propellant) are similar, based on this author's unpublished tabulated data.

REFERENCES

1. Environmental Statement for the Space Shuttle Program - Final Statement. NASA TM X-68541, 1972.
2. Environmental Impact Statement - Space Shuttle Program. NASA TM-82278, 1978.
3. Pellett, G. L.: Washout of HCl and Application to Solid Rocket Exhaust Clouds. Precipitation Scavenging (1974), ERDA Symp. Ser. 41 (CONF-741003), June 1977, pp. 437-465.
4. Satterfield, Charles N.; and Sherwood, Thomas K.: The Role of Diffusion in Catalysis. Addison-Wesley Pub. Co., Inc., c.1963, pp. 5-10.
5. Susko, Michael; and Stephens, J. Briscoe: Baseline Meteorological Soundings for Parametric Environmental Investigations at Kennedy Space Center and Vandenberg Air Force Base. NASA TM X-64986, 1976.
6. Cour-Palais, Burton G., compiler: Proceedings of the Space Shuttle Environmental Assessment Workshop on Tropospheric Effects. NASA TM X-58199, 1977.
7. Bird, R. Byron; Stewart, Warren E.; and Lightfoot, Edwin N.: Transport Phenomena. John Wiley & Sons, Inc., c.1960, pp. 409, 641-648.
8. Frössling, Nils: The Evaporation of Falling Drops. Beitr. Geophys., vol. 52, 1938, pp. 170-216.
9. Ranz, W. E.; and Marshall, W. R., Jr.: Evaporation From Drops - Part I. Chem. Eng. Prog., vol. 48, no. 3, Mar. 1952, pp. 141-146. Part II. Chem. Eng. Prog., vol. 48, no. 4, Apr. 1952, pp. 173-180.
10. Dingle, A. Nelson: Rain Scavenging of Solid Rocket Exhaust Clouds. NASA CR-2928, 1978.
11. Engelmann, Rudolf J.: The Calculation of Precipitation Scavenging. Meteorology and Atomic Energy - 1968, David H. Slade, ed., U.S. At. Energy Comm., July 1968, pp. 208-221. (Available from NTIS as TID-24190.)
12. Postma, A. K.: Effect of Solubilities of Gases on Their Scavenging by Raindrops. Precipitation Scavenging (1970), AEC Symp. Ser. 22 (CONF-700601), Dec. 1970, pp. 247-259.
13. Hales, J. M.: Fundamentals of the Theory of Gas Scavenging by Rain. Atmos. Environ., vol. 6, no. 9, Sept. 1972, pp. 635-659.
14. Slinn, W. G. N.: Precipitation Scavenging: Some Problems, Approximate Solutions, and Suggestions for Future Research. Precipitation Scavenging (1974), ERDA Symp. Ser. 41 (CONF-741003), June 1977, pp. 1-60.

15. Mason, B. J.: The Physics of Clouds. Second ed. Oxford Univ. Press, c.1971.
16. Foote, G. B.; and Du Toit, P. S.: Terminal Velocity of Raindrops Aloft. J. Appl. Meteorol., vol. 8, no. 2, Apr. 1969, pp. 249-253.
17. Pruppacher, Hans R.; and Klett, James D.: Microphysics of Clouds and Precipitation. D. Reidel Pub. Co., c.1978.
18. Marshall, J. S.; and Palmer, W. McK.: The Distribution of Raindrops With Size. J. Meteorol., vol. 5, no. 4, Aug. 1948, pp. 165-166.
19. Laws, J. Otis; and Parsons, Donald A.: The Relation of Raindrop-Size to Intensity. American Geophysical Union Transactions of 1943 - Part II, Twenty-Fourth Annual Meeting, Natl. Acad. Sci.-Natl. Res. Coun., Jan. 1944, pp. 452-460.
20. Mason, B. J.; and Andrews, J. B.: Drop-Size Distributions From Various Types of Rain. Q. J. R. Meteorol. Soc., vol. 86, no. 369, July 1960, pp. 346-353.
21. Waldvogel, A.: The N_0 Jump of Raindrop Spectra. J. Atmos. Sci, vol. 31, no. 4, May 1974, pp. 1067-1078.
22. Kelkar, V. N.: Size Distribution of Raindrops - Part I. Indian J. Meteorol. & Geophys., vol. 10, no. 2, Apr. 1959, pp. 125-136.
23. Kelkar, V. N.: Size Distribution of Raindrops - Part VI. Indian J. Meteorol. & Geophys., vol. 10, no. 2, Apr. 1968, pp. 143-148.
24. Knutson, Earl O.; and Fenton, Donald L.: Atmospheric Scavenging of Hydrochloric Acid. NASA CR-2598, 1975.
25. Fenton, Donald L.; and Purcell, Robert Y.: Atmospheric Scavenging of Solid Rocket Exhaust Effluents. NASA CR-2997, 1978.
26. Stewart, Roger B.; and Grose, William L.: Parametric Studies With an Atmospheric Diffusion Model That Assesses Toxic Fuel Hazards Due to the Ground Clouds Generated by Rocket Launches. NASA TN D-7852, 1975.
27. Stephens, J. Briscoe; and Stewart, Roger B.: Rocket Exhaust Effluent Modeling for Tropospheric Air Quality and Environmental Assessments. NASA TR R-473, 1977.
28. Dumbauld, R. K.; Bjorklund, J. R.; and Bowers, J. F.: NASA/MSFC Multilayer Diffusion Models and Computer Program for Operational Prediction of Toxic Fuel Hazards. NASA CR-129006, 1973.
29. Dumbauld, R. K.; Bjorklund, J. R.: NASA/MSFC Multilayer Diffusion Models and Computer Programs - Version 5. NASA CR-2631, 1975.

30. Stephens, J. Briscoe, and Hamilton, P. A.: Diffusion Algorithms and Data Reduction Routine for Onsite Launch Predictions for the Transport of Titan III C Exhaust Effluents. NASA TN D-7862, 1974.
31. Stephens, J. Briscoe, ed.: Atmospheric Diffusion Predictions for the Exhaust Effluents From the Launch of a Titan III C, Dec. 13, 1973. NASA TM X-64925, 1974.
32. Hwang, BoaChuan; and Gould, Robert K.: Rocket Exhaust Ground Cloud/Atmospheric Interactions. NASA CR-2978, 1978.
33. Susko, Michael; Hill, C. Kelly, and Kaufman, John W.: Downwind Hazard Calculations for Space Shuttle Launches at Kennedy Space Center and Vandenberg Air Force Base. NASA TM X-3162, 1974.
34. Stephens, J. Briscoe; Adelfang, S. I.; and Goldford, A. I.: Compendium of Meteorological Data for the Titan III C (AF-777) Launch in May 1975. NASA TM X-73338, 1976.
35. Stephens, J. B.; Adelfang, S. I.; and Goldford, A. I.: Compendium of Meteorological Data for the Viking A Launch in August 1975. NASA TM X-73339, 1976.
36. Stephens, J. B.; Adelfang, S. I.; and Goldford, A. I.: Compendium of Meteorological Data for the Viking B Launch in September 1975. NASA TM X-73340, 1976.
37. Solid Propellant Engineering Staff: Nozzle Exit Exhaust Products From Space Shuttle Boost Vehicle (November 1973 Design). Tech. Memo. 33-712 (Contract NAS7-100), Jet Propul. Lab., California Inst. Technol., Feb. 1, 1975.
38. Hsu, Hsiao-Ming: Numerical Simulations of Mesoscale Precipitation Systems. Ph. D. Diss., Univ. of Michigan, Feb. 1979.
39. Granett, A. L.; and Taylor O. C.: The Effect of Designated Pollutants on Plant Species. AMRL-TR-79-73, U.S. Air Force, Dec. 1979. (Available from DTIC as AD A078 933.)
40. Heck, Walter W.; Knott, William M.; Stahel, Edward P.; Ambrose, John T.; McCrimmon, James N.; Engle, Madeleine; Romanow, Louse A.; Sawyer, Alan G.; and Tyson, James D.: Response of Selected Plant and Insect Species to Simulated Solid Rocket Exhaust Mixtures and to Exhaust Components From Solid Rocket Fuels. NASA TM-74109, 1980.
41. Dingle, A. N.: Acid Rain: Microphysical Model. Proceedings of Shuttle Environmental Effects Program Review, Andrew E. Potter, ed., NASA CP-2110, 1980, pp. 65-82.
42. Pasquill, F.: Atmospheric Diffusion. D. Van Nostrand Co., Ltd., c.1962, pp. 165-178.

43. Pellett, G. L.; Sebacher, D. I.; Bendura, R. J.; and Wornom, D. E.: HCl in Rocket Exhaust Clouds: Atmospheric Dispersion, Acid Aerosol Characteristics, and Acid Rain Deposition. [Preprint] 80-49.6, Air. Pollut. Control Assoc., June 1980.
44. Brezonik, P. L.; Morgan, W. H.; Shannon, E. E.; and Putnam, H. D.: Eutrophication Factors in North Central Florida Lakes. Eng. Prog. at the Univ. of Florida, vol. XXIII, no. 8, Aug. 1969 (Bull. Ser. No. 134, Water Resources Res. Center Publ. No. 5, Florida Eng. & Ind. Exp. Sta.).
45. University of Central Florida: A Continuation of Base-Line Studies for Environmentally Monitoring Space Transportation Systems at John F. Kennedy Space Center. Volume II - Chemical Studies: Rainfall Soil Analysis. NASA CR-163122, 1980.
46. Likens, Gene E.; and Bormann, F. Herbert: Acid Rain: A Serious Regional Environmental Problem. Science, vol. 184, no. 4142, June 14, 1974, pp. 1176-1179.
47. Likens, Gene E.: Acid Precipitation. Chem. & Eng. News, vol. 54, no. 48, 1976, pp. 29-44.
48. Dochinger, L. S.; and Seliga, T. A., eds.: Proceedings of the 1st International Symposium on Acid Precipitation and the Forest Ecosystem. NEFES 77-1 FSGTR NE-23, Northeastern Forest Exp. Sta., Aug. 1976. (Available from NTIS as PB 25864511.)
49. Varshney, C. K.; and Dochinger, L. S.: Acid Rain: An Emerging Environmental Problem. Curr. Sci., vol. 48, no. 8, Apr. 20, 1979, pp. 337-340.
50. Likens, Gene E.; Wright, Richard F.; Galloway, James N.; and Butler, Thomas J.: Acid Rain. Sci. American, vol. 241, no. 4, Oct. 1979, pp. 43-51.
51. Brezonik, Patrick L.; Edgerton, Eric S.; and Hendry, Charles D.: Acid Precipitation and Sulfate Deposition in Florida. Science, vol. 208, no. 4447, May 30, 1980, pp. 1027-1029.
52. Cofer, W. R., III; and Pellett, G. L.: Adsorption and Chemical Reaction of Gaseous Mixtures of Hydrogen Chloride and Water on Aluminum Oxide and Application to Solid-Propellant Rocket Exhaust Clouds. NASA TP-1105, 1978.
53. Dawbarn, R.; and Kinslow, M.: Studies of the Exhaust Products From Solid Propellant Rocket Motors. AEDC-TR-76-49, U.S. Air Force, Sept. 1976. (Available from DTIC as AD A029 569.) (Also available as NASA CR-149674.)
54. Dawbarn, R.; Kinslow, M.; and Watson, D. J.: Analysis of the Measured Effects of the Principal Exhaust Effluents From Solid Rocket Motors. NASA CR-3136, 1980.

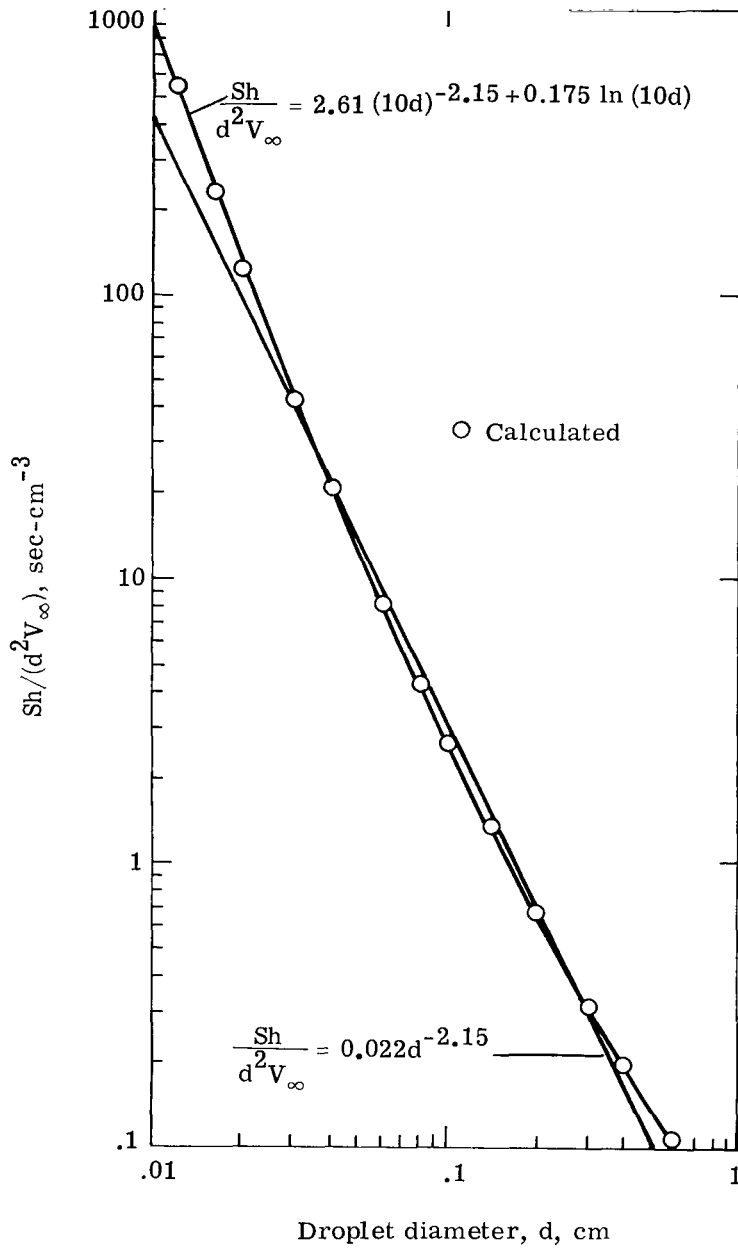


Figure 1.- Empirical fits of $Sh/d^2 V_\infty$ parameter for convective diffusion of HCl(g) to raindrops (modified Frössling) falling at terminal velocity in air at 15°C and 0.85 atm.

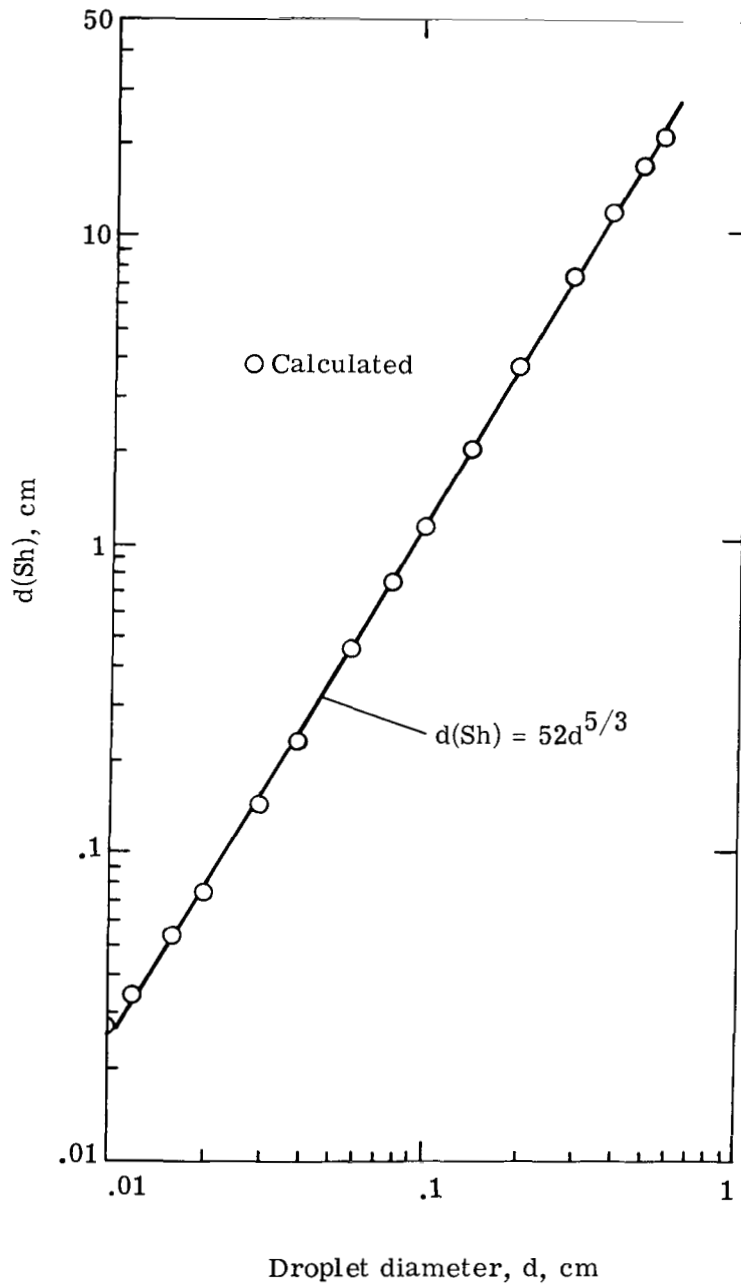


Figure 2.- Empirical fit of $d(\text{Sh})$ parameter for convective diffusion of $\text{HCl}(\text{g})$ to raindrops (modified Frössling) falling at terminal velocity in air at 15°C and 0.85 atm.

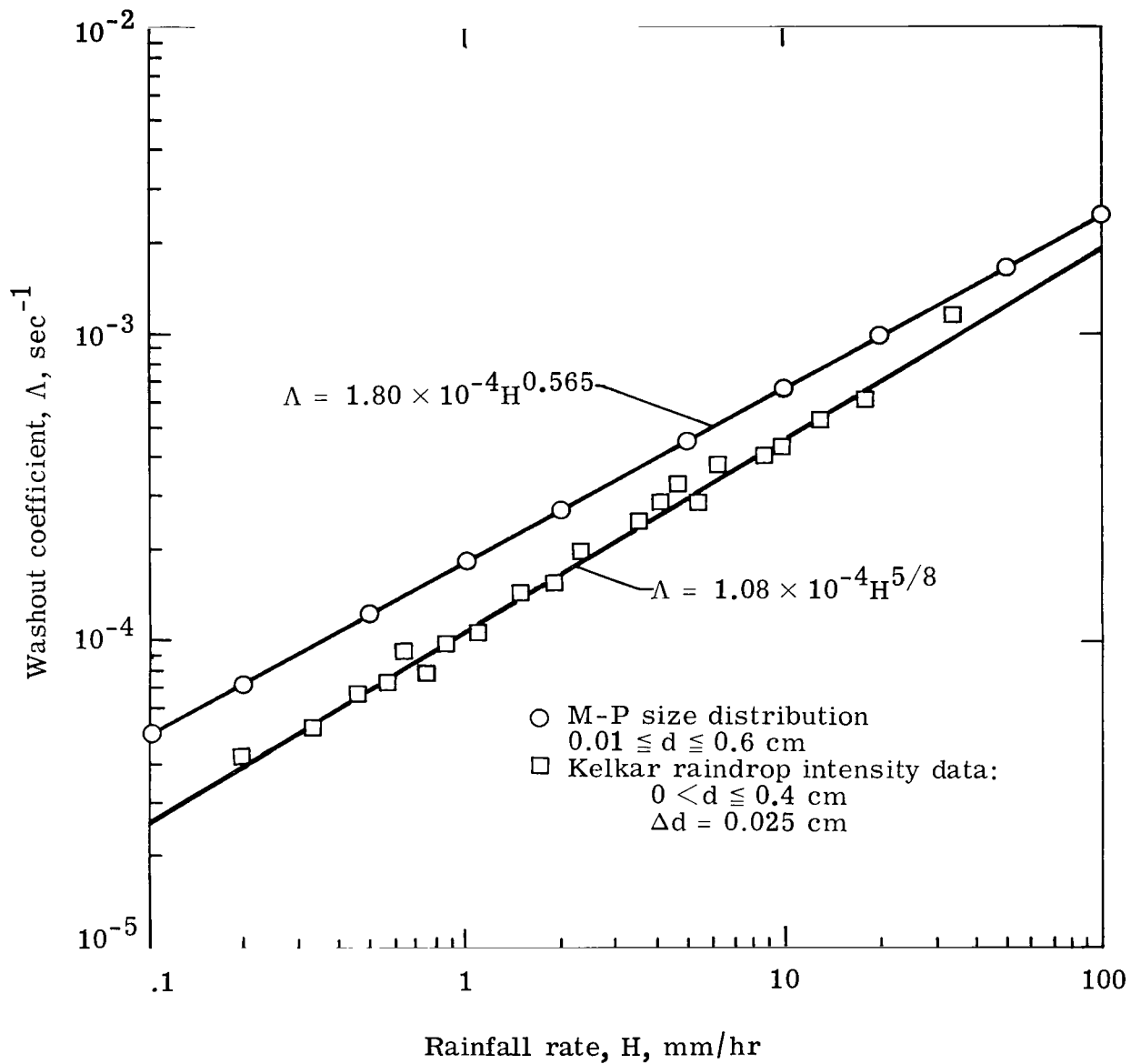


Figure 3.- Empirical fits of $\text{HCl}(g)$ washout coefficients based on modified Frössling equation and applied to Marshall-Palmer (M-P) raindrop size distribution function and Kelkar's raindrop intensity data. Expressions apply at 15°C and 0.85 atm.

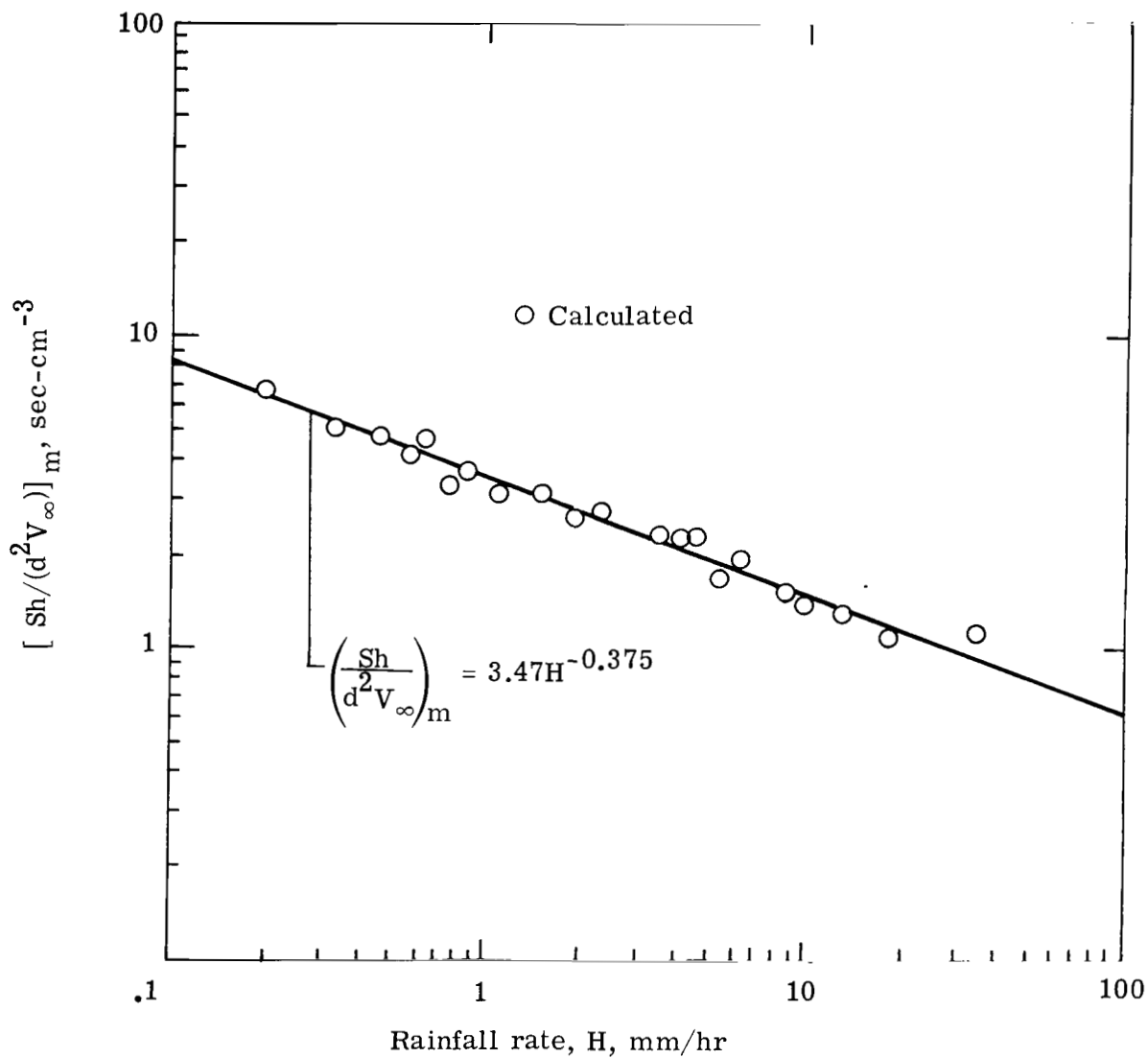


Figure 4.- Empirical fit of weighted mean Sh/d^2v_∞ parameter for convective diffusion of $\text{HCl}(g)$ to polydisperse raindrops (modified Frössling) falling with intensities measured by Kelkar for average rains. Expression applies at 15°C and 0.85 atm .

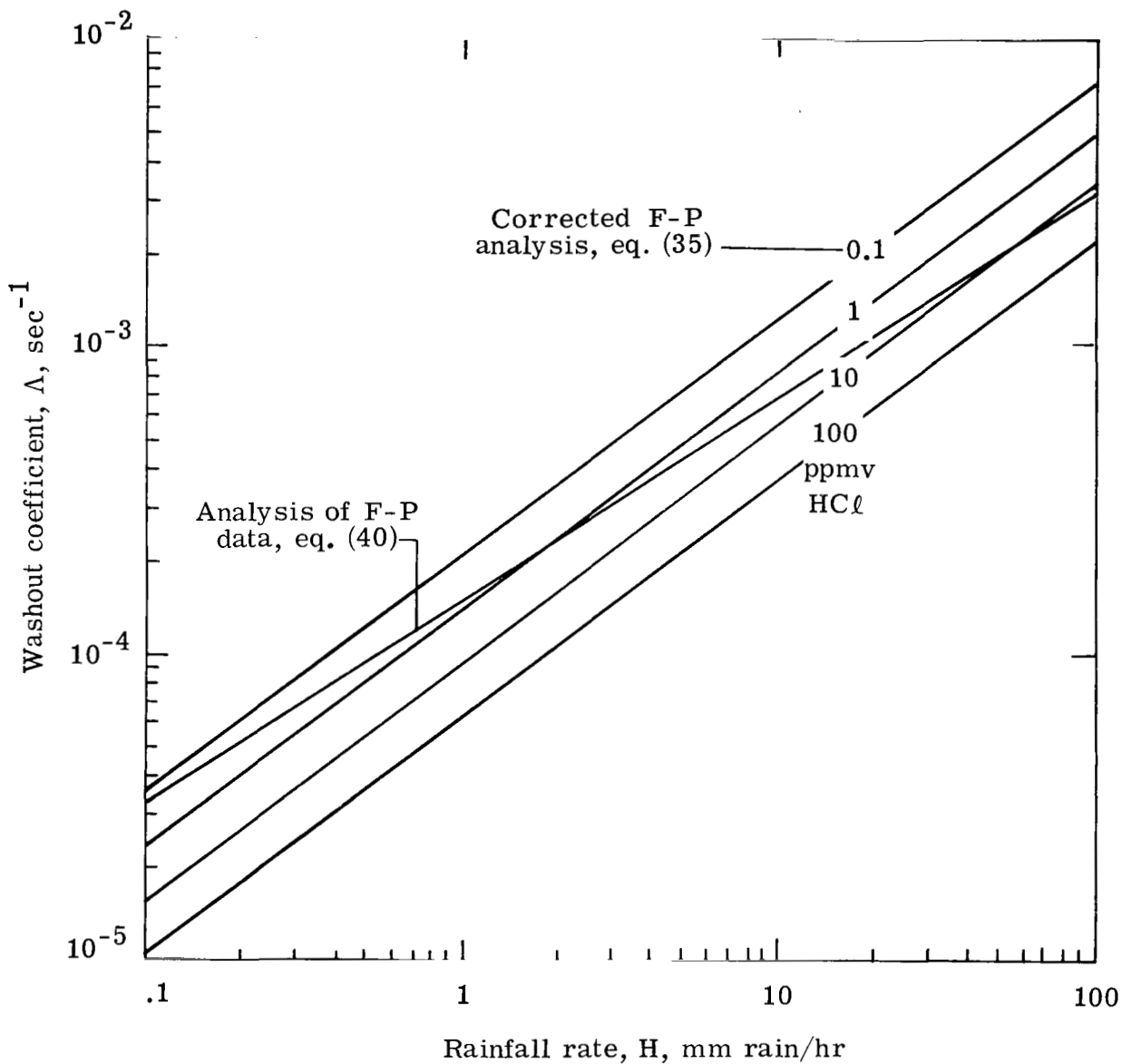


Figure 5.- Empirically deduced relationships for HCl(g + aq) washout based on Fenton and Purcell's (F-P) data (ref. 25) on scavenging of diluted SRM exhaust in laboratory chamber by uniform-size raindrops. They include power-corrected F-P expression (eq. (35)) and present independently deduced expression (eq. (40)).

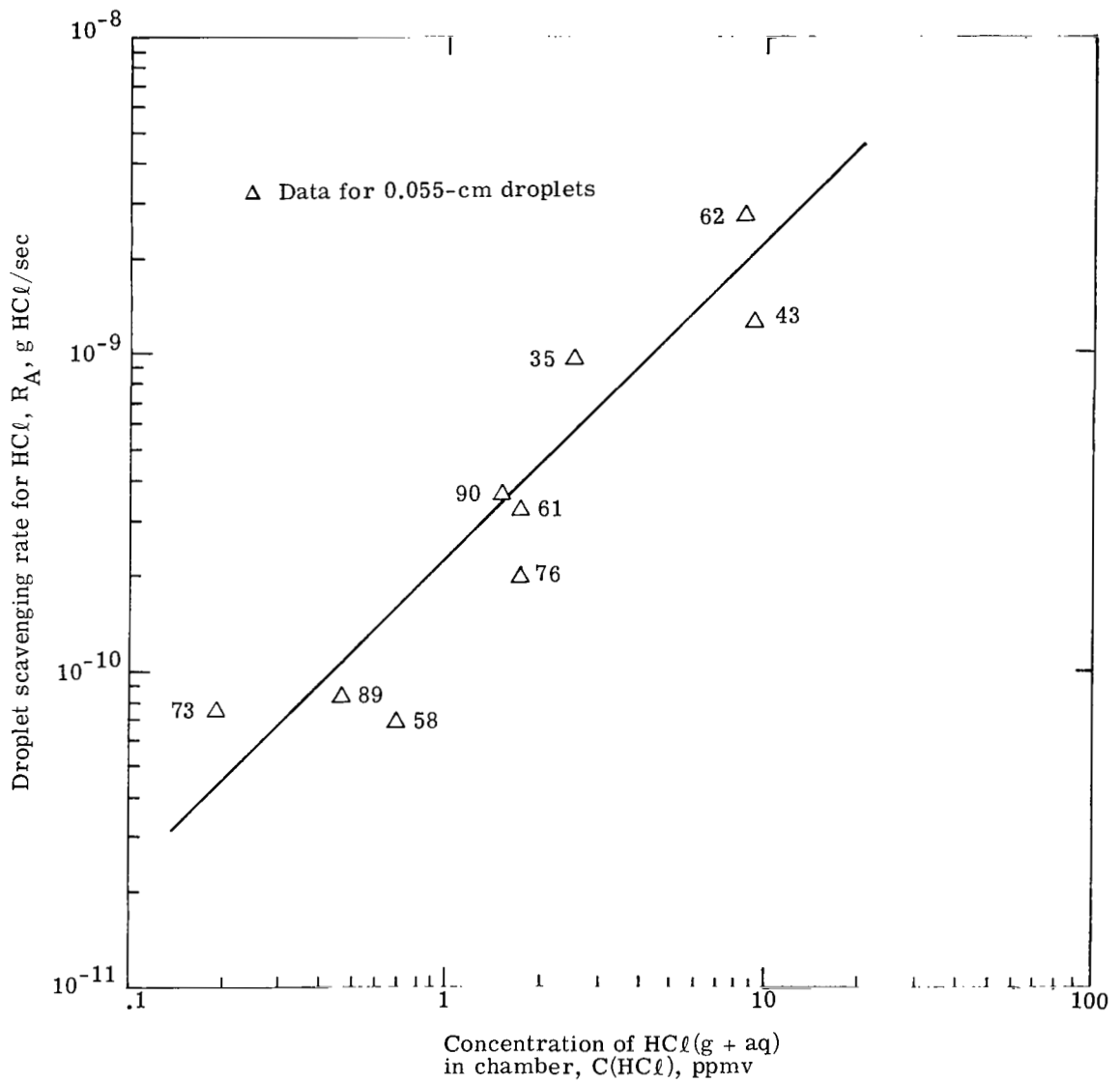


Figure 6.- Analysis of Fenton and Purcell's data (ref. 25) on laboratory scavenging of diluted SRM exhaust by 0.055-cm-diameter water droplets falling at terminal velocity. Solid line represents mean value of $R_A/C(HCl)$. Numbers represent relative humidity.

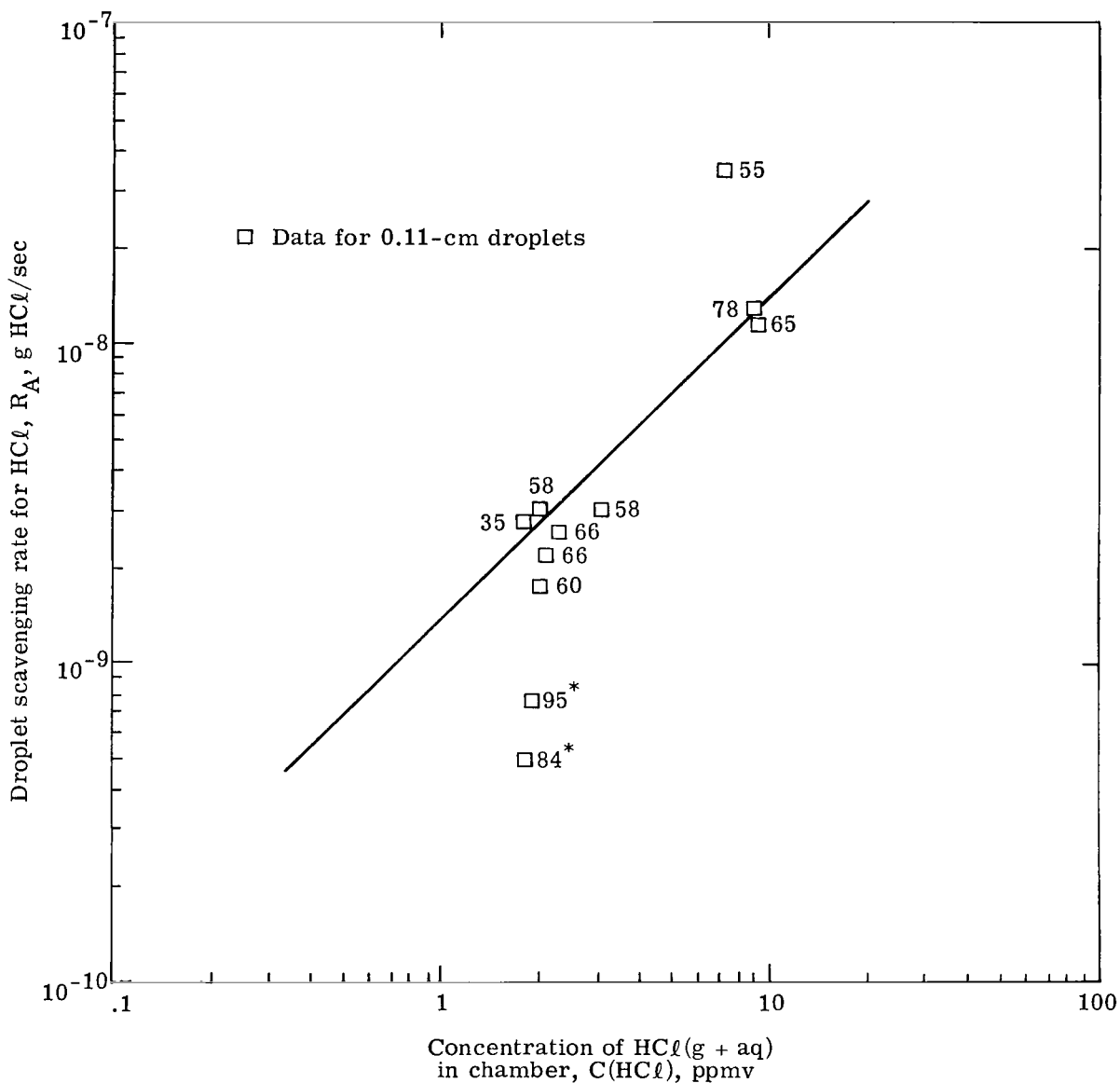


Figure 7.- Analysis of Fenton and Purcell's data (ref. 25) on laboratory scavenging of diluted SRM exhaust by 0.11-cm-diameter water droplets falling at terminal velocity. Solid line represents mean value of $R_A/C(HCl)$. Numbers represent relative humidity. Data points with asterisks had relatively large chloride corrections and are considered less reliable.

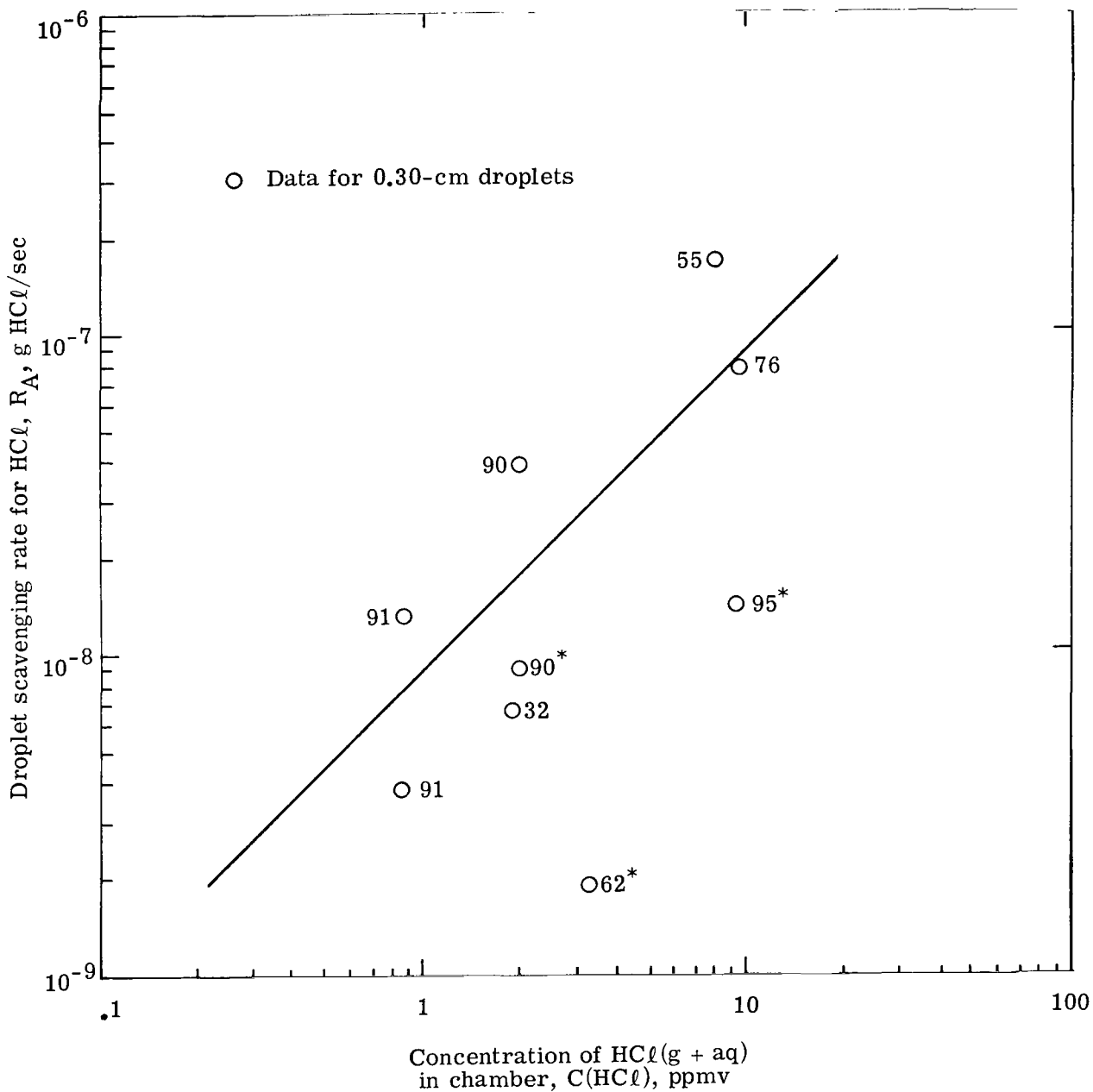


Figure 8.- Analysis of Fenton and Purcell's data (ref. 25) on laboratory scavenging of diluted SRM exhaust by 0.30-cm-diameter water droplets falling at accelerating subterminal velocity. Solid line represents mean value of $R_A/C(HCl)$. Numbers represent relative humidity. Data points with asterisks had relatively large chloride corrections and are considered less reliable.

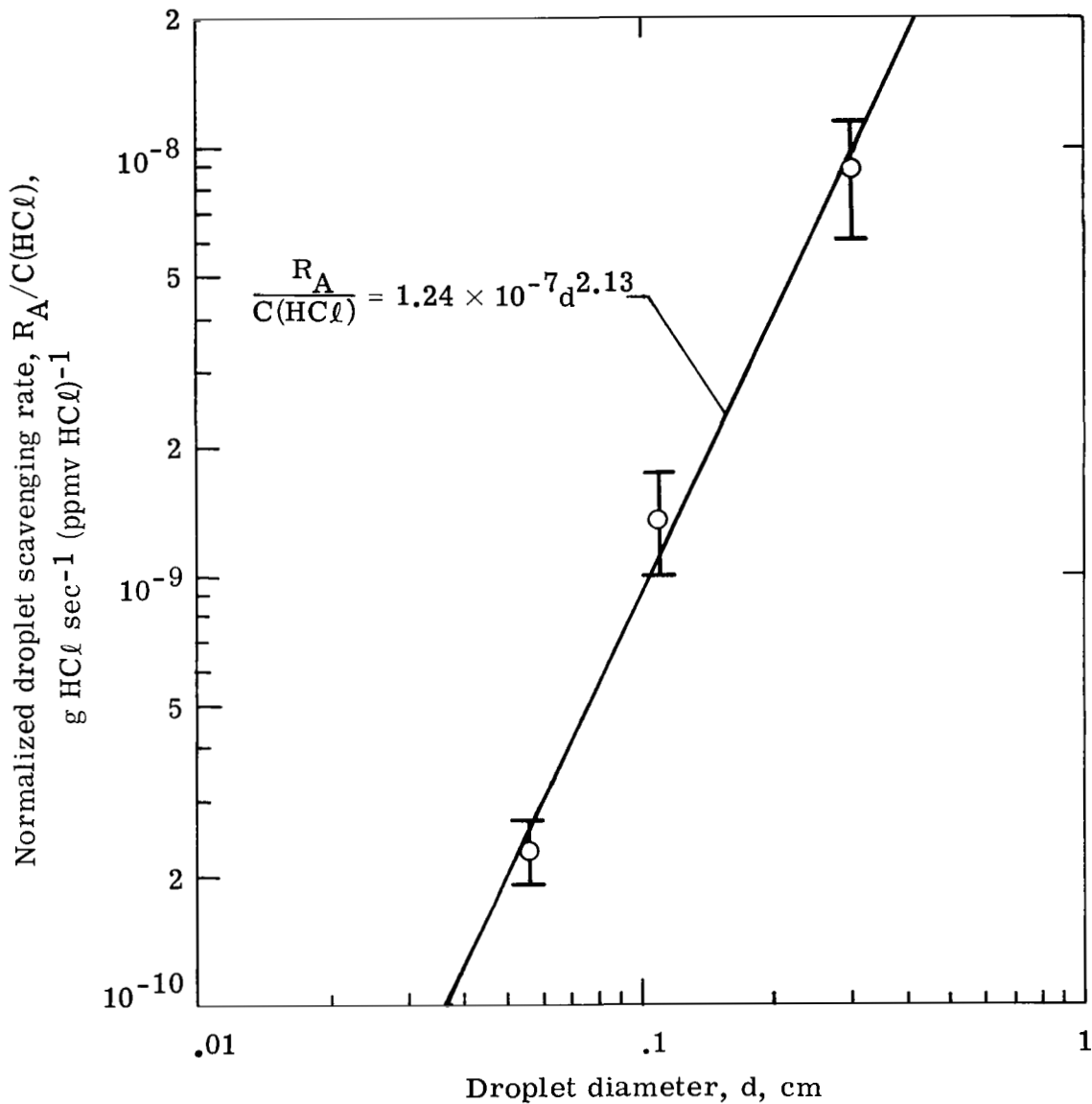


Figure 9.- Effect of droplet diameter on concentration-normalized HCl^l (g + aq) scavenging rate on a per-droplet basis. Least-squares fit of $\log [R_A/C(\text{HCl})]$ versus $\log d$ is shown for mean values of $R_A/C(\text{HCl})$ illustrated in figures 6 to 8. Vertical bars correspond to standard errors of mean values.

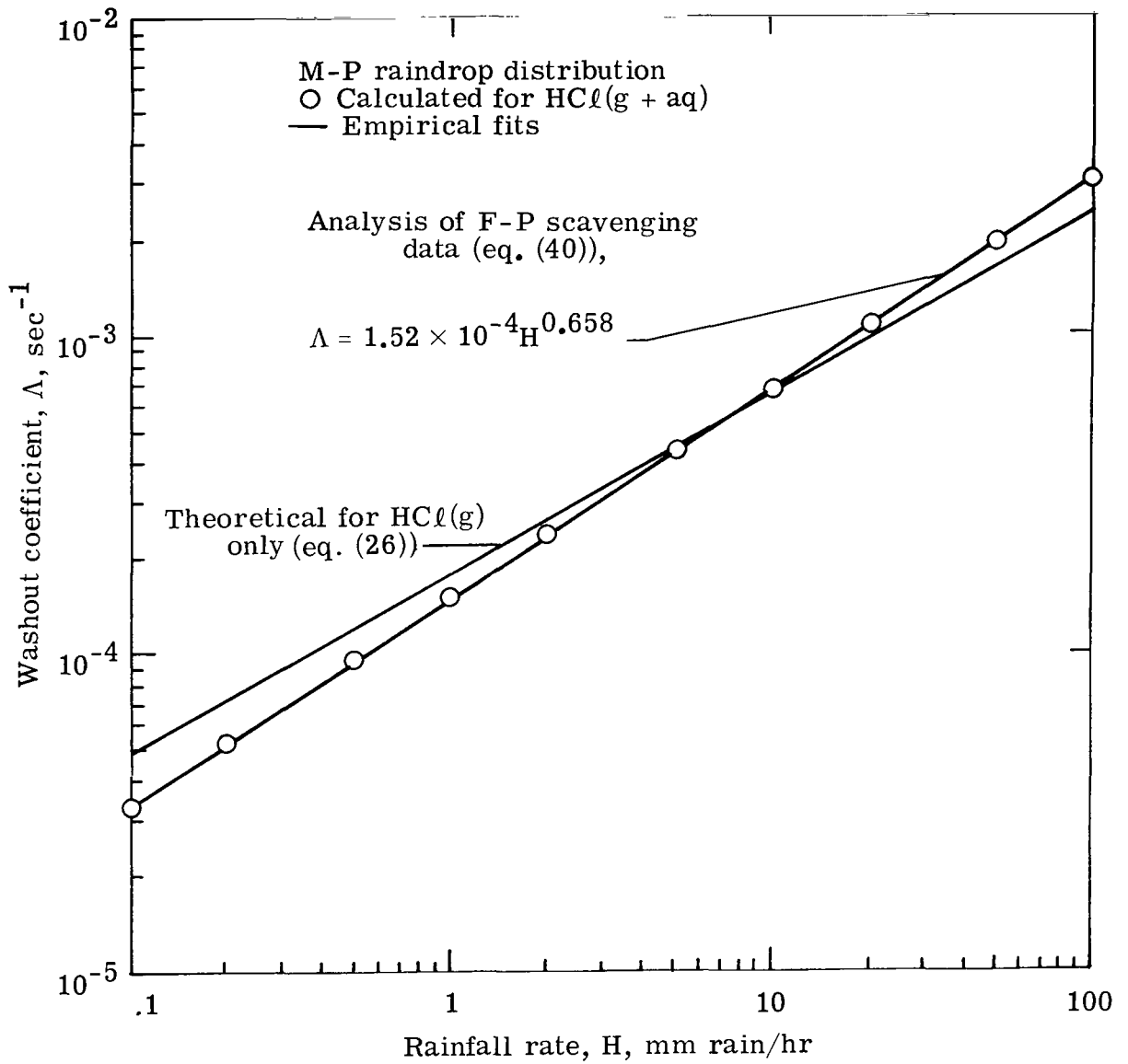
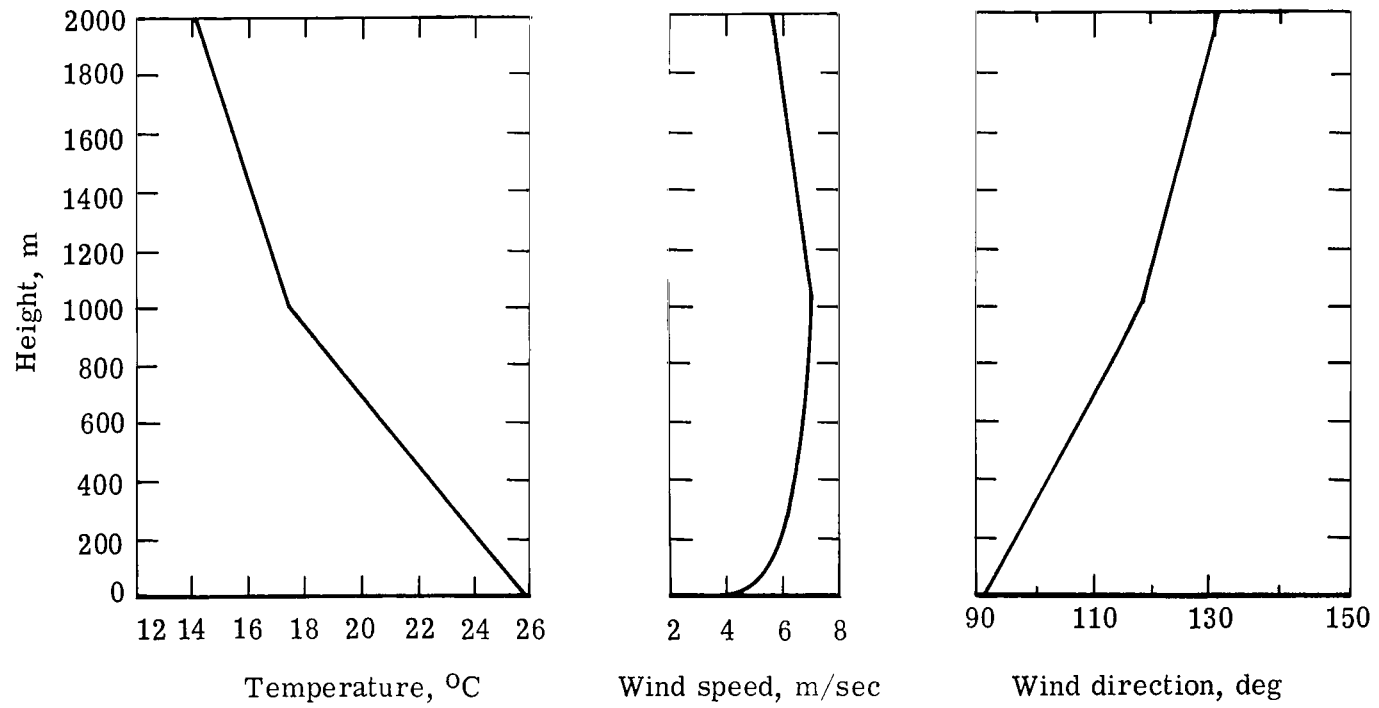
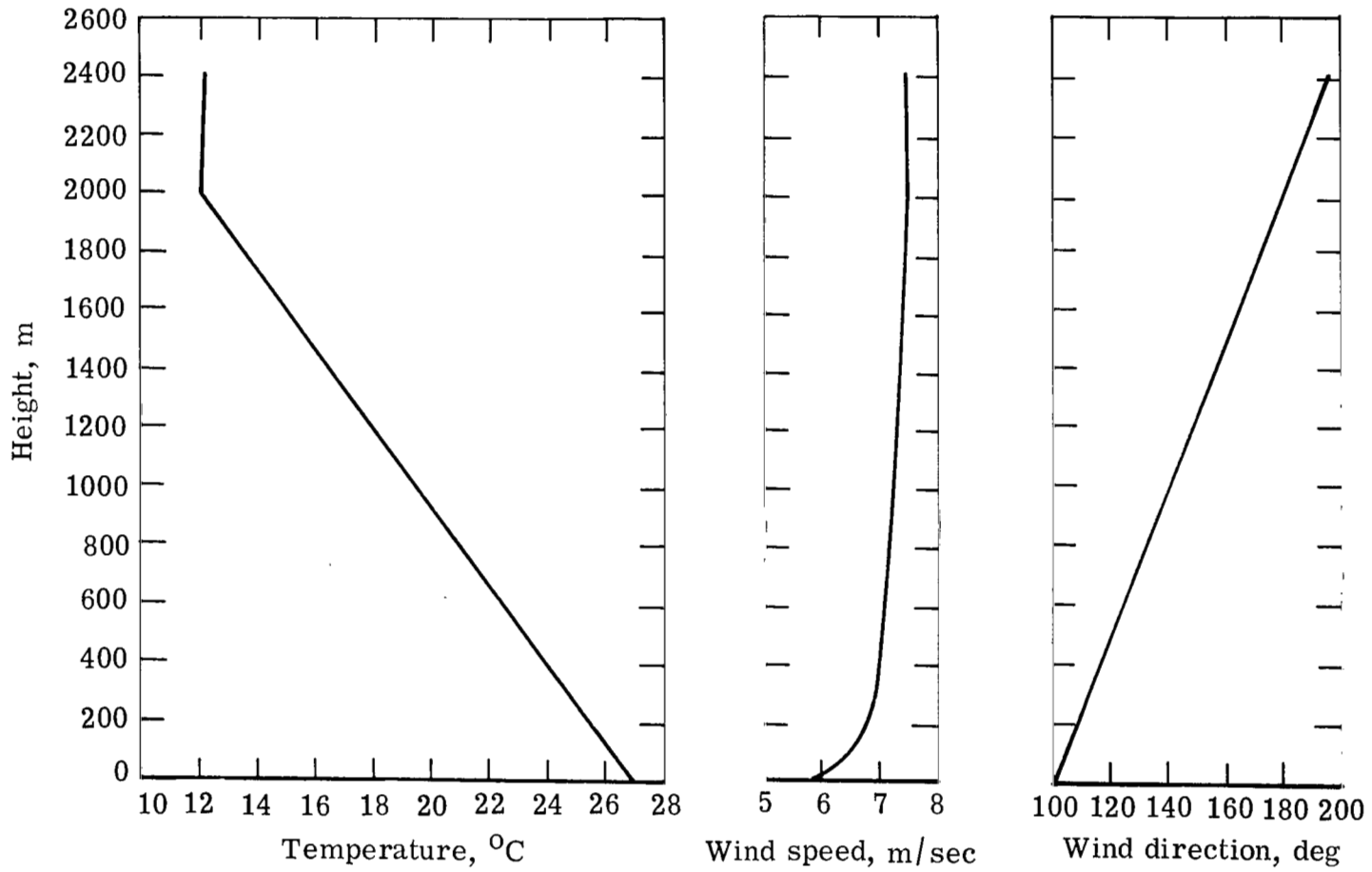


Figure 10.- Empirical fit of HCl(g + aq) washout coefficients (circles), based on present analysis of Fenton and Purcell's SRM exhaust rain scavenging data (ref. 25) and Marshall-Palmer (M-P) raindrop size distribution. Equation (26) for HCl(g) washout, based on modified Frössling equation and M-P distribution, is shown for comparison.



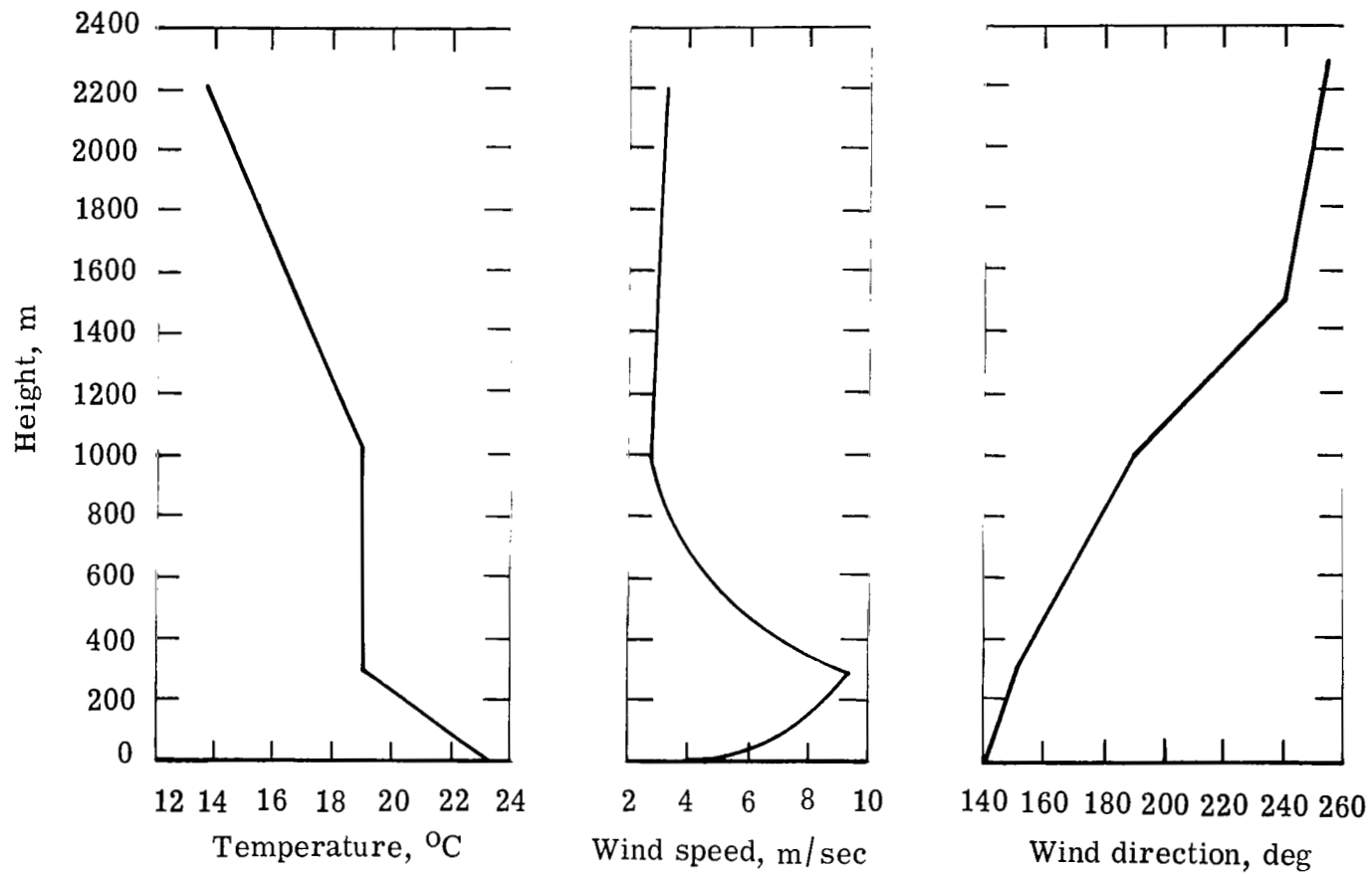
(a) For fall fair weather (FFW) meteorological regime (from ref. 33).

Figure 11.- Vertical profiles of temperature, wind speed, and wind direction at Cape Canaveral, Florida.



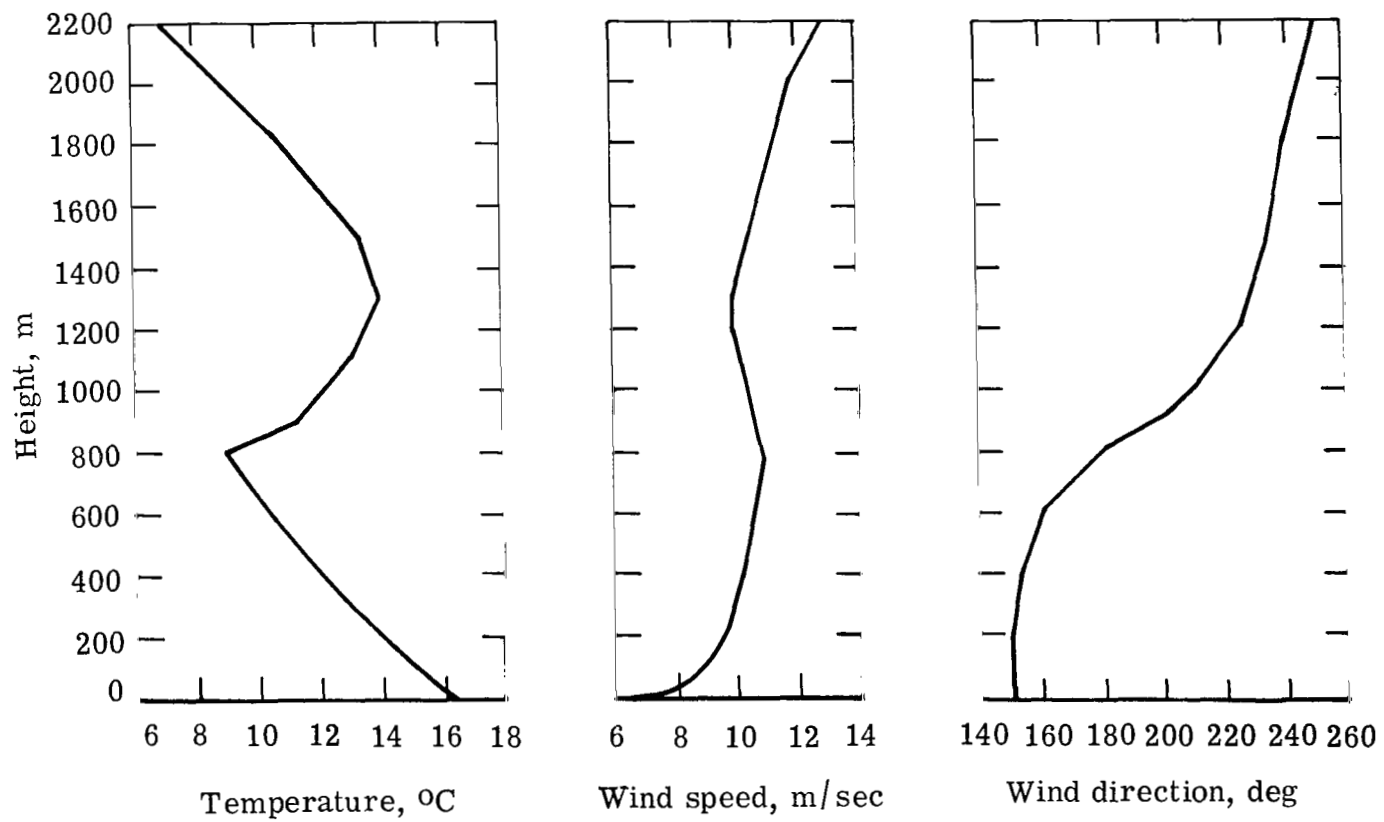
(b) For spring fair weather (SFW) meteorological regime (from ref. 33).

Figure 11.- Continued.



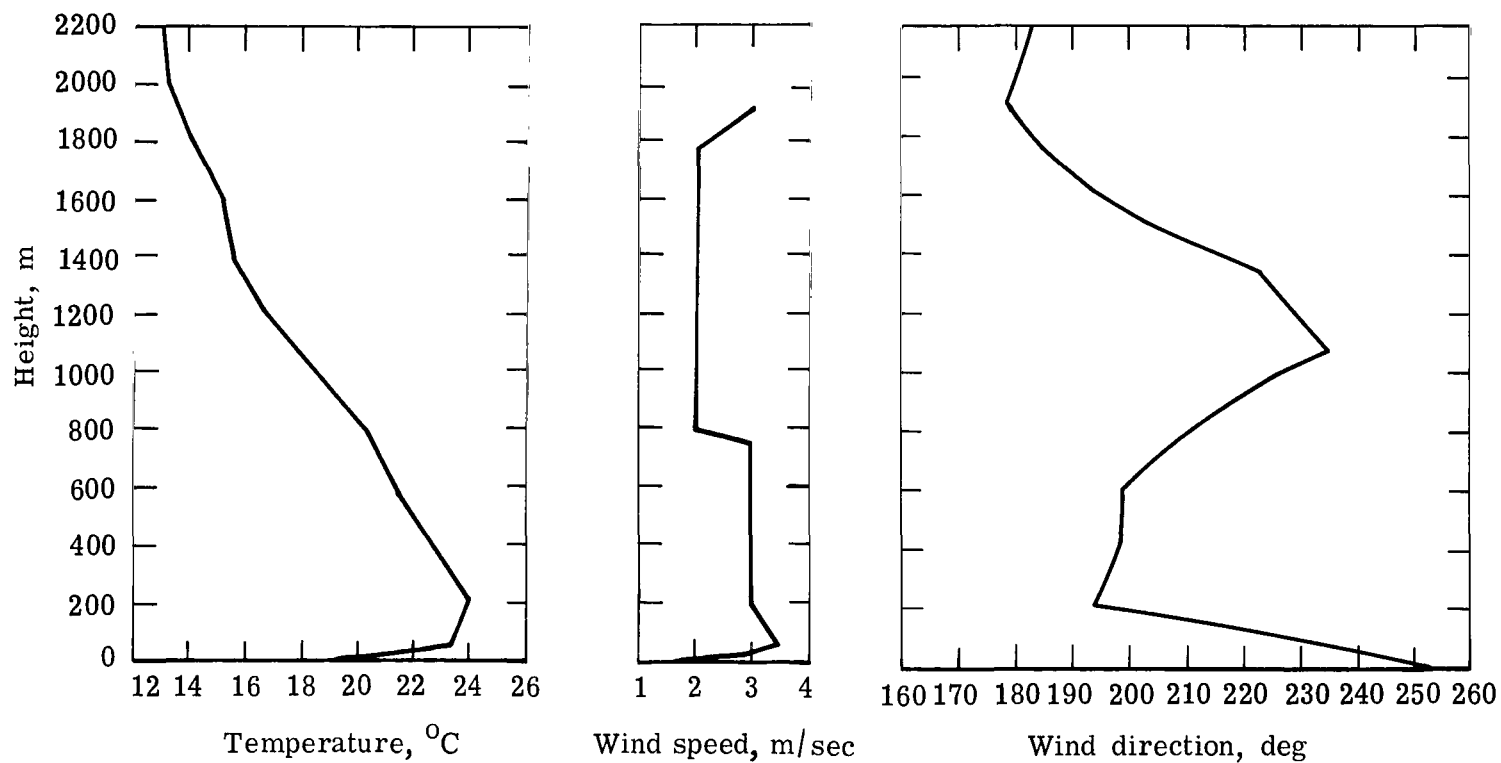
(c) For low-level sea breeze (LLSB) meteorological regime (from ref. 33).

Figure 11.- Continued.



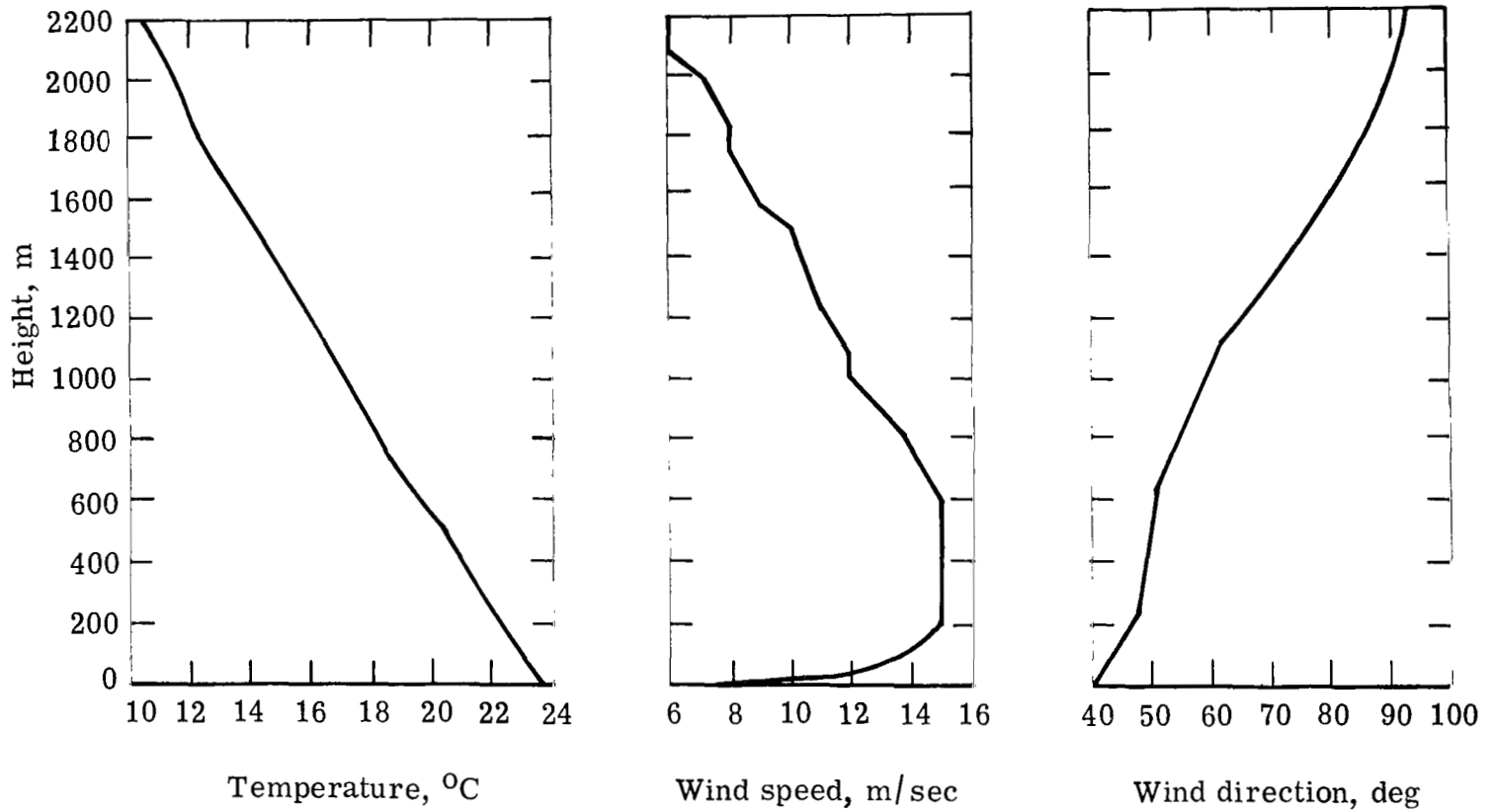
(d) For sea breeze (SB) meteorological regime (from ref. 28).

Figure 11.- Continued.



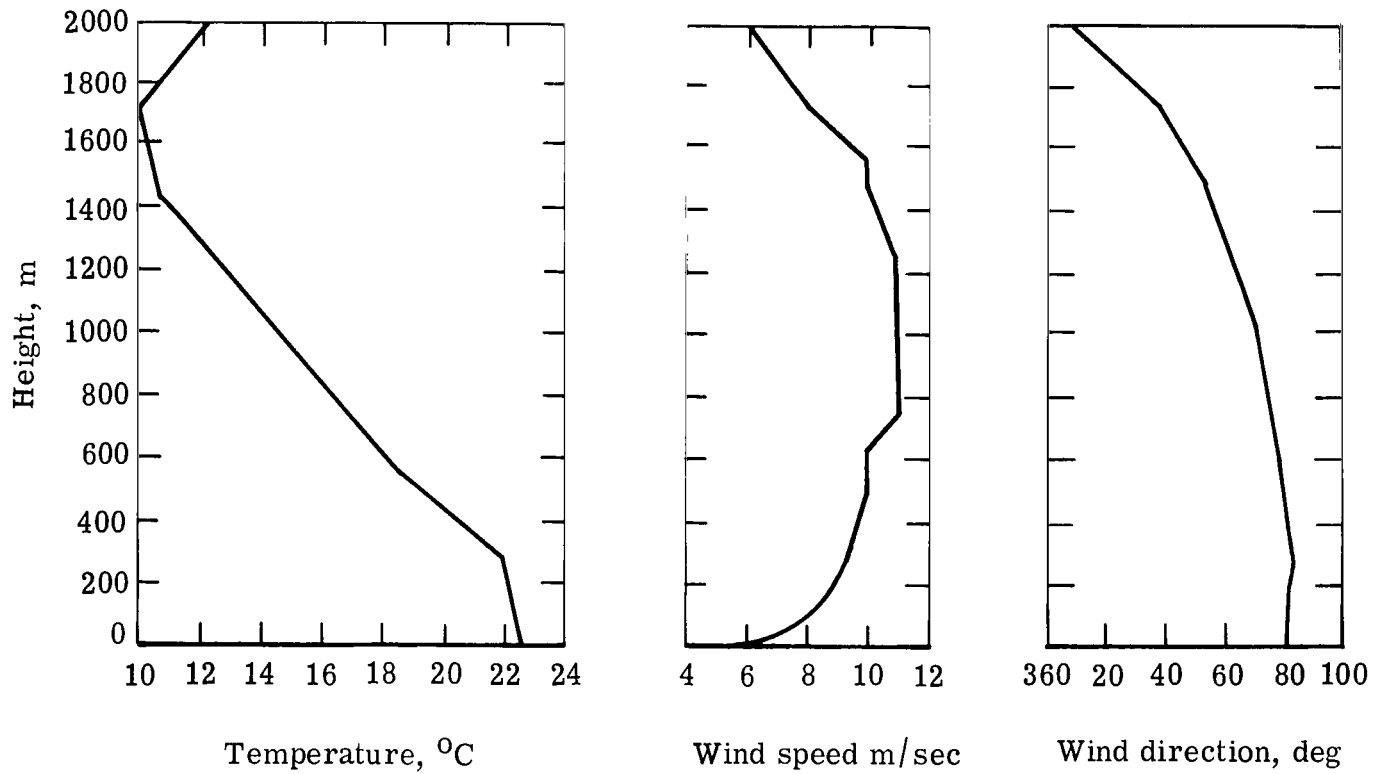
(e) For fair weather, pre-cold front (FW, Pre-CF) meteorological regime
(from ref. 33).

Figure 11.- Continued.



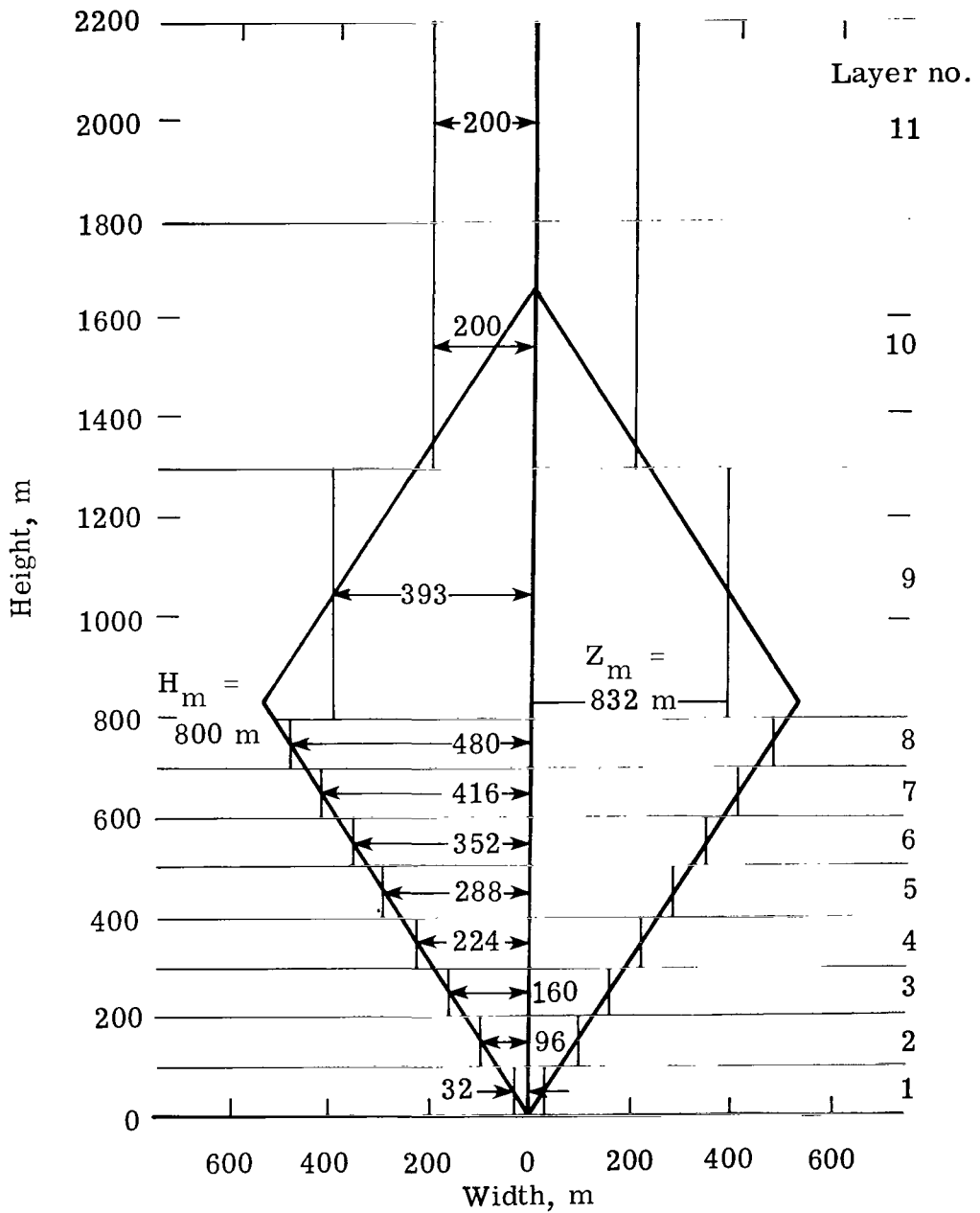
(f) For cold front passage (CFP) meteorological regime (from ref. 33).

Figure 11.- Continued.



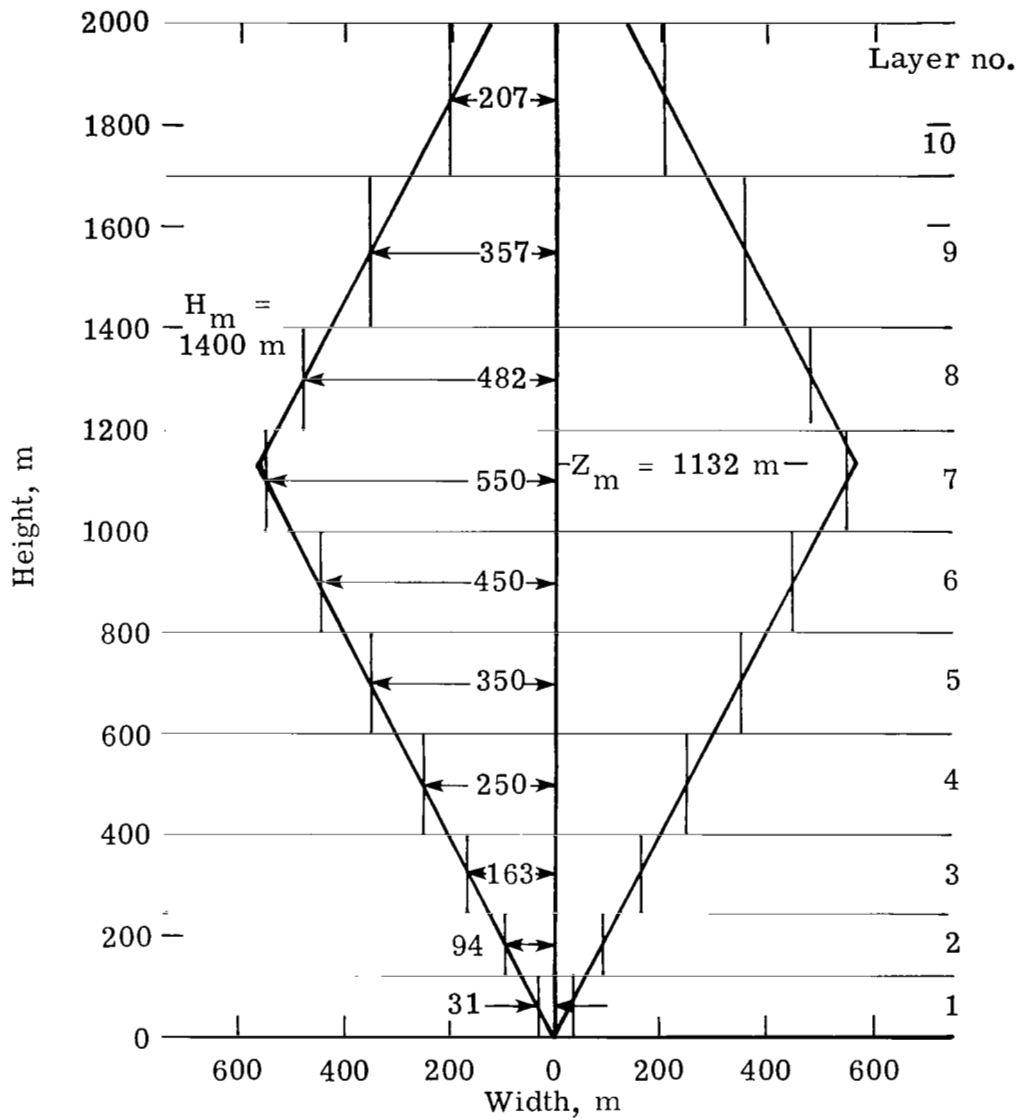
(g) Shortly after passage of cold front (Post-CFP) (from ref. 33).

Figure 11.- Concluded.



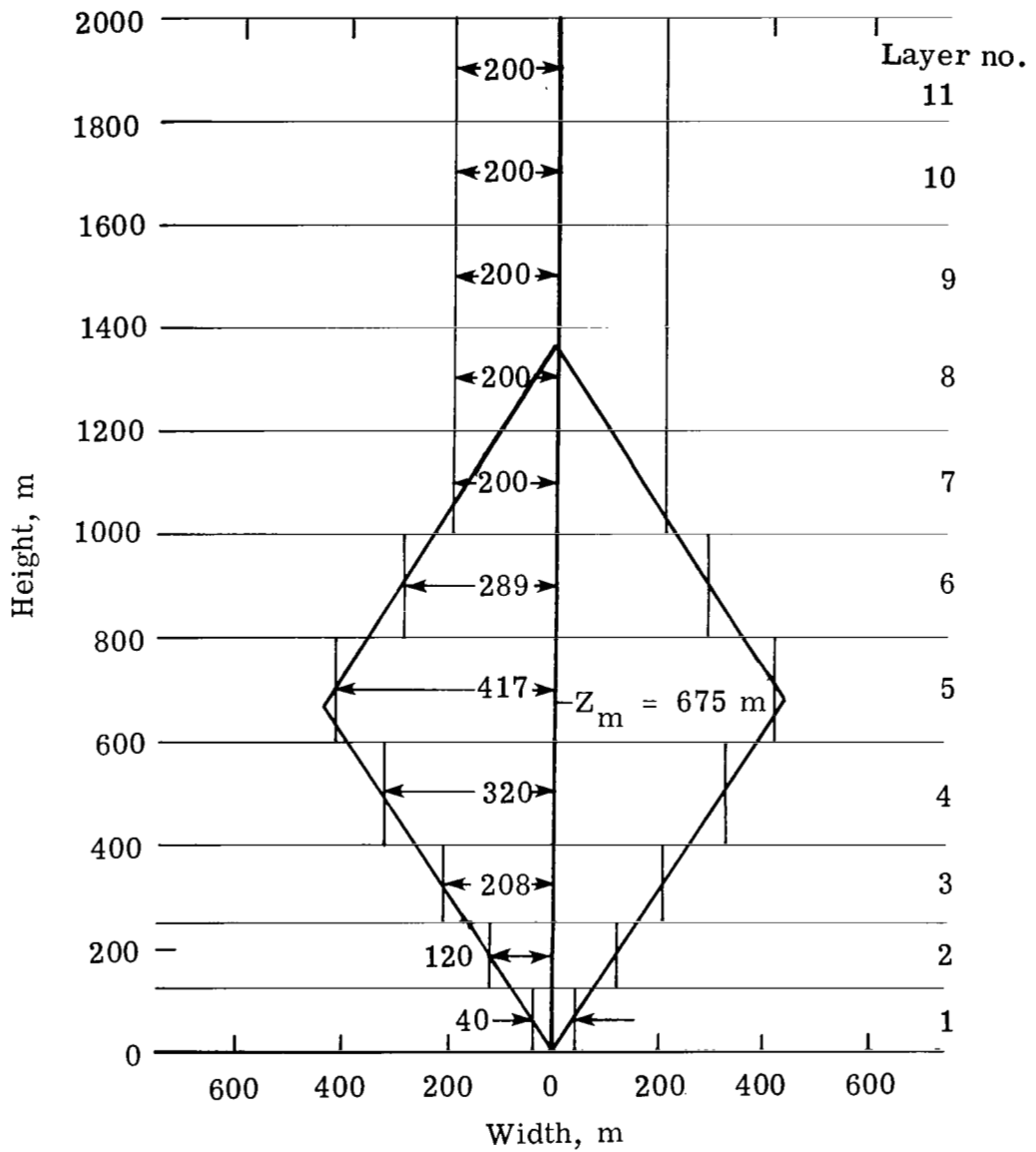
(a) For sea breeze (SB) meteorological regime. Height of cloud centroid is 832 m, and surface mixing-layer depth is 800 m (from ref. 28).

Figure 12.- Dimensions of stabilized ground cloud of Titan III exhaust products ($Q_I = 691$ cal/g) at Cape Canaveral, Florida.



(b) For post-cold front meteorological regime during normal launch (Post-CF) and during on-pad abort (Post-CF, pad abort) (from ref. 28).

Figure 12.- Continued.



(c) For cold front passage (CFP) meteorological regime (from ref. 28).

Figure 12.- Concluded.

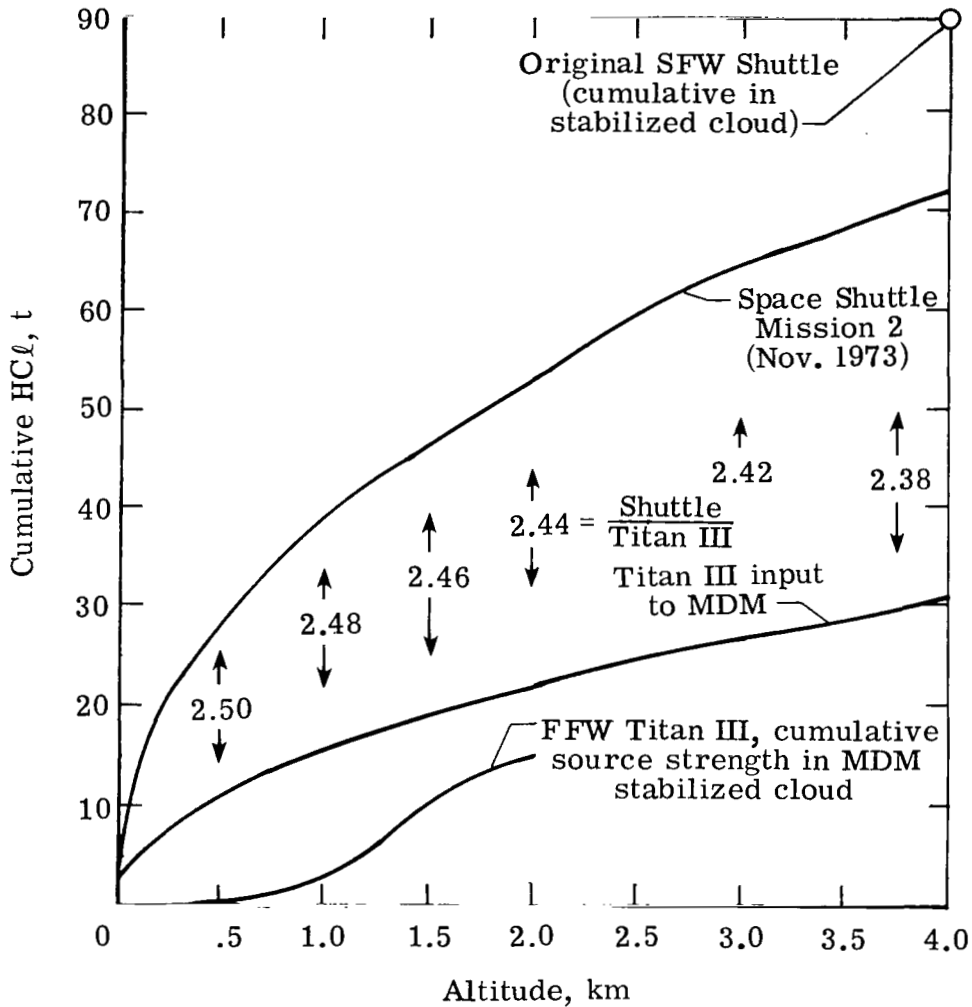


Figure 13.- Some HCl source-strength characteristics for Space Shuttle and Titan III SRM launches. Note that cumulative source strength in MDM-4(II) stabilized cloud is less than cumulative line source input.

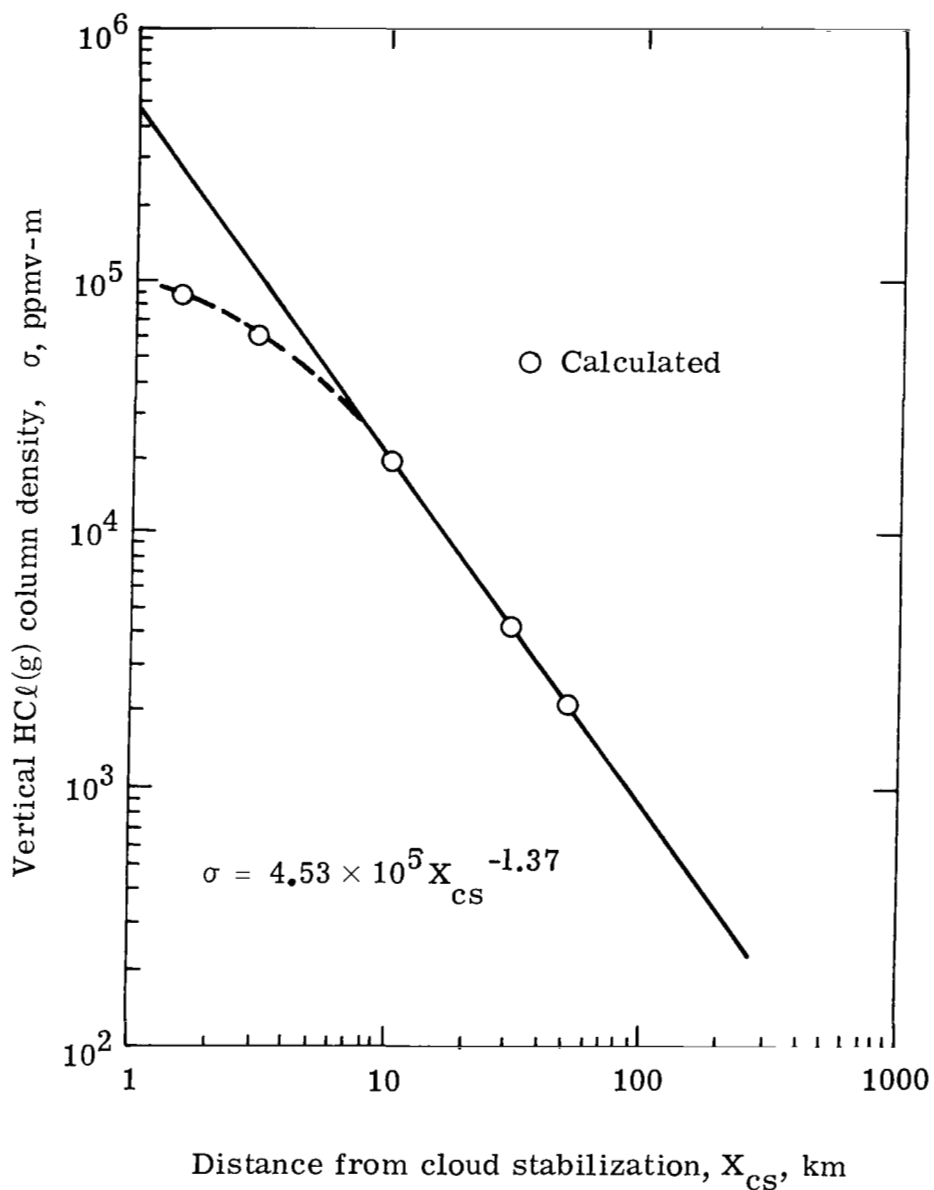


Figure 14.- Functional relationship used in reference 3 to characterize downwind dispersive decay of σ for Space Shuttle SRM exhaust cloud under SFW meteorological conditions. HCl source strength was $m_0 = 89 \times 10^6$ g HCl.

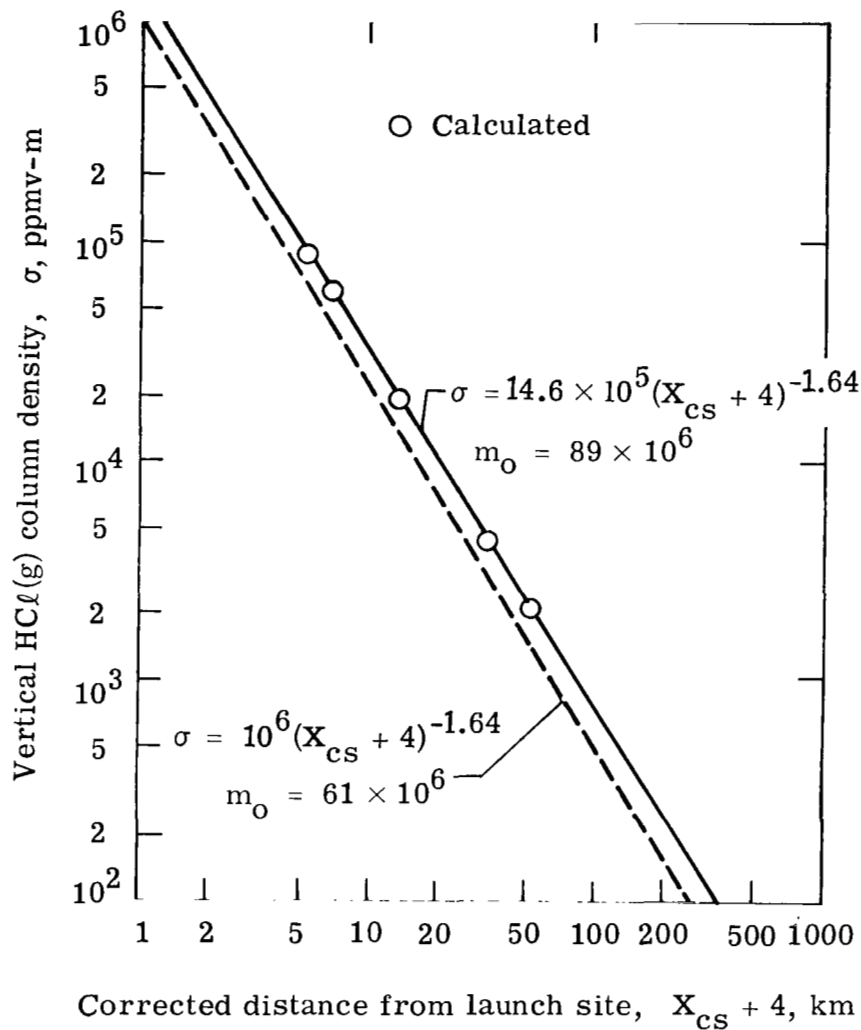


Figure 15.- Virtual-source-distance corrected empirical functions which characterize modified downwind dispersive decay of σ for Space Shuttle SRM exhaust cloud under SFW meteorological conditions. Functions for both original (89×10^6 g HCl) and presently modified (61×10^6 g HCl) stabilized-cloud source strengths are shown.

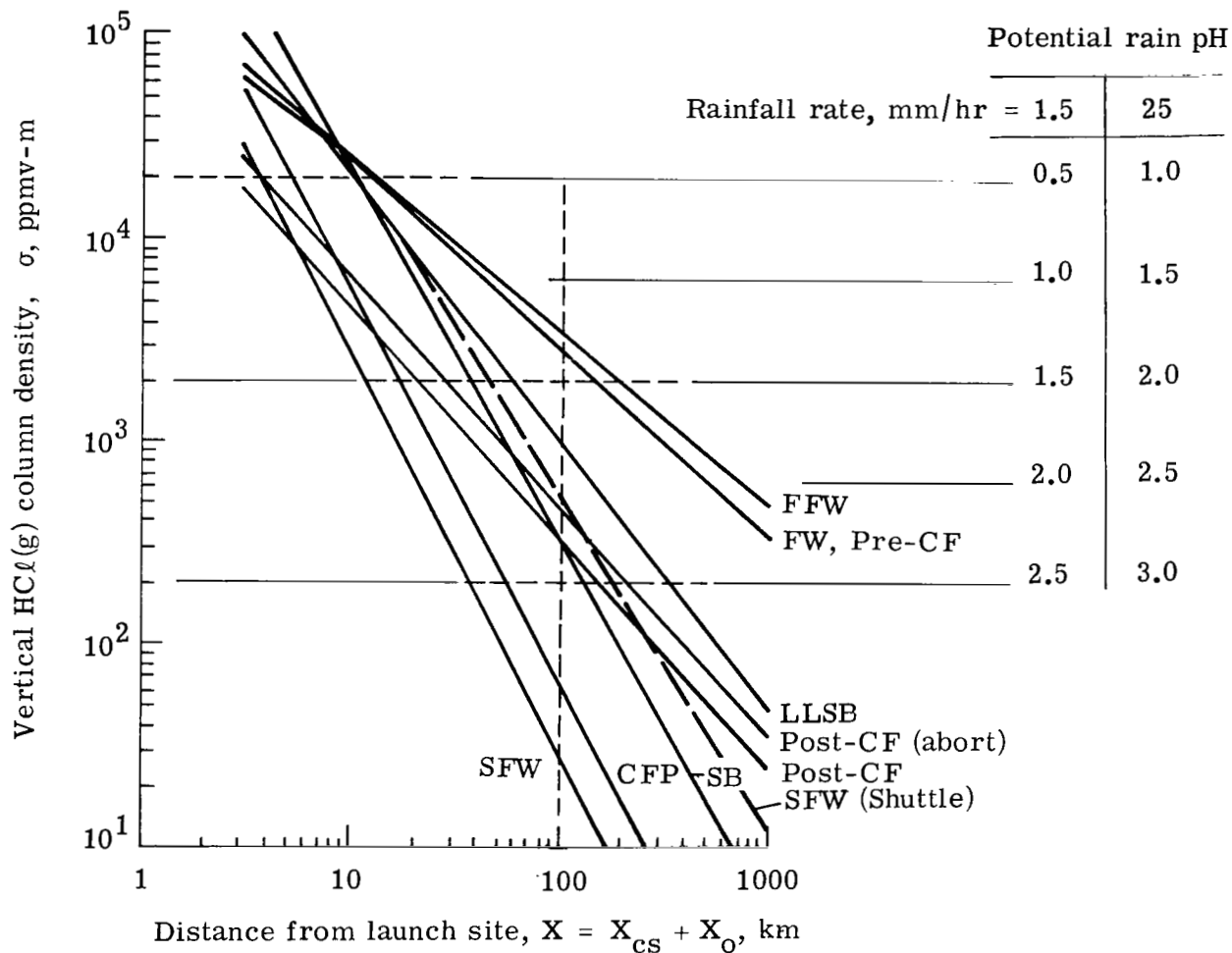


Figure 16.- Dispersive decay of σ and potential rain pH as function of downwind distance, for eight Titan III cases (solid lines) and one Space Shuttle case (dashed line) of exhaust cloud dispersion. Results are based on application of MDM-4(II) to seven standard meteorological regimes, equation (52) for pH_{pot} and equation (42) for Λ (geometric mean).

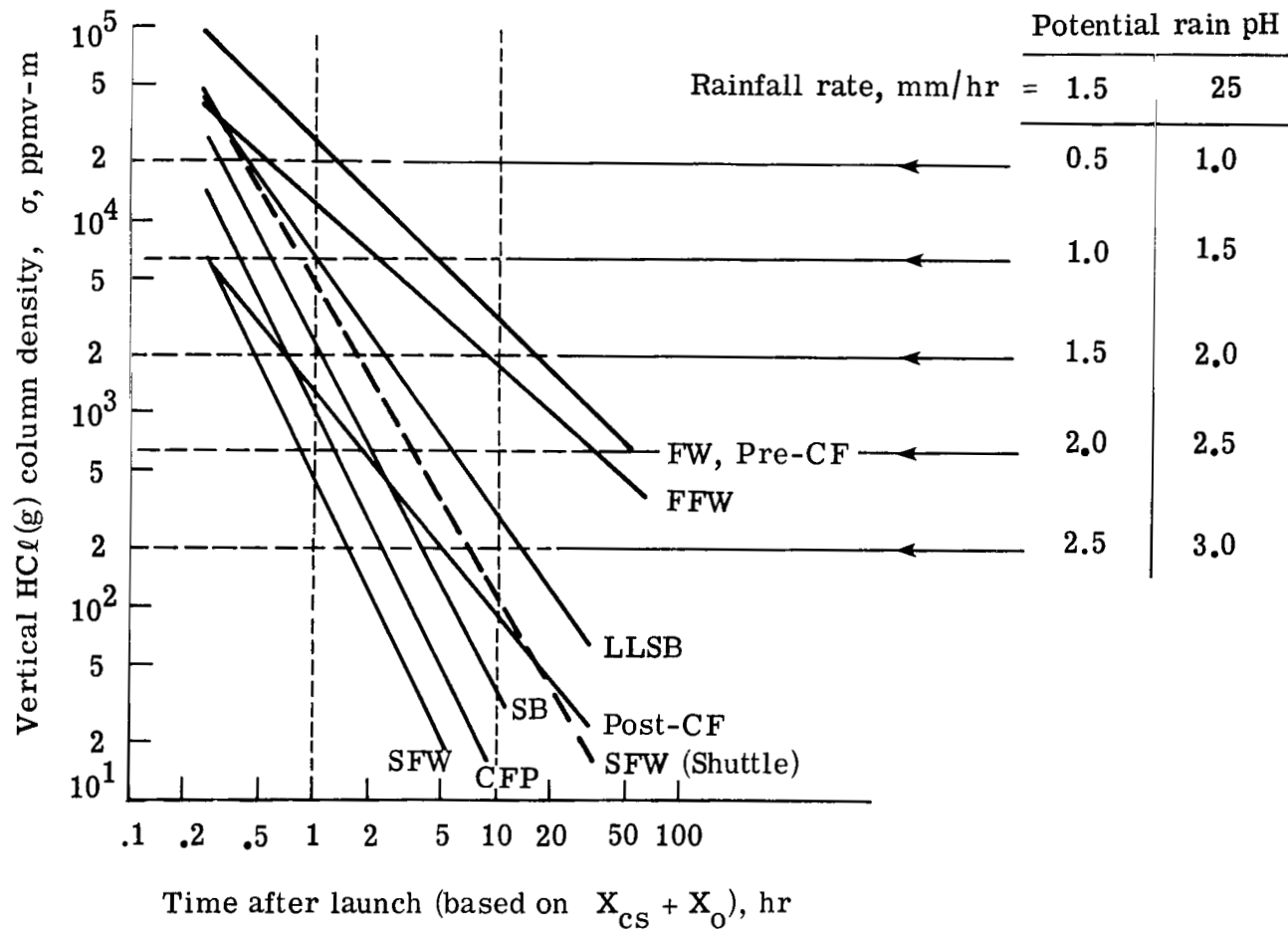


Figure 17.- Dispersive decay of σ and potential rain pH as function of downwind drift time, for seven Titan III cases (solid lines) and one Space Shuttle case (dashed line) of exhaust cloud dispersion. Results are based on application of MDM-4(II) to seven standard meteorological regimes, equation (52) for pH_{pot} and equation (42) for Λ (geometric mean).

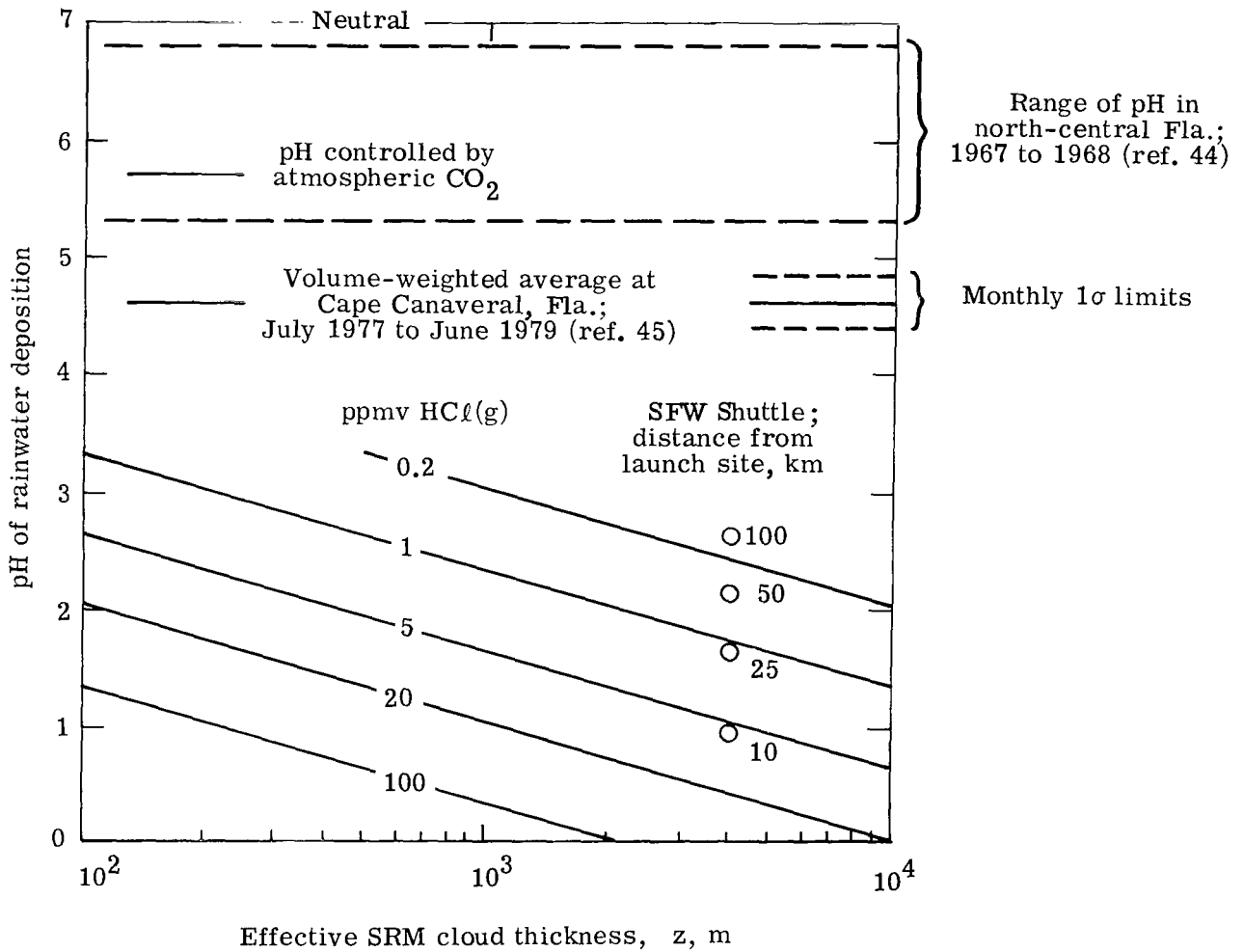


Figure 18.- Characteristic rain acidity for Florida area and relationships among potential pH, effective SRM cloud thickness, and vertically averaged HCl(g) concentration. The latter case was calculated for rainfall rate of 25 mm/hr using equation (46) with $t = 0$.

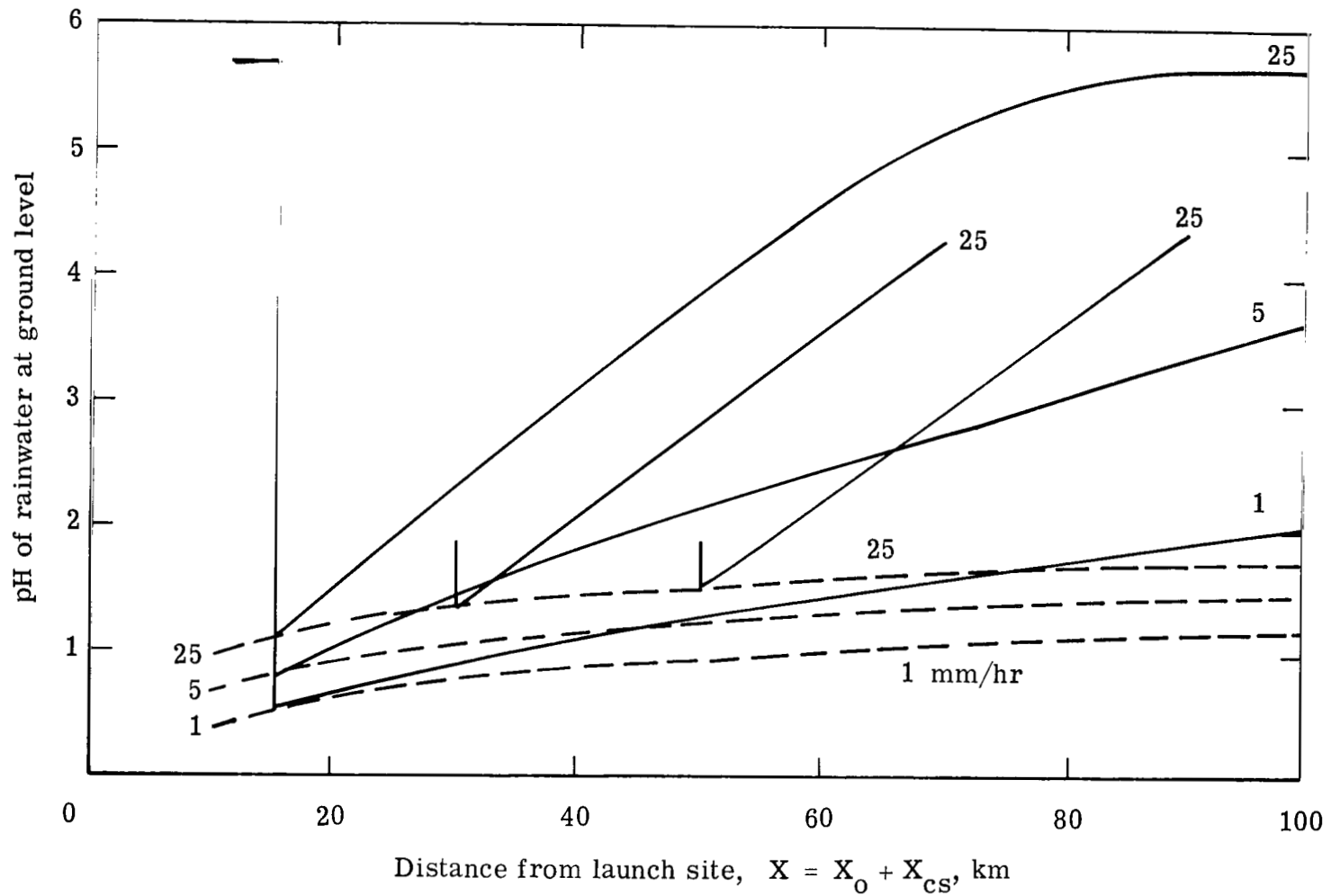


Figure 19.- Calculated volumetric-average rain acidity due to $\text{HCl}(\text{g})$ washout for FFW Titan III case. Potential rain pH (dashed line) applies at first onset of rain; pH of steady rain (solid line) reflects progressive washout, which was begun at 15, 30, and 50 km downwind.

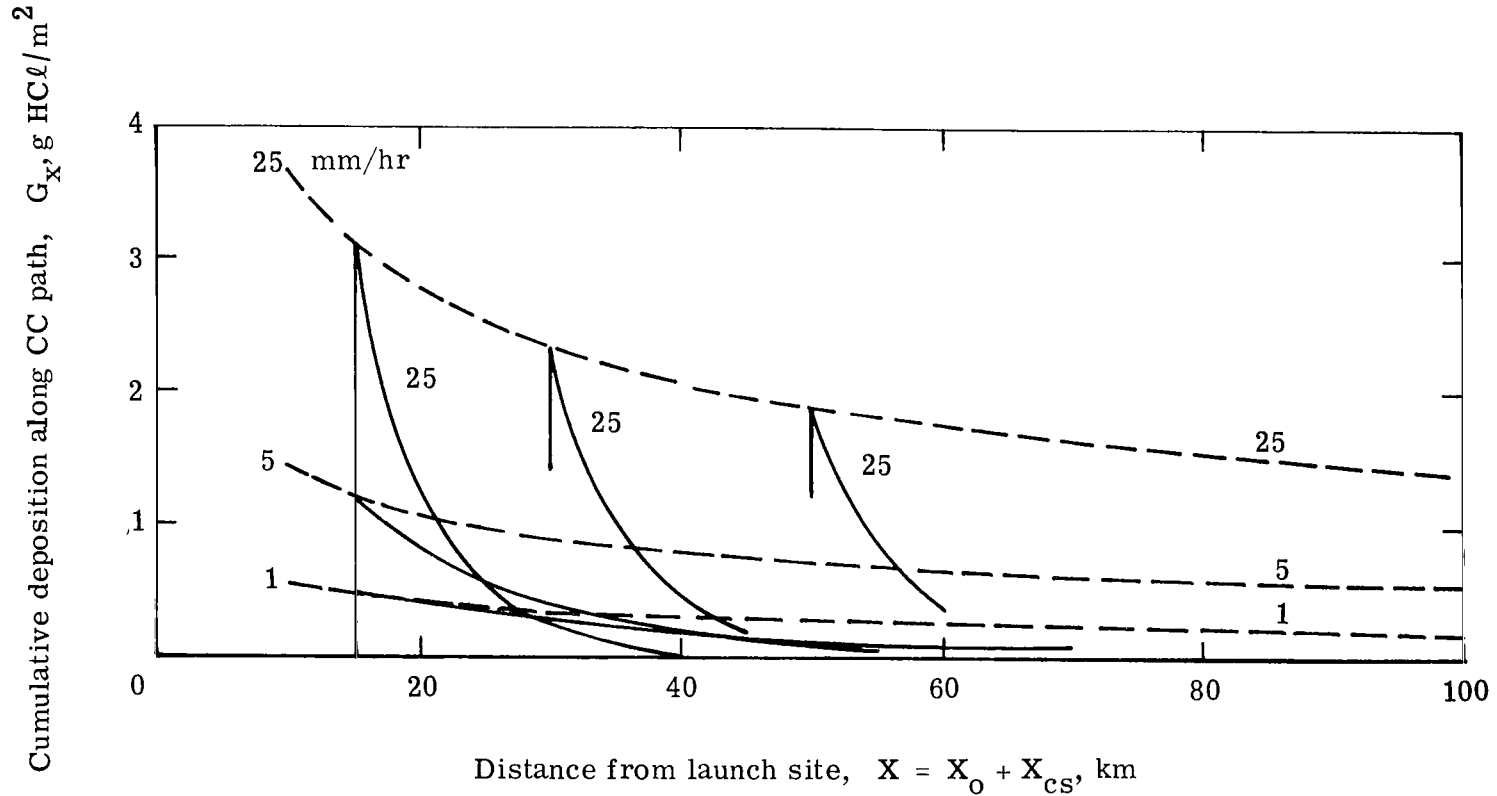


Figure 20.- Calculated cumulative HCl deposition per unit area along cloud-centroid path due to HCl(g) washout for FFW Titan III case. Potential deposition (dashed line) applies at first onset of rain for entire SRM cloud. Deposition after start of steady rain (solid line) reflects progressive washout, which was begun at 15, 30, and 50 km downwind.

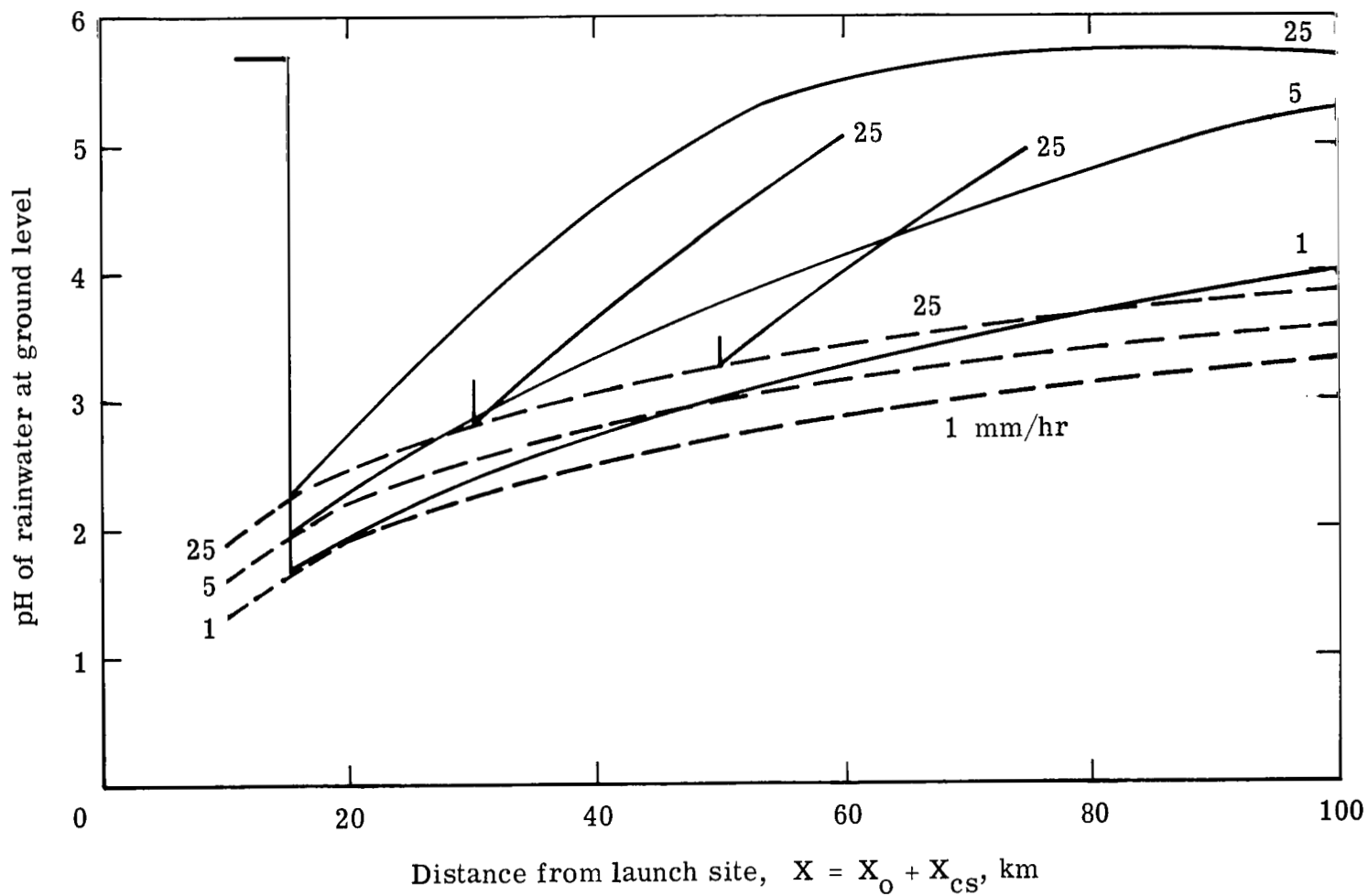


Figure 21.- Calculated volumetric-average rain acidity due to $\text{HCl}(g)$ washout for SFW Titan III case. Potential rain pH (dashed line) applies at first onset of rain; pH of steady rain (solid line) reflects progressive washout, which was begun at 15, 30, and 50 km downwind.

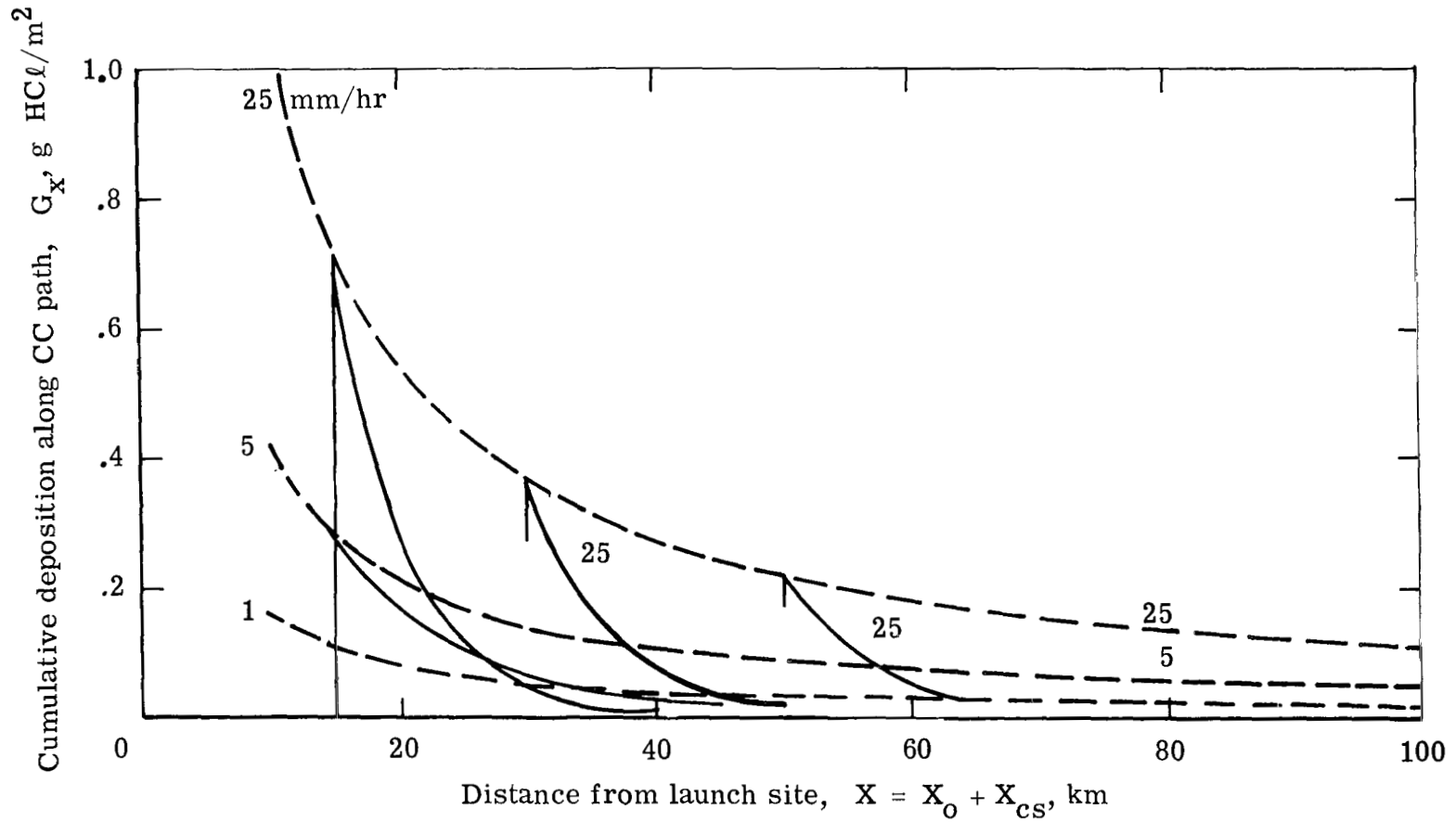


Figure 22.- Calculated cumulative HCl deposition per unit area along cloud-centroid path due to HCl(g) washout for SFW Titan III case. Potential deposition (dashed line) applies at first onset of rain for entire SRM cloud. Deposition after start of steady rain (solid line) reflects progressive washout, which was begun at 15, 30, and 50 km downwind.

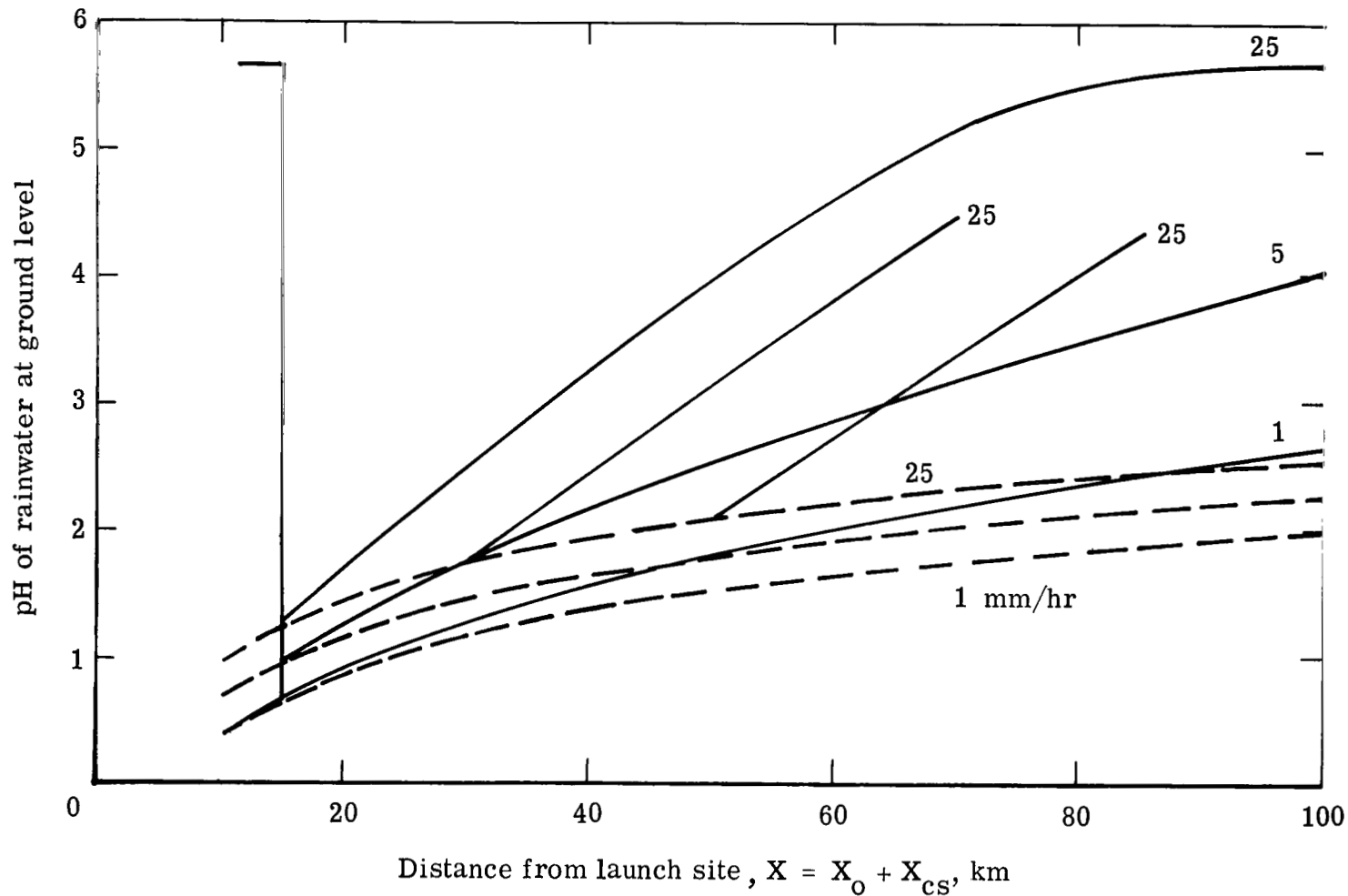


Figure 23.- Calculated volumetric-average rain acidity due to $\text{HCl}(\text{g})$ washout for source-strength-modified SFW Shuttle case. Potential rain pH (dashed line) applies at first onset of rain; pH of steady rain (solid line) reflects progressive washout, which was begun at 15, 30, and 50 km downwind.

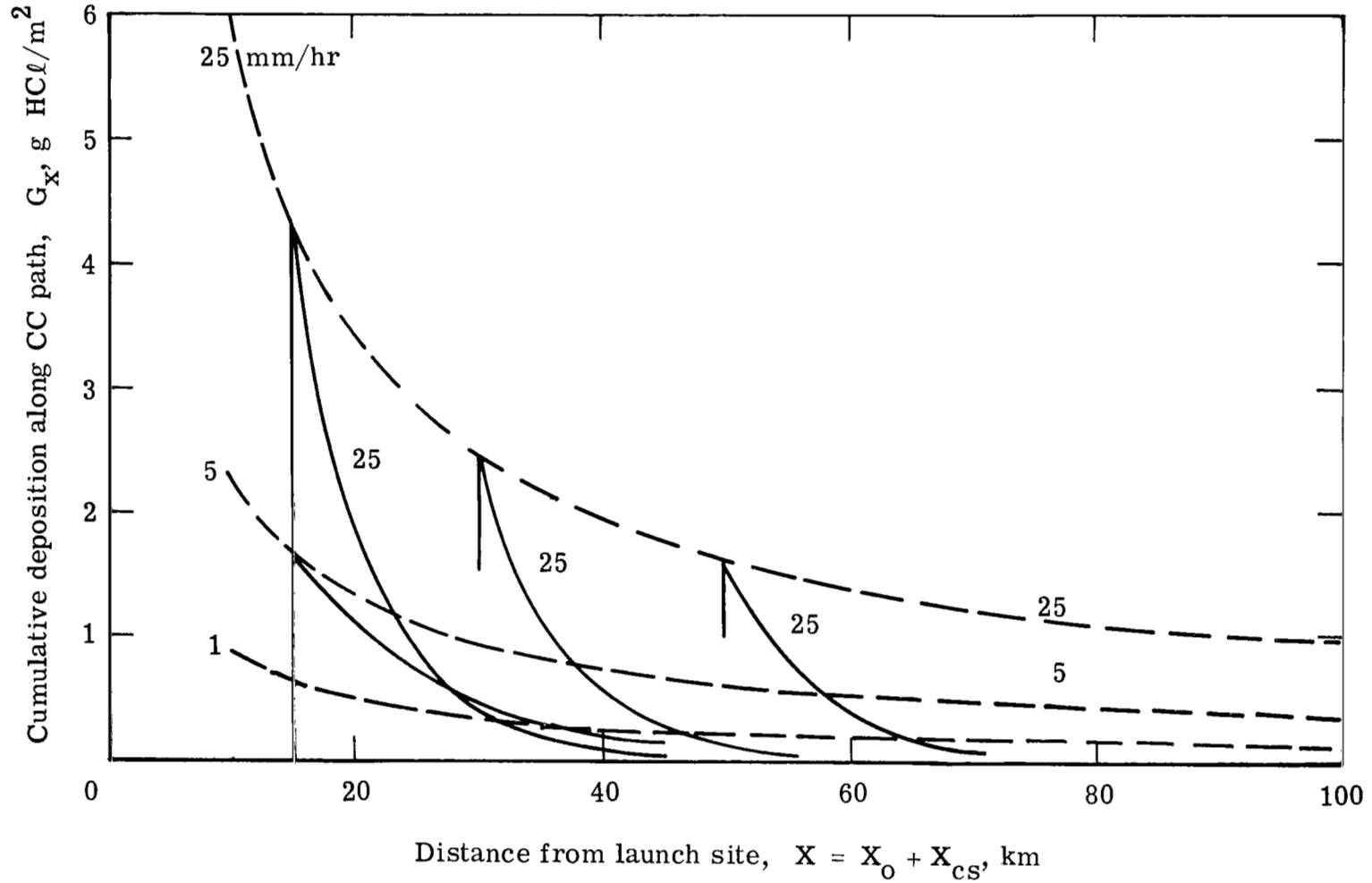


Figure 24.- Calculated cumulative HCl deposition per unit area along cloud-centroid path due to HCl(g) washout for source-strength-modified SFW Shuttle case. Potential deposition (dashed line) applies at first onset of rain for entire SRM cloud; deposition after start of steady rain (solid line) reflects progressive washout, which was begun at 15, 30, and 50 km downwind.

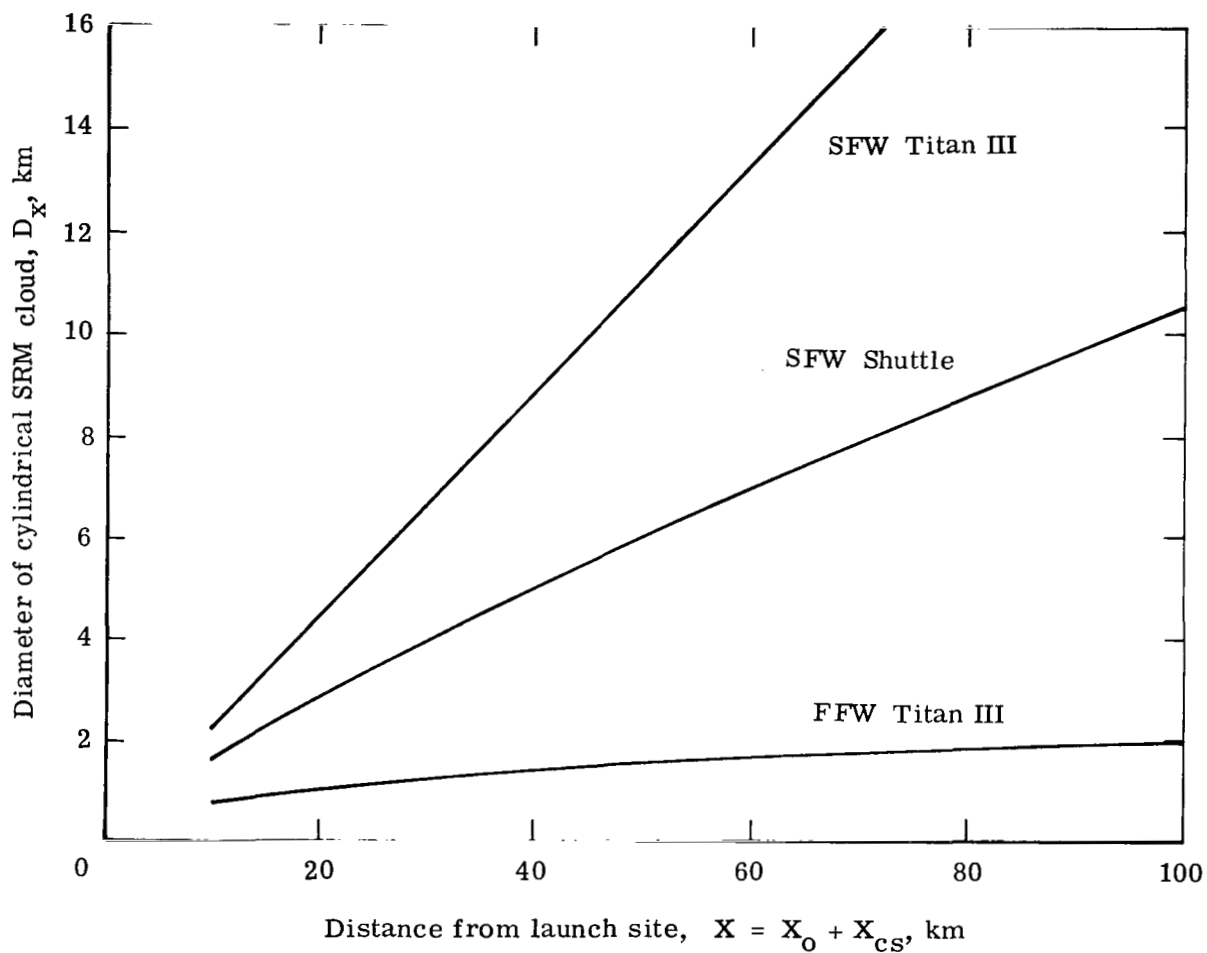


Figure 25.- Downwind growth of SRM exhaust cloud diameter for two extreme Titan III cases (SFW and FFW) and source-strength-modified SFW Shuttle case. Calculated for assumed right circular cylindrical geometry.

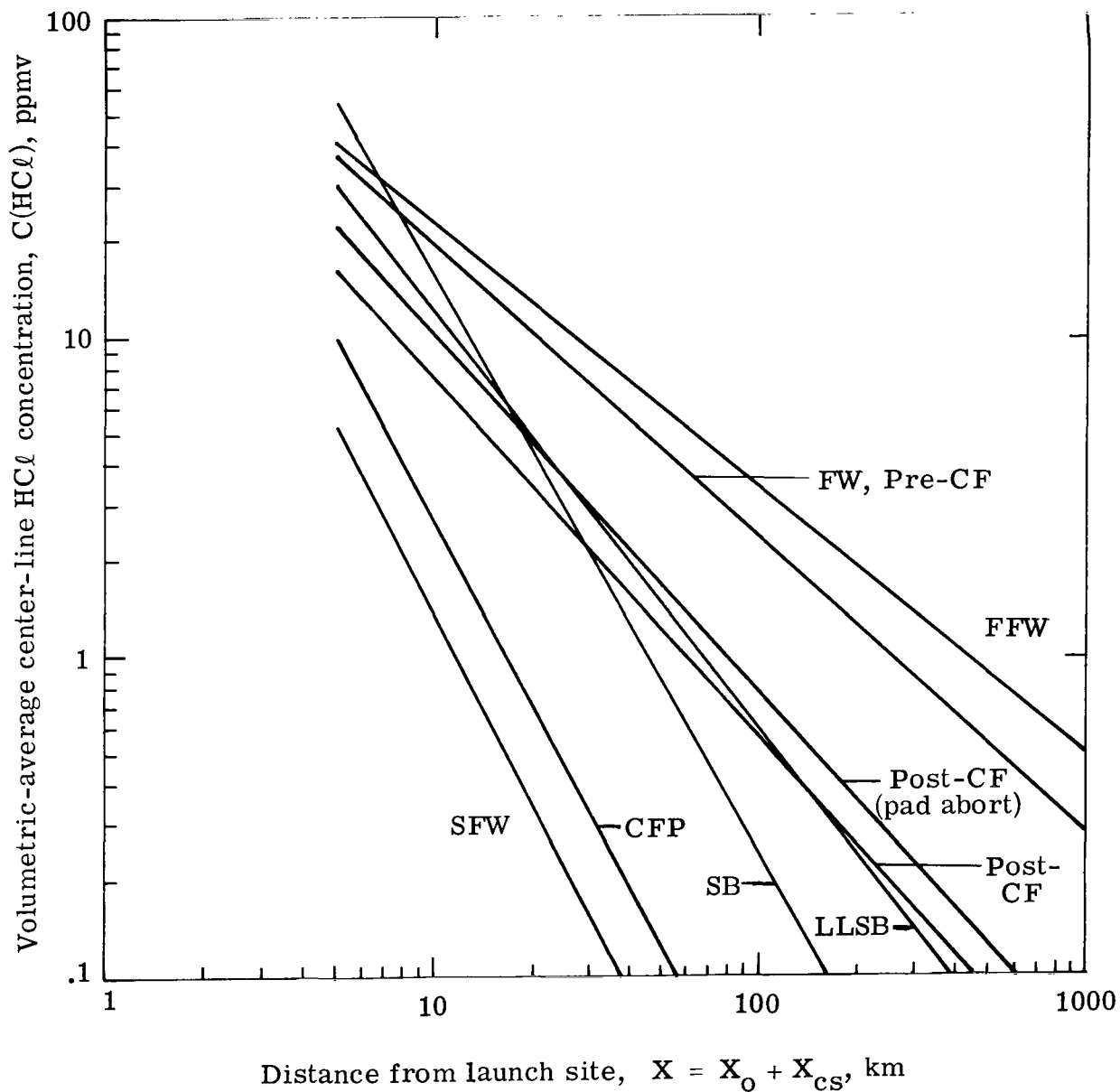


Figure 26.- Dispersive decays of volumetric-average HCl concentration calculated as functions of downwind distance for Titan III SRM exhaust clouds for seven standard meteorological conditions at Cape Canaveral, Florida.

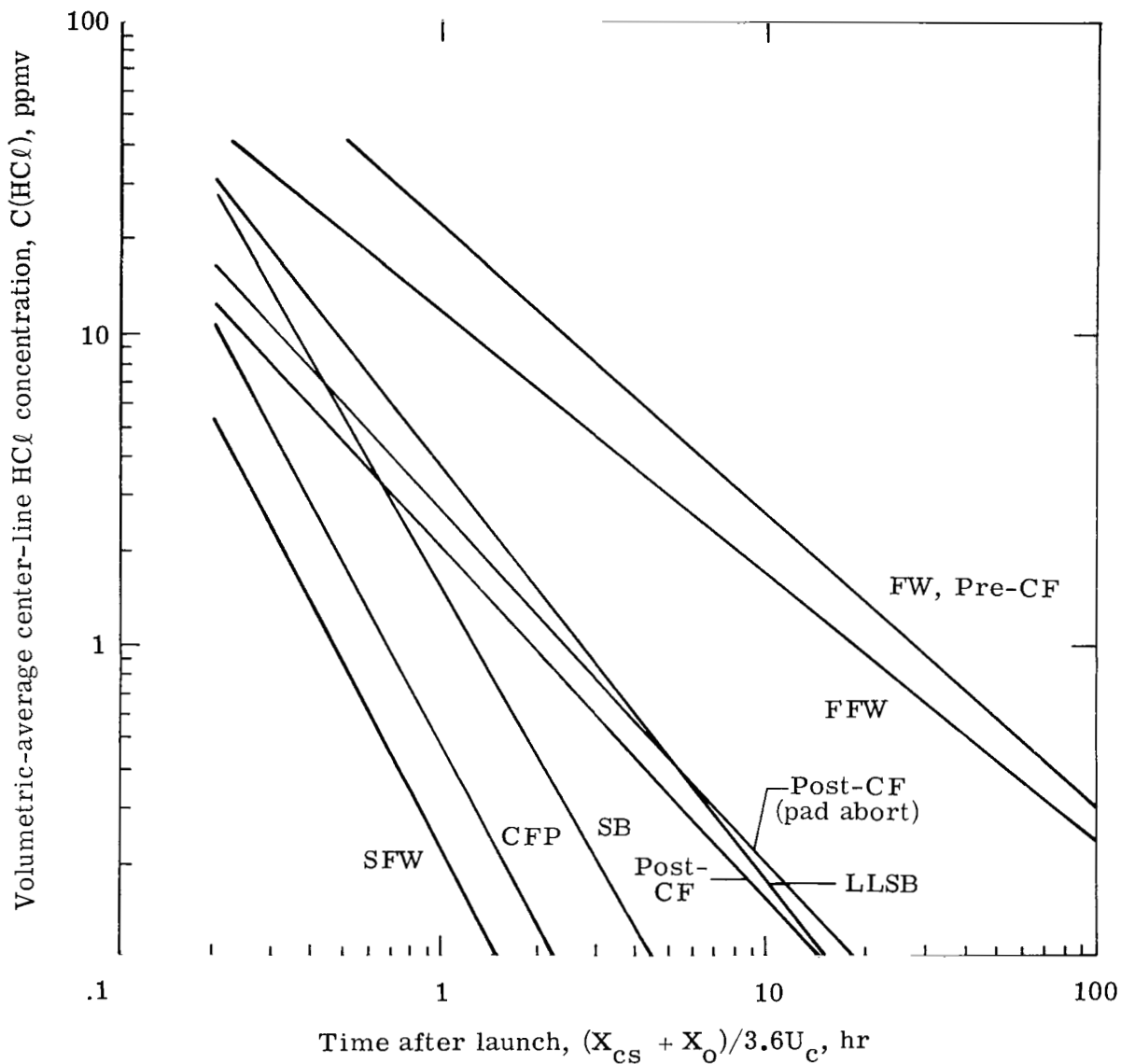


Figure 27.- Dispersive decays of volumetric-average HCl concentration calculated as functions of downwind drift time for Titan III SRM exhaust clouds for seven standard meteorological conditions at Cape Canaveral, Florida.

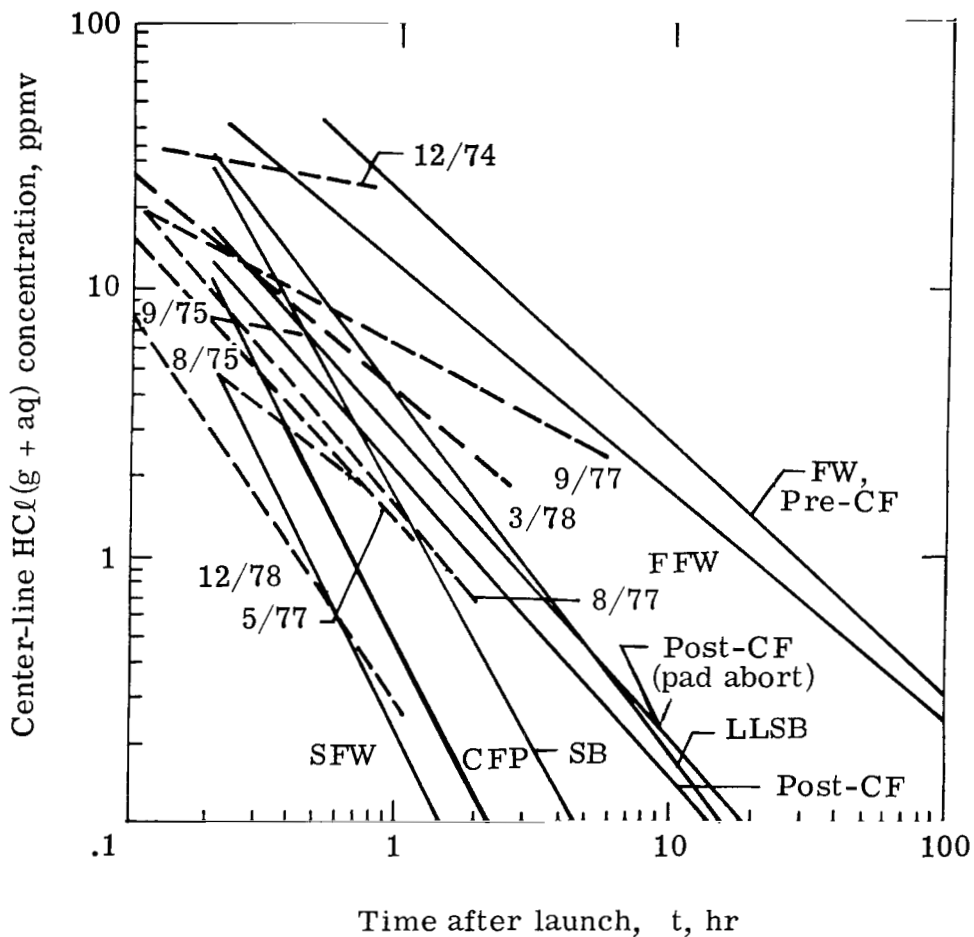


Figure 28.- Calculated decays (solid line) of in-cloud HC^l concentration (vertical average, cloud center line) are shown for seven standard meteorologies at Cape Canaveral, Florida. Empirical fits of experimental measurements (dashed line) of peak (≥ 1 sec) in-cloud HC^l are shown for eight Titan III launches at Cape Canaveral. Note that various calculated and experimental HC^l decays are not comparable on a one-to-one basis, since respective input and actual launch meteorologies differed (from ref. 43).

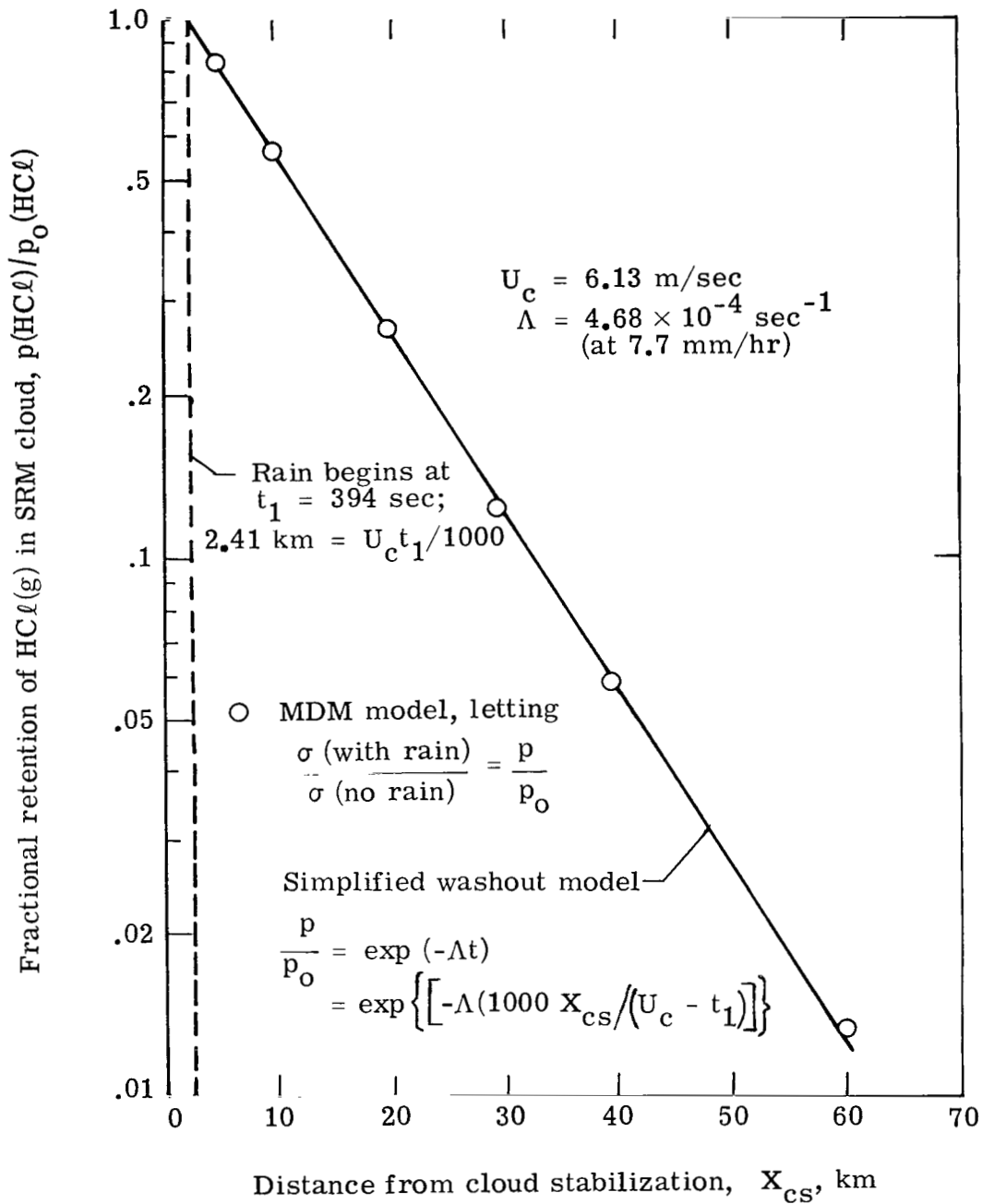


Figure 29.- Results of check on MDM-5(II) calculations of $\text{HCl}(g)$ washout from SRM exhaust clouds. Check examines equivalency (circles versus straight line) of calculated $\text{HCl}(g)$ retention in FFW Titan III exhaust cloud as determined by (a) ratio of calculated vertical $\text{HCl}(g)$ column densities for respective rain and no-rain cases and (b) present simplified washout model.

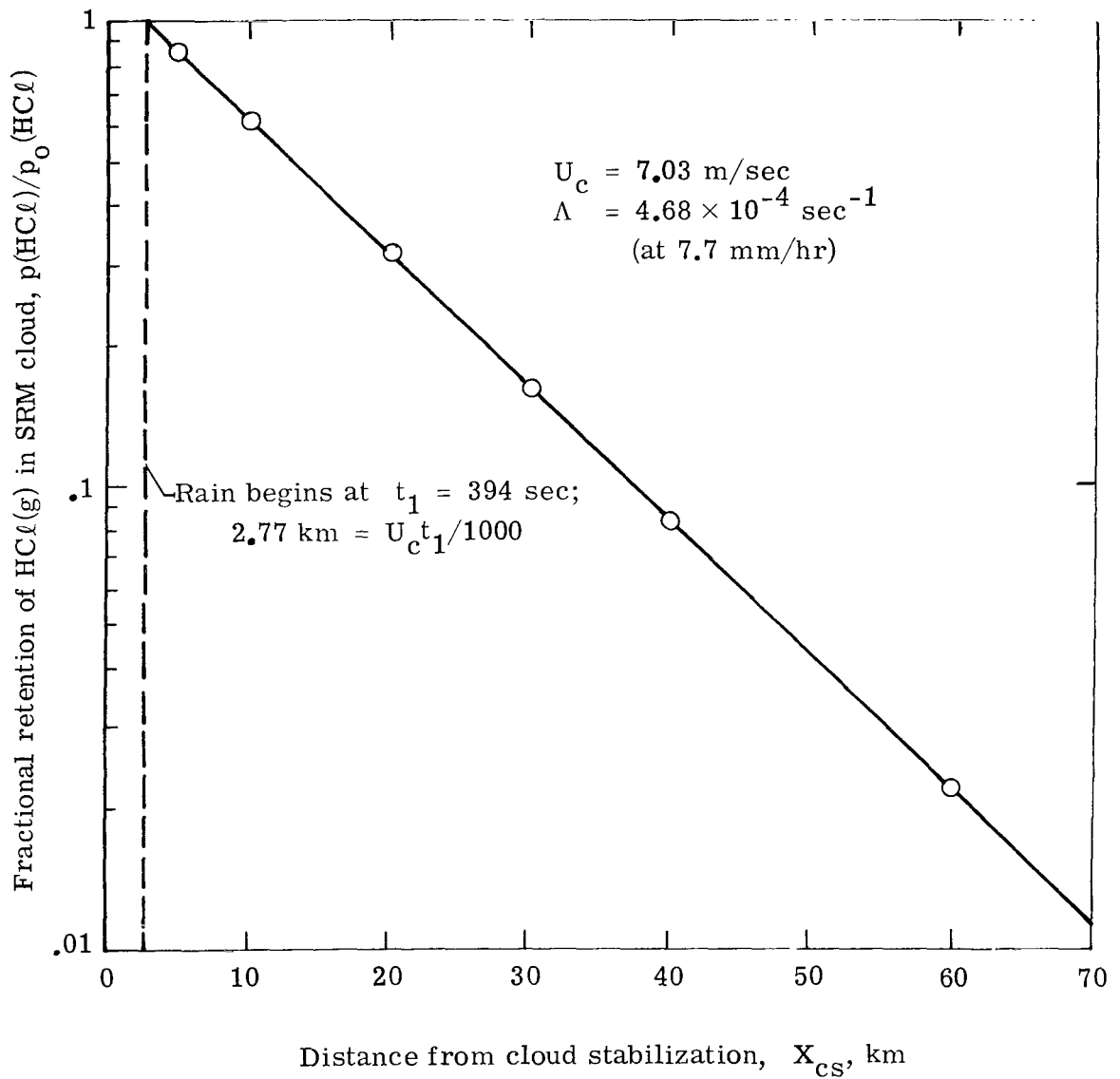


Figure 30.- Results of check on MDM-5(II) calculations of $\text{HCl}(g)$ washout from SRM exhaust clouds. Check examines equivalency (circles versus solid line) of calculated $\text{HCl}(g)$ retention in SFW Titan III exhaust cloud, using same procedure as in figure 29.

1. Report No. NASA TP-1801		2. Government Accession No.		3. Recipient's Catalog No.	
4. Title and Subtitle ANALYTIC MODEL FOR WASHOUT OF HCl(g) FROM DISPERSING ROCKET EXHAUST CLOUDS				5. Report Date May 1981	
7. Author(s) G. L. Pellett				6. Performing Organization Code 506-52-33-01	
9. Performing Organization Name and Address NASA Langley Research Center Hampton, VA 23665				8. Performing Organization Report No. L-14107	
12. Sponsoring Agency Name and Address National Aeronautics and Space Administration Washington, DC 20546				10. Work Unit No.	
15. Supplementary Notes				11. Contract or Grant No.	
16. Abstract				13. Type of Report and Period Covered Technical Paper	
<p>The potential is investigated that precipitation scavenging of HCl from large solid rocket (SRM) exhaust clouds may result in unacceptably acidic rain in the Cape Canaveral, Florida, area before atmospheric dispersion reduces HCl concentrations to safe limits. Several analytic expressions for HCl(g) and HCl(g + aq) washout are derived; a geometric mean washout coefficient ($\Lambda = 1.39 \times 10^{-4} H^{0.595} \text{ sec}^{-1}$, where H = mm rain/hr) is recommended. A previous HCl washout model is refined. It treats the idealized case of an independently generated vertical rainfall that overrides and scavenges an independently advecting and dispersing SRM cloud under stable stratification conditions. The resultant pH of rain and HCl deposition rate are functions of initial HCl source strength; dispersive power-law decay of vertical HCl column density σ; and mean wind speed, downwind rainfall onset, Λ, and H. Cumulative areal deposition of HCl G_x is based on an expanding cylindrical SRM cloud geometry. The washout model is applied to a refined Space Shuttle case (70 t HCl exhausted up to 4 km) and eight Titan III (60-percent less exhaust) dispersion cases. The σ decays were previously deduced by application of a multilayer Gaussian diffusion model to seven standard meteorological regimes for overland advection. The Titan III decays of σ and initial rain pH differed greatly among regimes; e.g., a range of >2 pH units was spanned at $X \geq 100$ km downwind and $t \geq 2$ hr. Environmentally significant pH's (≤ 1.5) for infrequent exposures were shown possible at $X \leq 50$ km and $t \leq 5$ hr for the two least dispersive Titan III cases. Representative examples of downwind rainwater pH and G_x are analyzed. Finally, factors affecting the validity of the results are discussed.</p>				14. Sponsoring Agency Code	
17. Key Words (Suggested by Author(s))			18. Distribution Statement		
Environmental pollution Precipitation scavenging Washout Hydrogen chloride			Acid rain Atmospheric dispersion		
			Unclassified - Unlimited		
			Subject Category 45		
19. Security Classif. (of this report)		20. Security Classif. (of this page)		21. No. of Pages	
Unclassified		Unclassified		90	
				22. Price	
				A05	